UNIVERSITY OF OKLAHOMA

GRADUATE COLLEGE

OPTIMIZATION OF RED BRICK DUST-BASED GEOPOLYMERS FOR USE IN

SUSTAINABLE CONSTRUCTION

A THESIS

SUBMITTED TO THE GRADUATE FACULTY

in partial fulfillment of the requirements for the

Degree of

MASTER OF SCIENCE

By

CODY A. BLACK
Norman, Oklahoma
2023

OPTIMIZATION OF RED BRICK DUST-BASED GEOPOLYMERS FOR USE IN
SUSTAINABLE CONSTRUCTION

A THESIS APPROVED FOR THE
SCHOOL OF CIVIL ENGINEERING AND ENVIRONMENTAL SCIENCE

BY THE COMMITTEE CONSISTING OF

Dr. Jeffery S. Volz, Chair

Dr. Royce W. Floyd

Dr. Shreya Vemuganti

Abstract

With the rising carbon dioxide levels affecting climate change, sustainable and eco-friendly alternatives to ordinary portland cement (OPC) are being investigated. To reduce the overall environmental impact, industrial waste products, such as fly ash and silica fume, have been used as partial substitutions for OPC in modern concrete mix designs. Other waste products can be used as replacements, and one such waste product is red brick dust (RBD). This research seeks to repurpose processed RBD through the utilization of geopolymerization processes.

Geopolymerization utilizes alkali activators, which cause the low-reactive RBD to interact more readily with its constituent parts to form a strong geopolymer base. Ground limestone, calcium hydroxide, and alumina were chosen and added to facilitate a stronger geopolymer reaction from the aluminosilicate. An extensive literature review was performed to understand the underlying principles and establish target ratios for the molar values of components. These target ratios were calculated based on the quantities of raw materials and alkali activators after converting to moles of calcium, silica, or alumina. Afterwards, each component was weighed based on content requirements, followed by modifications to the RBD geopolymer mixture using substitution by weight percent of RBD.

Brass 2"x2" mortar cubes were used to batch the specimens based on an Ancient Roman concrete approach. This involved utilizing target ratios provided by examples in Ancient Roman concrete. Multiple mix designs were used, along with ambient and oven curing methods, to determine an optimized region in which RBD geopolymers showed the

highest compressive strength. Uniaxial compressive testing and calorimetry reports allowed for the identification of strength properties and gel phases, respectively. Stagnation of geopolymerization was an issue during this study based on calorimetry results. Generally, underdeveloped calorimetry peaks led to undesirable compressive strengths. This was indicative of a failure in either the dissolution process or the polymerization and hardening phase.

Once the data was analyzed for the 2"x2" mortar cubes, a secondary approach emerged known as hybrid gel compatibility. This approach focused on the possible existence of hybrid gels inside the RBD geopolymer mixture. The 3"x6" cylinder series adopted the hybrid compatibility approach, followed by additional batching and testing with new mix designs. Compressive strength results were overlayed onto ternary diagrams, and a maximum compressive strength zone was identified. Seven-day ambient-cured, 28-day ambient-cured, and oven-cured compressive strengths were analyzed against ACI codes to establish compressive strength limits and achieve the goal of this research: to find a sustainable alternative to OPC with improved or similar material characteristics through the optimization of low-reactive aluminosilicates and geopolymerization techniques.

Acknowledgements

I began my journey to achieve a better life through my entrance into the United States Marine Corps in 2013. At the time, I was facing numerous personal issues, including two DUI charges and a drug possession charge. Through the Marine Corps, I was able to overcome and put the past behind me. They provided me with a sense of purpose and dedication to not only myself but also to those around me. This newfound commitment was combined with hard work and the ability to reach for success, as exemplified by my meritorious promotions that followed. Sadly, surgery due to an accident caused a separation from service in 2017. Afterwards, my plans for an engineering career still prevailed, so I transitioned into the Architectural Engineering program at the University of Oklahoma in Spring 2018. During my first semester, I faced hardship with a diagnosis of T-cell lymphoma. Despite this, I persevered and completed my classes at a full-time student status while undergoing treatments and surgeries.

All of this led to an inspiration to research and experiment with Ancient Roman concrete, which further drove me to learn about geopolymers. I tested my experiments by creating 2"x2" mortar cubes using oven-cured bricks, which were crushed with a man-powered crusher. I brought the finished products to Dr. Volz, and the rest is explained in this document. So, I would like to thank my wife, Carly Black, who was there with me during the cancer treatments, brick-breaking, and questionable forging practices. I would like to thank my immediate family for being there for me when I was so lost in this world, especially after I left the Marine Corps. I have a personal blessing and thank you to my spiritual mentor, Denny Madory. He helped me crawl back from a terrible place mentally,

Table of Contents

List of Tables

List of Figures

Chapter 1: Introduction

1.1 Background

According to Davidovits (2020), the term "geopolymer" was first coined by his team in the 1970s and has since been widely utilized by many researchers and scientists. The author describes geopolymers as "ceramic-like inorganic polymers produced at low temperatures, usually below 100°C." These geopolymers are linked together via covalent bonds provided by the alumina (Al_2O_3) and silica (SiO_2) sheets. An alkali solution is applied to the aluminosilicates, which allows the Al_2O_3 and SiO_2 to enter a free state. Afterward, the sheets of Al_2O_3 and SiO_2 realign into interconnected chains depending on the presence of sodium (Na) or calcium (Ca). Finally, polymerization and hardening can occur, leading to strength development based on ambient or elevated temperature scenarios (Davidovits, 2020). A simplified geopolymerization process, shown in Figure 1-1, was used for this research project. The processes are summarized into three main phases: Aluminosilicate Dissolution, Gel Precipitation, and Polymerization and Hardening.

Figure 1-1: Gel Phase Descriptors for Geopolymer Research

It should be noted that Davidovits (2020) describes this process as being limited by reactivity and heat conditions. Normally, the polymerization and hardening phase

progresses within the 15-hour mark at ambient curing conditions, while increased heat during curing moves up this timetable. Davidovits (2020) showed, in Figure 1-2, that researchers were able to use highly reactive kaolinite clay and activate it with sodium hydroxide (NaOH). Davidovits and his team found that the alkali-activated kaolinite clay polycondensed into hydrated sodalite at 100°C to 150°C. Initially, geopolymerization research was conducted on clay-based or industrial waste-based aluminosilicates, then progressed to other sources.
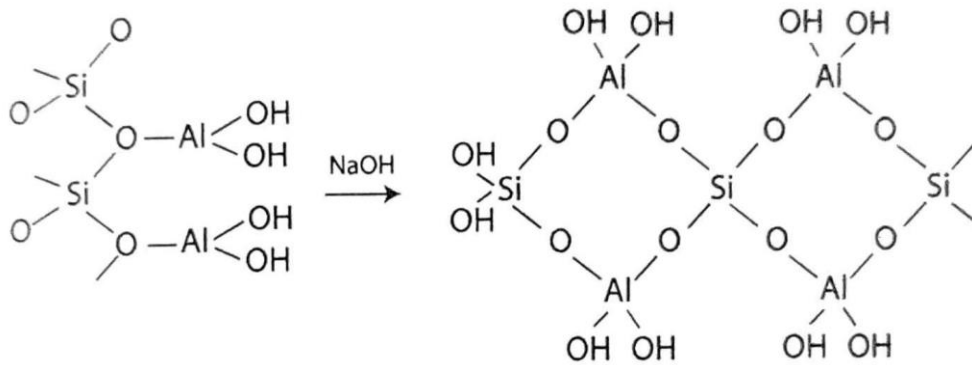
Figure 1-2: Polycondensation of Aluminosilicate in Alkali Solution (Davidovits, 2020)

One such material was red brick dust (RBD). Wong et al. (2018) found that "brick is the second most widely used construction material after concrete" and "it is treated as construction and demolition waste if there are damages during the manufacturing, construction, and demolition activities." The authors detailed the impact of RBD on the environment and proposed an alternative solution to this issue. Their conclusion pointed to RBD as an effective way to reduce waste accumulation in landfills through

geopolymerization (Wong et al., 2018). Further research into RBD and other demolition debris is needed to assess the feasibility of its use in the construction field.

The repurposing of these aluminosilicates has the potential to alter climate change and provide an eco-friendly alternative to ordinary portland cement (OPC). Climate change has become increasingly influential in modern life, with carbon dioxide (CO_2) playing a pivotal role. Cement production and curing account for roughly 5% to 8% of global CO_2 emissions, according to Scrivener et al. (2018). In addition, Scrivener et al. (2018) mentioned that OPC is "the largest manufactured product on Earth by mass." These two factors serve as a warning for continued use of OPC and point to the need for alternative materials, such as RBD.

1.2 Goals, Objectives, and Scope of Work

The overarching goal of this research was to find a sustainable alternative to OPC with improved or similar material characteristics through the optimization of low-reactive aluminosilicates and geopolymerization techniques. The following is a discussion of the objectives and scope of work that were pursued to achieve this goal. Two approaches were used to adapt and accommodate unexpected changes in the RBD geopolymer mixture as objectives shifted and changed during the experiment.

Based on the variability in the geopolymerization processes, a range of objectives was needed to identify and overcome saturation issues within the RBD geopolymer mixture. The initial objective was to find an optimal activator ratio by testing various hydroxide (OH) molarity values and then evaluating their corresponding target ratios. The optimum

OH molarity was crucial for identifying the amount of alkali activators present. Once an optimal alkali concentration was found, the molar ratios were adjusted for the following: Ca/SiO_2, $Ca/(Al_2O_3 + SiO_2)$, Al_2O_3/SiO_2, and SiO_2/Al_2O_3. These ratios determined the strength properties and geopolymerization progression through the addition of raw materials. The chosen values were based on a literature review and represent an Ancient Roman concrete approach.

A separate approach, known as hybrid gel compatibility, was also found during the literature review. Ternary diagrams can be used to identify regions for strength development based on hybrid gels formed from the aluminosilicates and other components. This secondary strategy focused on forming gel chains within the RBD composition through ratios of Ca:Si:Al molar percentages. When those Ca:Si:Al contents were plotted against compressive strengths, a better understanding of gel chains and strength properties occurred. This shifted the objectives to locating an area of maximum compressive strength and finding gel formation indicators through calorimetry readings.

The RBD geopolymer research accomplished the evolving cycle of objectives through a comprehensive work plan designed to satisfy the overarching goal. As shown in Figure 1-3, the scope of work was separated into five main tasks: Target Ratios and Hybrid Gel Theory, RBD Processing, Testing and Analysis, RBD Modification, and Series Advancement. Within these main tasks, there are additional subtasks for achieving the objectives and advancing the 2"x2" mortar cube and 3"x6" cylinder recipes. These tasks included a literature review, acquiring processed RBD for batching and testing,

compressive and calorimetry tests, and selection of promising specimens for series advancement.
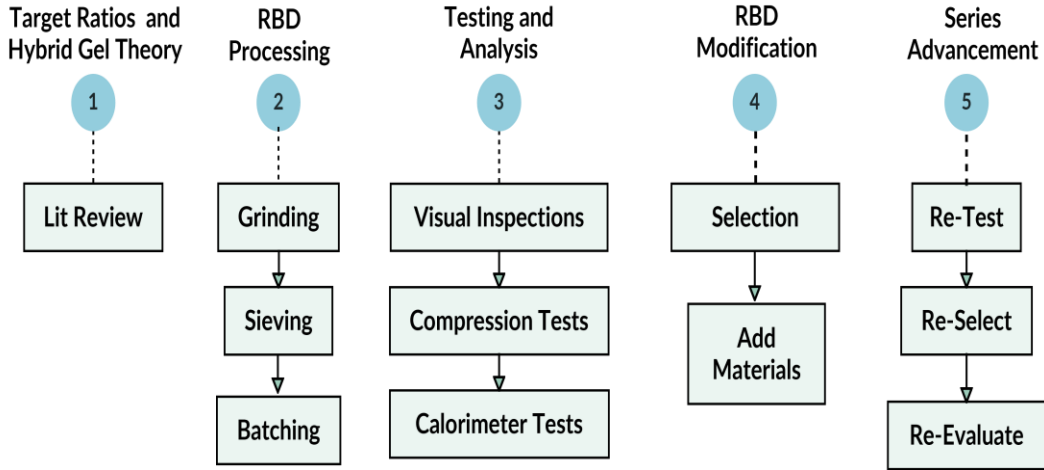
Figure 1-3: Flowchart for Scope of Work

1.3 Research Plan

Optimization of the RBD geopolymer mixture was evaluated based on the highest compressive strengths and well-developed calorimetry peaks. The initial research paradigm used 2"x2" mortar cubes with multiple samples per group. The geopolymer mortar cubes were batched and tested, mimicking ASTM Standard C305 (2020) and ASTM Standard C109/C109M (2021), respectively. Curing techniques attempted to follow prescribed ASTM Standards. However, the oven and ambient curing models were modified to accommodate the unique properties of the RBD geopolymer mixture. The molds used for the 2"x2" mortar cubes were brass and showed good resistance to the highly alkaline environment.

The research was scaled up for the 3"x6" cylinder series, and reusable plastic molds were utilized for ambient and oven-curing models. ASTM Standard C192/C192M (2019) and ASTM Standard C39/C39M (2021) were used for 3"x6" cylinder batching and testing with modifications to adjust for the curing conditions. The main modification was the use of airtight storage units to prevent excess water evaporation for ambient-cured samples. Oven-cured samples were sealed with plastic lids to prevent moisture removal. All specimens and alkali solutions were allowed to reach ambient conditions before batching and testing occurred.

1.4 Outline

Five chapters and three appendices define the structure of this document and serve as a guide for the target audience. The current chapter is designated Chapter 1 and provides the introduction and background information. The paper is designed as a story to help move the reader through the material without overcomplicating underlying principles and mechanisms. Therefore, the literature review organically falls into Chapter 2 position with a thorough explanation of the information acquired for this research. This is followed by Chapter 3, which includes the formulations, results, and analysis of the 2"x2" mortar series. The target ratios in this section were focused on the Ancient Roman concrete theories provided by Jackson et al. (2017).

A modified approach was adopted for Chapter 4, and the new hybrid gel compatibility theory was implemented based on Garcia-Lodeiro et al. (2011) and Luo et al. (2023) for the 3"x6" cylinders series. Ternary diagrams allowed for further exploration of geopolymer

processes and enabled a better understanding of the Ca:Si:Al components. Chapter 5 finalized the research project with conclusions inferred from experiments and recommendations based on the findings. The three appendices, at the end, serve as a depository for sample imagery, compressive strength results, and calorimetry reports.

Chapter 2: Literature Review

The Literature Review was based on three main topics: (1) Calcium Silicate Hydrate (C-S-H) and Al-Substituted Variant, (2) Geopolymer Gels and Compatibility, and (3) Alkali Concentrations, Raw Materials, and Curing Techniques. These topics encompassed the entirety of variables necessary for optimization of RBD-based geopolymers. Most research studies used highly reactive Ca source with a few using brick waste-based geopolymers. This current RBD research utilized low Ca aluminosilicates, with Ca sources added, to activate the geopolymerization process. Observations and similarities were needed to provide a comprehensive overview of molar ratios, chemical activity, and curing processes.

2.1 Calcium Silicate Hydrate (C-S-H) and Al-Substituted Variant

The unique properties of Calcium Aluminate Silicate Hydrate (C-A-S-H) are derived from the C-S-H bonds traditionally found in OPC. Taylor (1986) discussed the process of C-S-H formation and how the chemical structure is formed. The article focused on how high or low Ca/Si ratios can affect either jennite or tobermorite crystallization. The optimal range for tobermorite formation was found to be Ca/Si = 0.8 to 1.2, while a higher range of Ca/Si = 1.4 to 2.2 produced jennite instead (Taylor, 1986). These results can be used to find Ca/Si ratios that produce Al-tobermorite and C-A-S-H gels. However, Al suggestions are lacking in this research, along with geoformations that are still being analyzed for non-standard aluminosilicates, such as RBD.

The Ca/Si ratio controls the strength characteristics of cementitious materials, along with the substitution of metal ions, such as Al^{3+} or Fe^{3+}. Richardson and Groves (1993) determined optimal Ca/Si ratios that allowed for Al substitution in place of Ca, leading to the creation of Al-tobermorite structures. The authors indicated that "at high Ca/Si ratios, the Al or Fe preferentially substitute for Ca in octahedral sites, and at low Ca/Si ratios they substitute for Si in tetrahedral sites." Their study outlined that a range of Ca/Si ratios from 0.8 to 1.2 would enable the substitution of Al into the C-S-H chains with a limiting Ca/Al ratio of 0.15. In addition, a linear relationship was proposed for the substitution of Al_2O_3 into C-S-H chains, yet the actual pairing mechanisms are still being investigated (Richardson and Groves, 1993). These values can be integrated into RBD target ratios to help guide C-S-H and C-A-S-H gel production. Target ranges are crucial to forming the proper environment and are currently lacking in RBD geopolymer research.

Experiments and geochemistry investigations were crucial for identifying the process of geopolymerization. Davidovits (2020) is considered the seminal work on geopolymer chemistry and serves as a foundation for understanding the chemical structures of geopolymers. The author analyzed the covalent bridging mechanisms for Ca-based geopolymers and provided diagrams for understanding the three-dimensional layouts. The Ca-based geopolymers possessed silicon (Si)/aluminum (Al) ratios of 1 to 3 with Ca-rich aluminosilicates, such as ground granulated blast furnace slag (GGBFS). These Ca-based specimens incorporated tobermorite-like structures into three-dimensional layouts known as (K, Ca)-cyclo-ortho-(sialate-disiloxo). The chemical formula was written as 3CaO-

Al_2O_3-$3SiO_2$ and was normally accompanied by calcium silicate hydrate (C-S-H) chains (Davidovits, 2020).

Examples of C-S-H chains and their Al-substituted variant, C-A-S-H, were investigated by Jackson et al. (2013). The authors conducted an analysis of lime clasts found in hydraulic cement subjected to seawater and other environmental factors. The article discusses the Ca/Si ratios found in ancient Roman cement, examples of C-A-S-H production in the field, and the material properties of Al-tobermorite. The relict lime clasts and the cementitious binder were both found with Al-substituted tobermorite (Al-tobermorite) structures within their interconnected networks. The formation of these Al-tobermorite sites is indicative of C-A-S-H chains within the specimens and is hypothesized to be directly responsible for the increased strength properties of ancient Roman cement over time (Jackson et al., 2013). This type of research into Roman cement can potentially assist in better understanding the mechanisms and hydrate chains behind RBD geopolymers.

Jackson et al. (2017) investigated the presence of C-A-S-H gels in Roman concrete against various concrete core samples from different geographical sites. Their goal was to determine the difference between Roman seawater mortar and other types of cement. A ternary diagram, shown in Figure 2-1, was used to depict the Ca, Al, and Si contents found in core samples from various geological deposits. Results indicated that a high Ca/Si ratio with low to no Al content was typical of OPC, while a range of 10% to 15% Al by analysis signified Al-tobermorite in the Roman mortar. This research identified the Ca/Si, Si/Al, and Ca/Al ratios that were used for naturally occurring Al-tobermorite formations.

Furthermore, Jackson et al. (2017) addressed the importance of geopolymer research and how it serves to "further understanding of multiple pathways to low-temperature Al-tobermorite crystallization."
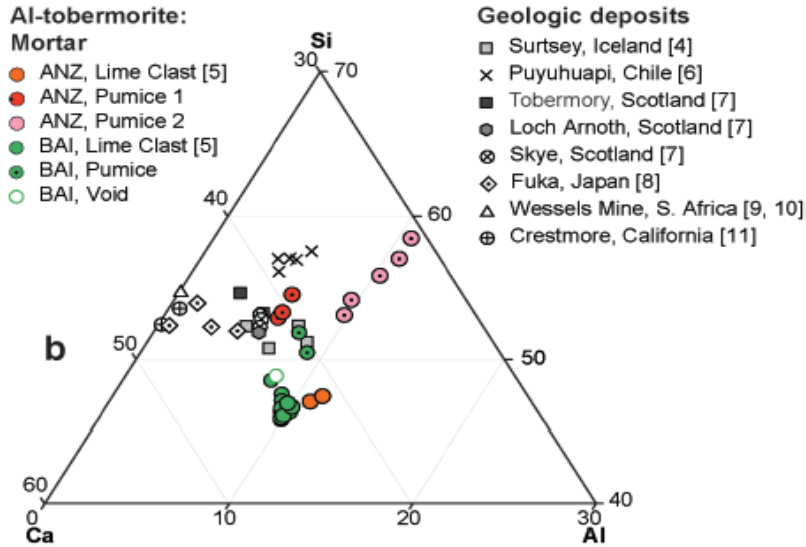
Figure 2-1: Ternary Diagram of Ca, Al, and Si Contents Present in Core Samples from Different Geological Deposits (Jackson et al., 2017)

2.2 Geopolymer Gels and Compatibility

In addition to C-S-H and C-A-S-H gels, there are also Sodium Aluminate Silicate Hydrate (N-A-S-H) gels. As shown in Figure 2-2, Provis and Bernal (2014) explored the chemistry of N-A-S-H and C-A-S-H formation, along with multiple binder systems and aluminosilicate sources. It should be noted that MgO was used to balance gel formations in GGBFS-based geopolymers. Yet, the formation process is similar for aluminosilicates balancing with other metal oxides, such as FeO, under alkali activation. Their research investigated fly ash, GGBFS, and metakaolin as aluminosilicates and found that differing

levels of Ca have a significant effect on gel creation. Low Ca levels normally led to N-A-S-H dominant gels, while high Ca indicated C-A-S-H dominant chains.
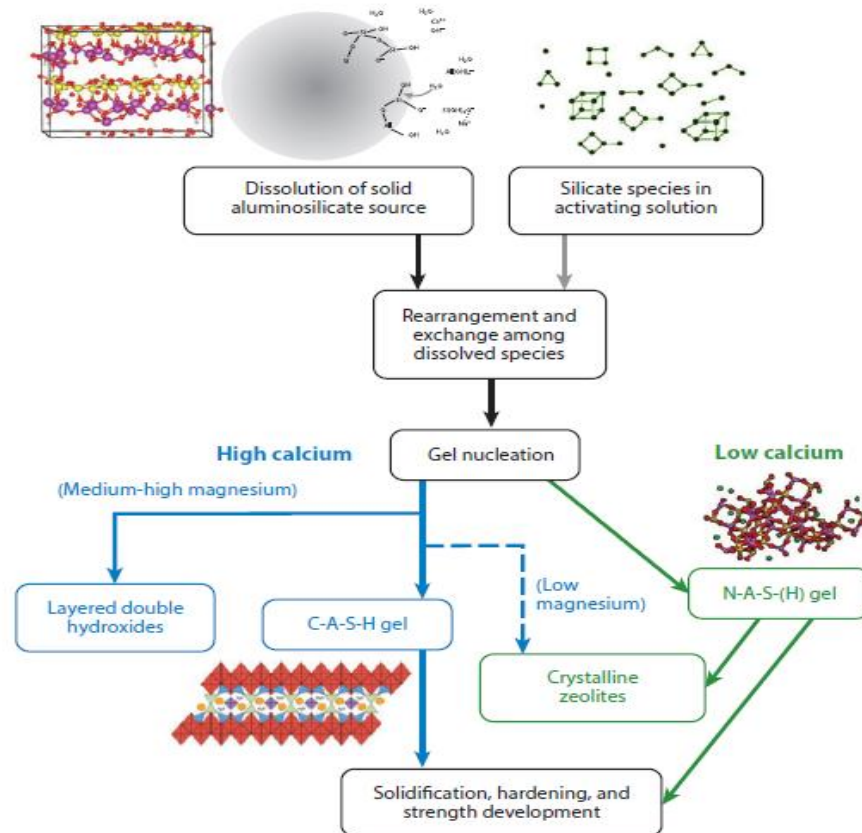
Figure 2-2: Geopolymer Phases for Gel Formation and Hardening
(Provis and Bernal, 2014)

Based on Provis and Bernal (2014), the underlying mechanisms for fly ash-based geopolymers and blended co-existence systems were the primary focus. The fly ash-based systems provided similarity to RBD geopolymers with low Ca contents. These geopolymer systems rely heavily on Al cross-bridging and N-A-S-H formations to provide strength properties. In addition, the blended systems were integral in understanding the

compatibility between C-A-S-H and N-A-S-H gels. A combination of fly ash and GGBFS allowed for an examination of these blended systems, pointing to hybrid gel existence, which was not well understood in the research.

Wang et al. (2019) also investigated fly ash-based geopolymers with a comparative review of alkali-activated geopolymers versus sulfate-activated geopolymers. Their review provided additional information on C-A-S-H and N-A-S-H gel production. The research indicated strength properties and dissolution rates for each gel, allowing for a better understanding of the underlying mechanisms. C-A-S-H gels formed first in fly ash-based geopolymers. The initial creation of C-A-S-H gels allowed for short-term strength to develop within the fly ash-based geopolymer. Next, N-A-S-H gels formed under a depleted Ca scenario, leading to increased strength in later stages.

Garcia-Lodeiro et al. (2011) applied a ternary diagram to help determine the Ca:Si:Al content levels needed for either N-A-S-H or C-A-S-H gel formation. They theorized that the SiO_2, calcium oxide (CaO), and Al_2O_3 contents of aluminosilicate and alkali activators combine to form random variations of C-S-H, C-A-S-H, and N-A-S-H gels. The ternary diagram, shown in Figure 2-3, was used to demonstrate C-A-S-H and N-A-S-H chain production. C-A-S-H gels formed with Ca around 50%, Si values below 50%, and Al contents lower than 15%. N-A-S-H gels precipitated with lower Ca and higher Si and Al contents.

In addition to the element molar ratios, the pH of the specimens played a significant role in gel formation. A high pH above 12 favored C-A-S-H gels as the Ca2+ ions decomposed the N-A-S-H gels and created additional C-A-S-H chains. At a pH below 12,

the N-A-S-H gels were predominantly stable only when the Ca sources were exhausted (Garcia-Lodeiro et al., 2011). This led to N-A-S-H gels being stalled at high pH during the initial polymerization phase.
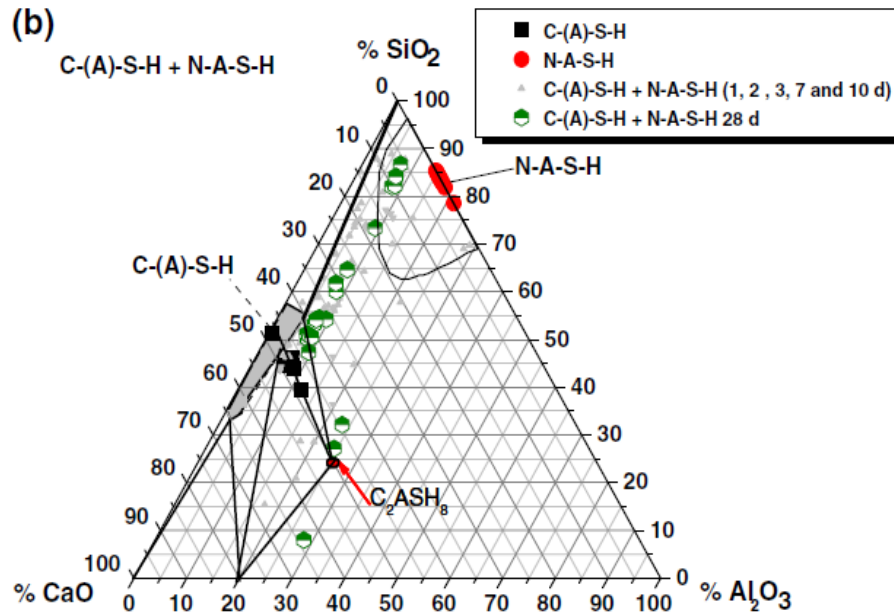
Figure 2-3: Ternary Diagram of C-A-S-H and N-A-S-H Gel Formation Based on CaO, SiO2, and Al2O3 Content Values (Garcia-Lodeiro et al., 2011)

This article addressed the compatibility of N-A-S-H and C-A-S-H gels and found a prioritizing order for C-A-S-H gels under the optimal ranges. As shown in Figure 2-4, there is also value in considering additional gel formations known as hybrid gels. Along with C-A-S-H and N-A-S-H zones, Garcia-Lodeiro et al. (2011) found areas where these two chains interlocked and created distinct (N, C)-A-S-H chains. They described the target ratios for this zone as the following: "The compositional range for Ca-modified (ion-exchanged) (C, N)-A-S-H gels is $0 < Na_2O/Al_2O_3 < 1.85$, $0 < CaO/SiO_2 < 0.3$, $0.05 <$

Al$_2$O$_3$/SiO$_2$ < 0.43". This provided molar ratios compatible with (N, C)-A-S-H gels and an ability to explore regions outside the Ancient Roman concrete ternary zones.
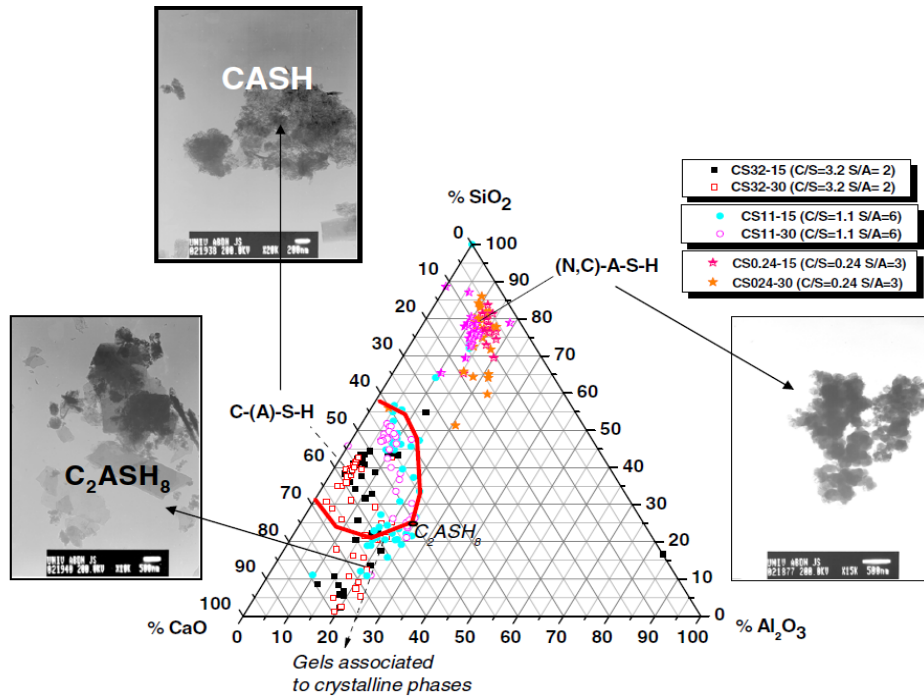
Figure 2-4: Ternary Diagram of C-A-S-H and (N, C)-A-S-H Formation Based on CaO, SiO$_2$, and Al$_2$O$_3$ Content Values (Garcia-Lodeiro et al., 2011)

Luo et al. (2023) further delved into the hybrid gel theory and discovered interesting results for (N, C)-A-S-H, Na-dominant gel, and (C, N)-A-S-H, Ca-dominant gel. As shown in Figure 2-5, their research was able to determine two distinct hybrid gels between the N-A-S-H and C-A-S-H regions. The premise was based on trying to prove the interference of Ca availability in the binder mechanisms. Their outcome became an explanation of hybrid gel behavior and how they interact instead of just Ca-based gel production.

This research found correlations between Ca availability, dissolution rate, and content ratios, leading to Ca being the determining factor in gel creation. They concluded that "with

a partial ion exchange between Na^+ and Ca^{2+}, a hybrid binder consisting of isolated C-(N)-A-(S)-H type gel and N-(C)-A-S-H type gel is resulted" (Luo et al., 2023). The two-hybrid gels increased strength development based on optimal Ca:Si:Al contents. Furthermore, gel interactions were finalized when an equilibrium state was established. This allowed for an exploration of multiple gels within the geopolymer mixture and further reinforced the need for compatibility understanding.
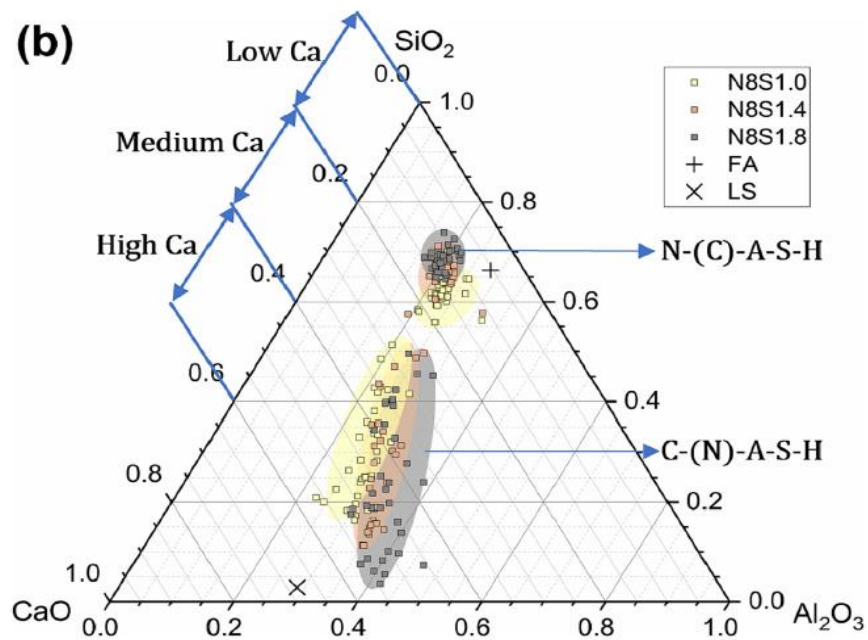
Figure 2-5: Ternary Diagram of Hybrid Gel Production Zones
(Luo et al., 2023)

With N-A-S-H, C-A-S-H, (N, C)-A-S-H, and gel compatibility explored, the final gel to uncover was the (C, N)-A-S-H gel. Walkley et al. (2016) focused on the C-A-S-H dominant region of the ternary diagrams and how (C, N)-A-S-H gels interact with N-A-S-H gels. They found that high Al levels and lower Ca levels led to the failure of the cross-

bridging feature. The C-A-S-H gels can only substitute a limited amount of Al before reaching an oversaturated state. The Ca contents needed to lower for the N-A-S-H gels to start up-taking the leftover Al present.

Figure 2-6 reveals a steep decrease in Al/Si molar ratios within the first 28 days of curing, followed by either a decline or an increase. The uptick in Al/Si molar ratios suggests the substitution of Si into the geopolymer framework. Moreover, high Al samples have prompted the formation of N-A-S-H gels, while N-A-S-H production has been constant under low Al ratios. Within a Ca-high and Ca-low environment, (C, N)-A-S-H formation persists until either Ca availability is too restricted, or Al can no longer bridge into C-A-S-H dominant zones.

In addition to understanding (C, N)-A-S-H zones, Walkley et al. (2016) provided ambient curing windows outside the 28-day threshold. This helped to reinforce the idea of geopolymerization occurring continually throughout their lifecycle. The geopolymerization process takes place over 48 hours for initial hardening, then 28 days for final hardening. However, there are processes still happening well into 180 days of curing, and further investigation is warranted.
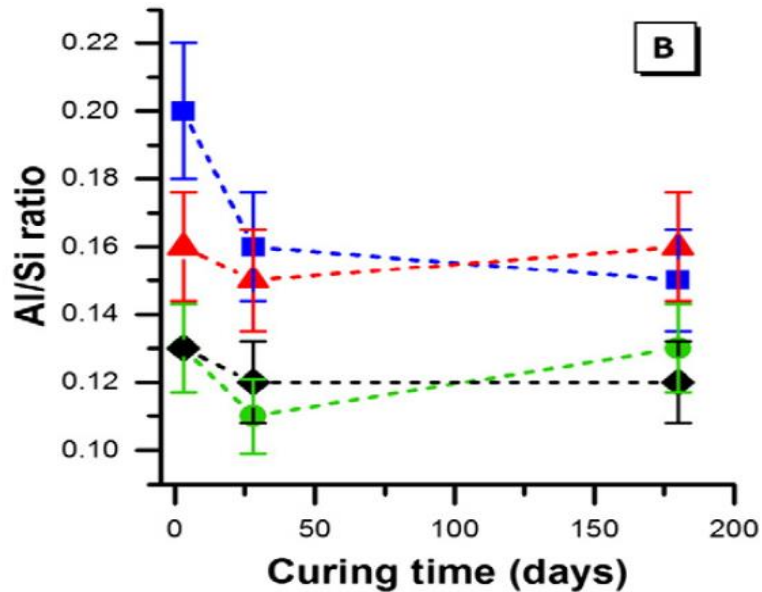
Figure 2-6: Al/Si Molar Ratios For 180 Day Ambient Curing Cycle
(Walkley et al., 2016)

2.3 Alkali Concentrations, Raw Materials, and Curing Techniques

Robayo-Salazar et al. (2016) studied samples produced with RBD, sand, NaOH, sodium silicate (Na_2SiO_3), and water. From these findings, sodium oxide (Na_2O)/SiO_2 ratios and the addition of OPC were the determining factors for achieving optimal compressive strength. By adding Na_2SiO_3 to raise the SiO_2/Al_2O_3 ratio of the material and the Na_2O/SiO_2 ratio of the alkali solution, the compressive strengths for each sample were analyzed based on Figure 2-7. Their results revealed that a Na_2O/SiO_2 ratio of 0.12 and a SiO_2/Al_2O_3 ratio of 6.6 yielded the samples' highest compressive strength.
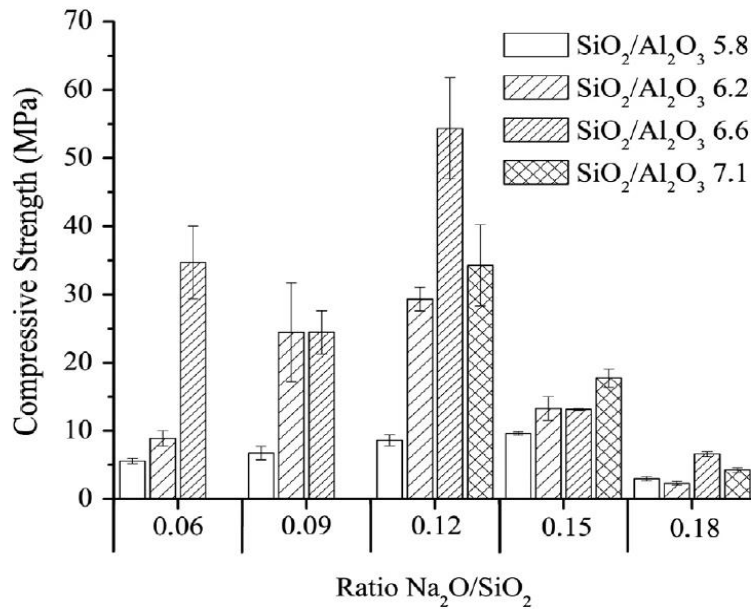
Figure 2-7: Bar Plot of SiO$_2$/Al$_2$O$_3$ Ratios Plotted With Compressive Strength (MPa) vs. Na$_2$O/SiO$_2$ Ratios (Robayo-Salazar et al., 2016)

Next, the RBD geopolymers were modified with 0% to 20% OPC substitution by weight, which enhanced the strength of the RBD geopolymers that were batched with NaOH and Na$_2$SiO$_3$, shown in Figure 2-8. The 20% OPC by weight and Na$_2$SiO$_3$ sample produced the highest compressive strength at ambient temperature (25°C) and a Na$_2$O/SiO$_2$ ratio of 0.12 (Robayo-Salazar et al., 2016). These results show how the geopolymerization process can be manipulated to further the aluminosilicate reactions.
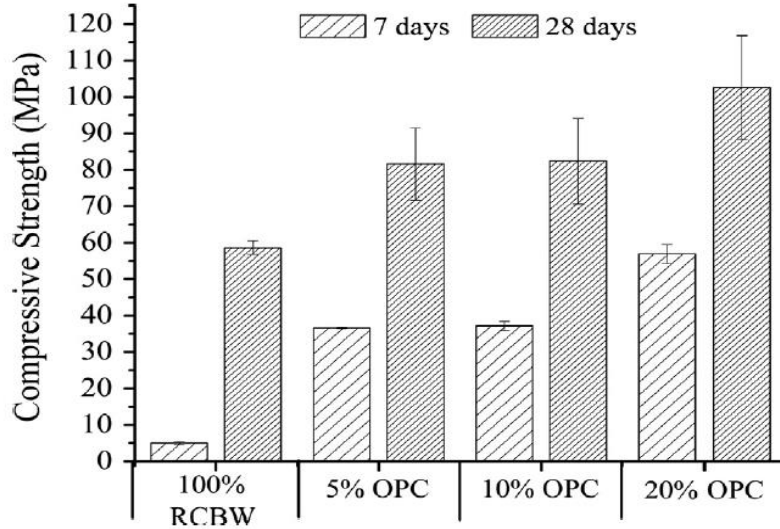
Figure 2-8: Bar Plot of OPC Addition Plotted With Compressive Strength (MPa) vs. Sample (Robayo-Salazar et al., 2016)

As Robayo-Salazar et al. (2016) mentioned, finding the ratios of NaOH to Na_2SiO_3 is an important step toward optimal strength development. Youssef et al. (2019) conducted a study that examined the Na_2SiO_3/NaOH ratios for GGBFS and ground waste brick (GWB) geopolymers. Their study focused on the mechanical properties of 100% GWB with 0% GGBFS by weight, then continued through each iteration up to 0% GWB with 100% GGBFS by weight. The 80/20 (GGBFS/GWB) geopolymer was selected, and testing continued using this sample and a range of Na_2SiO_3/NaOH ratios from 1.5 to 3 by weight, shown in Figure 2-9.
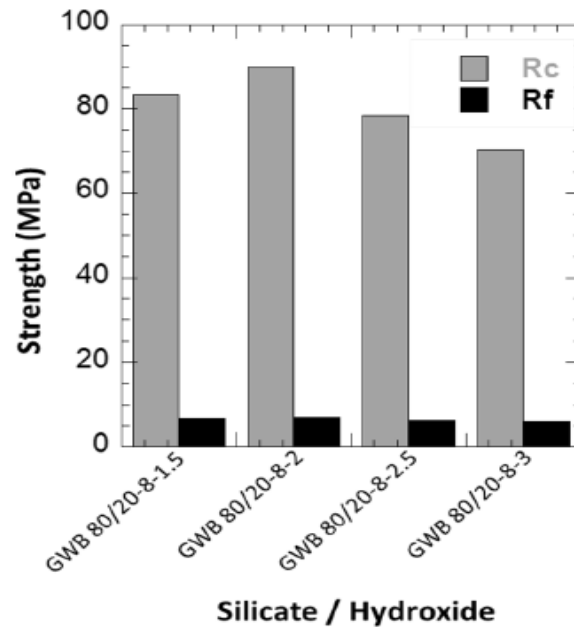
Figure 2-9: Bar Plot of R_c (Compression) and R_f (Flexure) Strength (MPa) Against Na_2SiO_3/NaOH ratios (Youssef et al., 2019)

The compressive strength was maximized at 90 MPa (13,050 psi) with a Na_2SiO_3/NaOH ratio of 2.0. Increasing the Na_2SiO_3/NaOH ratio above 2.0 decreased compressive strength values due to the oversaturation of Na^+ ions. Decreasing the Na_2SiO_3/NaOH ratio below 2.0 resulted in a lack of OH^- ions, which are needed for the dissolution of the aluminosilicates (Youssef et al., 2019). These findings show the need for balancing the Na_2SiO_3/NaOH ratio and are crucial for predicting boundaries for RBD geopolymer mix designs.

Firdous and Stephan (2019) examined the SiO_2/Na_2O ratios and investigated a novel composite index, the silica modulus. The authors explored this silica modulus as the controlling variable in determining the optimum strength of pozzolan-based geopolymers. The compressive strength vs. silica modulus curves, displayed in Figure 2-10, indicated a

21

variation in peaks and slopes depending on the materials tested and the specific silica modulus. This study reveals that a range of NaOH concentrations can alter both the heights and gradients of the silica modulus curve. Generally, a silica modulus value of 0.6 falls within an increasing gradient, while a value of 1.1 is situated within a decreasing gradient (Firdous and Stephan, 2019). These results can be used to dictate the outer ranges for the silica modulus curve, yet this data only applies to natural pozzolan-based geopolymers.
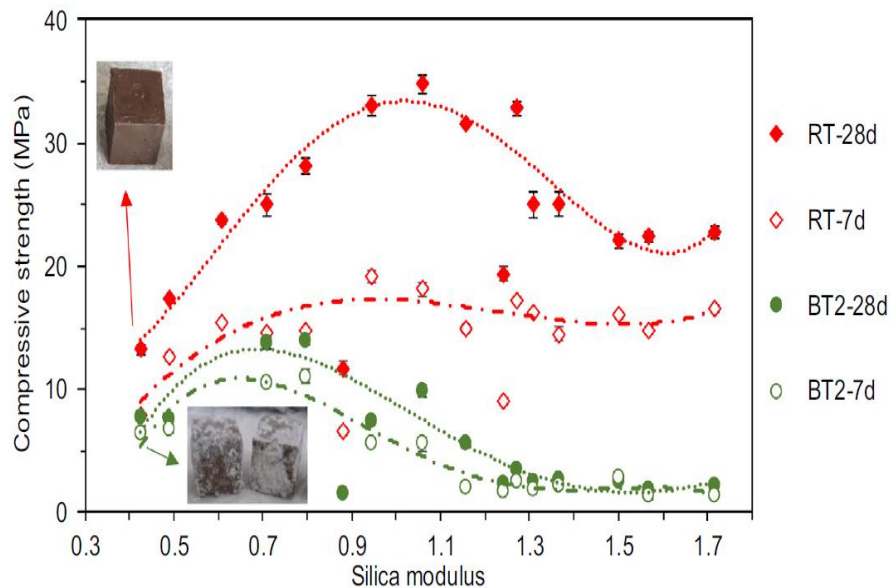
Figure 2-10: Compressive Strength (MPa) of Pozzolan-Based Geopolymers vs. Silica Modulus (SiO$_2$/Na$_2$O) (Firdous and Stephan, 2019)

Zhang et al. (2012) advanced silica modulus research with compressive strength and calorimetry analysis of alkali-activated metakaolin. Their findings uncovered correlations between heat peaks and solution dissolution and hardening phases, as well as confirming an upper limit for silica modulus for initial strength development. Figure 2-11 shows the compressive strengths for each silica modulus, and Figure 2-12 highlights dissolution by a

marked initial thermal spike, followed by polymerization and hardening, which register a secondary heat evolution. Temperatures and silica modulus offer another avenue for geopolymer optimization and serve to improve the quality of the RBD geopolymer mixture.

The silica modulus increase led to a decrease in compressive strengths, as manifested by lower secondary calorimetry peaks. According to their research, compressive strengths can be optimized through a prolonged initial heat spike, while weaker secondary peaks indicate decreased strength characteristics. There appears to be a correlation between increased initial peak maximums and more effective strength development. However, high-energy initial peaks often result in inadequate hardening and polymerization, resulting in weakened specimens. Conversely, when a well-developed secondary heat evolution occurs, the strength characteristics are usually enhanced. These theories can be applied to RBD geopolymer systems and improve understanding of alkali concentrations.
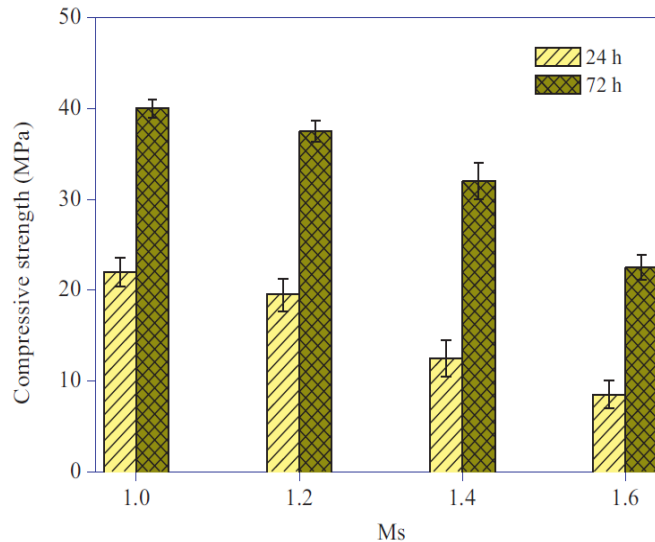
Figure 2-11: Bar Plot of Compressive Strengths Versus Silica Modulus (Zhang et al., 2012)
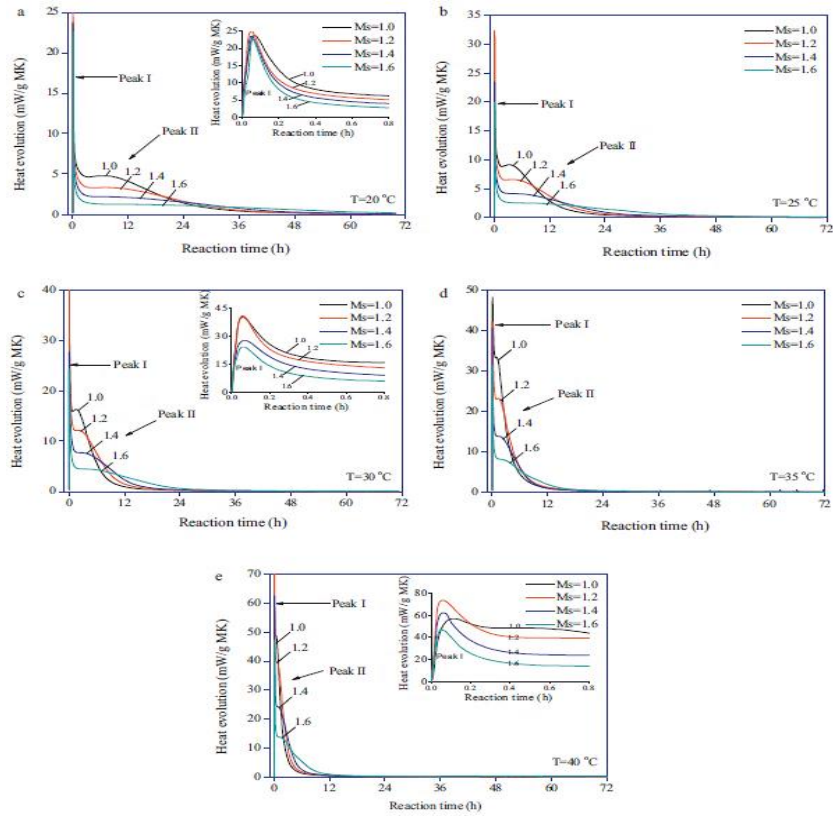
Figure 2-12: Calorimetry Results for Specimens Undergoing Increased Temperature from 20 °C (a) to 40 °C (e) (Zhang et al., 2012)

Low-reactive aluminosilicate materials, like RBD, need additional minerals to produce desired mechanical behaviors that match or exceed OPC. One such compound is calcite (CaCO$_3$), found naturally in limestone. Kalinkin et al. (2020) found that the addition of CaCO$_3$, ranging from 0% to 10% by weight, gradually increased the compressive strength of fly-ash based geopolymers. Their paper claims this additional strength is attributed to CaCO$_3$, which becomes "…the centers of the formation of the sodium containing aluminosilicate hydrate gel - the main cementing phase of the geopolymer." This seeding effect offers a promising mechanism for increasing the compressive strength of geopolymers. Research utilizing the seeding effect on low-reactive aluminosilicate

24

materials, such as RBD, is currently limited. Further exploration is needed before $CaCO_3$ can be used in any geopolymer matrix with percentages above 10% substitution by weight.

These seeding effects are not limited to $CaCO_3$. Temuujin et al. (2009) investigated the addition of quicklime (CaO) and hydrated lime ($Ca(OH)_2$) to fly ash-based geopolymers. Their results showed that ambient-cured specimens benefited from the addition of both compounds, while oven-cured specimens tended to lose strength. This paper also noted the possibility that $Ca(OH)_2$ is more beneficial than CaO due to mechanisms that allow for the further dissolution of the aluminosilicate material. This study only investigated 1% to 3% substitution of CaO by weight and 1.3% to 3.9% substitution of $Ca(OH)_2$ by weight. Investigation of $Ca(OH)_2$ beyond these thresholds should proceed with caution. The cost of the materials will need to be weighed against the overall benefits.

The final compound of interest for this RBD research is Al_2O_3. Tchakoute et al. (2012) demonstrated that the substitution of Al_2O_3 in volcanic ash-based geopolymers can lead to moderate increases in compressive strength, while the metakaolin counterparts experienced a reduction in compressive strength. The authors postulated that this was due to the low Al_2O_3 content of 15.41% in the volcanic ash, which allowed for a greater increase in Al_2O_3 compared to the high Al_2O_3 content of 40.48% in the metakaolin. This article provides a chemical breakdown of the volcanic ash that closely mimics that of RBD and utilizes an Al_2O_3 range of 0% to 40% substitution by weight. As such, this can be used with Robayo-Salazar et al. (2016) to apply a range of Al_2O_3 to RBD geopolymers.

Beyond the Na_2SiO_3/NaOH ratio, silica modulus, and material selection, the compressive strength of geopolymers is also affected by the curing method (Davidovits,

2020). Nurruddin et al. (2018) reviewed current research on curing geopolymers and found that oven curing offers higher compressive strength than ambient curing. Although the mechanisms responsible for this higher strength are unknown, this review points to changes in geopolymerization due to the different catalyst temperatures. Oven curing temperatures can vary from 60°C to 140°C, and time can change from 4 hours to 24 hours. One of the reasons for the range of temperatures and timing was the loss of water at a rapid rate. An improper oven-curing protocol led to the unwanted evaporation of water molecules needed to advance the geopolymerization process (Nurruddin et al., 2018). Oven-based curing was reported as the most effective curing method, yet ambient-cured geopolymers should be investigated for loss of water issues and strength development.

Finally, an environmental analysis was needed to determine the efficacy of optimizing RBD geopolymers, as an OPC alternative would need to be less polluting. Robayo-Salazar et al. (2017) conducted an environmental impact assessment to ascertain the least polluting compound among various alkali-activators and OPC additions. Their findings showed that OPC exhibited almost 50% higher CO_2 emissions than red clay brick waste (RCBW) geopolymers. A better indication of performance and emissions was potential global warming ($KgCO_{2eq}$) normalized by compressive strength (MPa), shown in Figure 2-13.
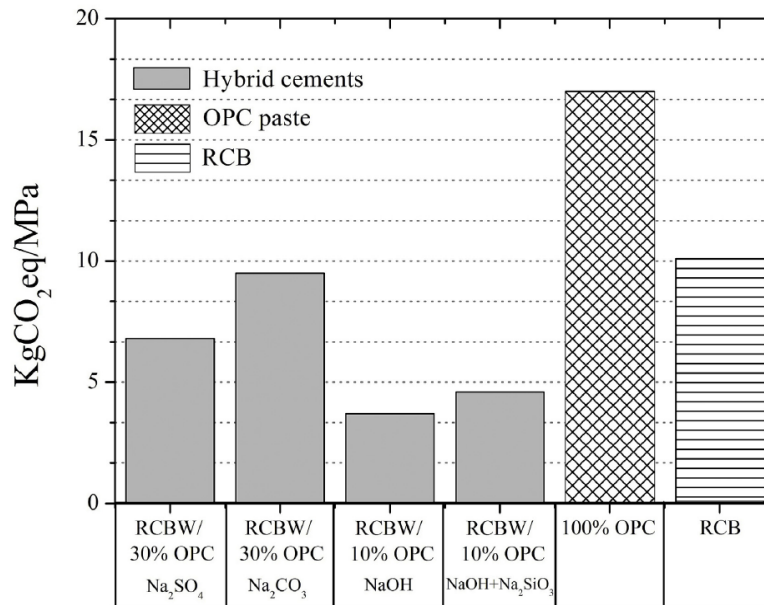
Figure 2-13: Bar Plot of Global Warming Potential (KgCO$_{2eq}$) Normalized by Compressive Strength (MPa) vs. RCBW Variants (Robayo-Salazar et al., 2017)

These results focused on RBD geopolymers activated with NaOH, Na$_2$SiO$_3$, sodium sulfate (Na$_2$SiO$_4$), or sodium carbonate (Na$_2$CO$_3$). NaOH and Na$_2$SiO$_3$-based RCBW geopolymer with 0% OPC by weight was labeled RCB, and the KgCO$_{2eq}$/MPa for RCB was 37.5% more efficient than OPC (Robayo-Salazar et al., 2017). The RCBW geopolymer with 10% OPC substitution by weight and activated with NaOH and Na$_2$SiO$_3$ showed better results due to the increased strength development. The 10% OPC drastically raised the compressive strength, which decreased the overall KgCO$_{2eq}$/MPa. However, OPC should be avoided, and other sources of calcium still need to be investigated.

Chapter 3: RBD Geopolymer Optimization

Optimization of the RBD geopolymer was essential for the successful completion of the first stage of research. Using the processed RBD, the initial series of tests focused on evaluating various alkali activators for maximum compressive strength, followed by trials with $Ca(OH)_2$, powdered limestone, and alumina addition. The same source was used for each raw material throughout the experiments, and deviations from the prescribed procedure were kept to a minimum. The molar and percentage ratios were determined according to the molar values and weight respectively, unless stated otherwise.

3.1 Materials and Methods

3.1.1 Materials Background

The RBD acquisition began with the use of an industrial-size ball mill. The ball mill pulverized the bricks into usable RBD. The unfiltered RBD was placed in a #40 sieve and processed to remove organic debris and detritus. The processed RBD was placed into an oven set at $235^{o}F$ for at least 24 hours. This step ensured proper moisture removal using ASTM Standard C566 (2019). A handheld X-ray fluorescence (HHXRF) machine was used on the finished RBD to acquire the chemical composition of the representative sample. Table 3-1 shows the chemical composition of the powdered RBD. Existing molar ratios were determined based on the weight percentages provided by the XRF report. Initial molar ratios were calculated to be the following: $Ca/Si = 0.07$, $Ca/(Al+ Si) = 0.06$, $Al_2O_3/CaO = 1.65$, $SiO_2/Al_2O_3 = 8.15$, and $Na_2O/SiO_2 = 0.07$.

Table 3-1: Chemical Composition of Processed RBD

Mineral	Sample Value (ppm)	Percent of Whole
SiO_2	141497	48.9
Al_2O_3	29456	10.2
CaO	9840	3.3
Fe_2O_3	58439	20.2
MgO	0	0.0
MnO	496	0.2
Na_2O	9441	3.2
K_2O	11534	4.0
Trace Minerals	29017	10.0
Total	289720	100.00

To improve the performance of the RBD geopolymer, two sets of parameters, shown in Table 3-2 and Table 3-3, were investigated based on the addition of OPC, GGBFS, or fly ash as additives (Robayo-Salazar et al., 2016; Youssef et al., 2019; Taylor, 1986; Richardson and Groves, 1993; Jackson et al., 2013; Jackson et al. 2017; Provis and Bernal, 2014: Luo et al., 2023; Garcia-Lodeiro et al., 2011). Instead of utilizing heavily reactive cementitious materials, this research aimed to enhance the strength of the RBD by controlling the base components silica, alumina, and calcium. The calcium sources utilized incorporated powdered limestone and $Ca(OH)_2$. The powdered limestone was Duda Energy Food Grade 97% Calcium Carbonate from ground limestone, and the $Ca(OH)_2$ was HiMedia Calcium Hydroxide, Purified.

Table 3-2: Target Molar Ratios (Set 1)

Target Ratio	Target Value
Ca/Si Molar Ratio	0.8-1.2
Ca/(Si+Al) Molar Ratio	0.74-0.90
SiO_2/Al_2O_3 Molar Ratio (Alkali & RBD)	5.80-6.50
Al_2O_3/CaO Molar Ratio	0.15-0.25
Al_2O_3/SiO_2 Molar Ratio (All Components)	Max = 0.43
Na_2O/Al_2O_3 Molar Ratio	Max = 1.85
Na_2O/SiO_2 Molar Ratio	0.10-0.13

Table 3-3: Ternary Limits for Ratios (Set 2)

Target Ratio	Target Value
% CaO for Solution, Ternary Diagram Limits	30%-45%
% SiO_2 For Solution, Ternary Diagram Limits	40%-55%
% Al_2O_3 For Solution, Ternary Diagram Limits	10%-25%
% Na_2O For Solution, Ternary Diagram Limits	Max = 15%

NaOH sourced from Belle Chemical's Sodium Hydroxide - Pure - Food Grade was employed as the primary alkali activator. Robayo-Salazar et al. (2016) and Youssef et al. (2019) reported that the incorporation of NaOH plus Na_2SiO_3 as alkali activators could result in enhanced strength properties to the geopolymer matrix of cementitious materials. Optimal mix ratios for both activators are provided in Table 3-4. The Na_2SiO_3, in the form of "water glass," a commercial sodium silicate, was assumed to have an average chemical composition of 10% Na_2O, 30% Hydrated Na_2SiO_3, and 60% Water.

Table 3-4: Optimized Alkali Concentrations

Target Ratio	Target Value
Na_2SiO_3/NaOH Ratio (by wt.)	2.0 - 3.0
NaOH Molarity (M)	6M - 7M
Na_2O % Concentration (by wt.)	7% - 10%

3.1.2 Experimental Procedure

Using a known chemical profile, the first step of the research focused on verifying the alkali concentrations of the activators. Previous studies revealed a range of NaOH and Na_2SiO_3 concentrations that were sufficient to commence dissolution of the aluminosilicate species (Robayo-Salazar et al., 2016; Youssef et al., 2019). NaOH was dissolved in water within glass jars with molarity (M) of the NaOH set at 5M, 7M, and 9M. As there is no standard, 24 hours of dissolution was considered suitable for homogeneity and heat dispersion during the reaction. The dissolved NaOH was added first, followed by the "water glass" at a ratio of 2.0, 2.5, and 3.81 Na_2SiO_3/NaOH by weight.

Before the blending of RBD and liquid materials, following ASTM Standard C305 (2020), the dry materials were mixed for 3 mins to help evenly distribute the components. To ensure a liquid/solids (L/S) ratio of 0.35, the available amount of water in the "water glass" was set as the baseline, and the remaining quantity was added accordingly. This L/S ratio was increased to 0.35 from 0.25 due to potential workability issues from the addition of $CaCO_3$ (Robayo-Salazar et al., 2016). After 3 mins of mixing, 2 mins of setting, and 2 more mins of mixing, the RBD geopolymer was formed into 2"x2" mortar cube molds and tamped in keeping with ASTM Standard C305 (2020).

After casting, two specimens per series were subjected to 28 days of ambient curing or 24 hours of oven curing at 150˚F (Nurruddin et al., 2018). Subsequently, the oven-cured samples were checked for strength characteristics against the ambient-cured samples after resting for 24 hours at room temperature. Ambient-cured samples were kept in sealed containers to prevent excess water loss, while oven-cured samples were unable to be

accommodated. Water loss can be an issue during both curing conditions, leading to water on the surface of ambient-cured samples and microcracks in oven-cured samples. Uniaxial compressive tests were conducted using ASTM Standard C109/C109M (2021), while calorimeter testing followed ASTM Standard C1753/C1753M (2021).

After conducting tests to evaluate the SiO_2/Al_2O_3 molar ratio, Na_2O/SiO_2 molar ratio, and molarity of NaOH, a representative sample was chosen based on the highest compressive strength and calorimeter heat evolution reports. A contribution diagram, shown in Figure 3-1, was used to select the target values and included the following: NaOH content for Na_2O values in Na_2O/SiO_2, Na_2SiO_3 content for SiO_2 values in SiO_2/Al_2O_3, and moles of NaOH/liter of H_2O for NaOH molarity. The same procedures from the previous stage were implemented with updated values based on the results, and then Ca, Si, and Al contents were analyzed based on prior research to obtain new target ratios (Taylor, 1986; Richardson and Groves, 1993; Jackson et al., 2013; Jackson et al. 2017).

Methodology
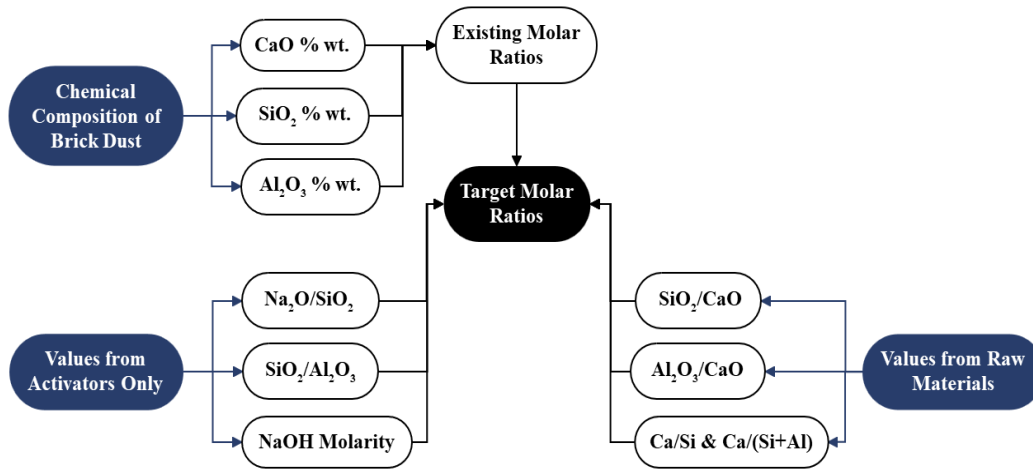
Figure 3-1: Method Flowchart for Determining Molar Ratio Contributions

The initial phases of the study focused on establishing the molar ratios of CaO/SiO_2, $CaO/(Al_2O_3+SiO_2)$, Al_2O_3/CaO and SiO_2/Al_2O_3 for the entire geopolymer system rather than only the activators and precursor materials. Each phase added a single raw material, with $Ca(OH)_2$ added initially to regulate Ca levels before replacing it with powdered limestone when the $Ca(OH)_2$ reached 6% substitution by weight (Temuujin et al., 2009). Subsequent phases further increased the substitution rate of the powdered limestone, beginning with 12% and ending with 36% (Kalinkin et al., 2020). The final phase adjusted the Al_2O_3 levels by adding ground alumina in 5% substitutions by weight that were increased to 15% (Tchakoute et al., 2012). Before introducing the alkaline liquids for each phase, the solids were mechanically mixed to achieve equal distribution throughout the RBD geopolymer mixture. Evaluation of the mixtures was done according to ASTM

Standard C305 (2020) and ASTM Standard C109/C109M (2021) using 2"x2" mortar cubes.

Representative samples were collected and tested in each step of the process until a final selection of RBD geopolymer mix designs was completed, with the outcome based on the compressive strength of the samples. A further batching phase was conducted to assess 5M NaOH and Na_2SiO_3/NaOH (by wt.) of 2.0, 5M NaOH and Na_2SiO_3/NaOH (by wt.) of 2.5, and 7M NaOH and Na_2SiO_3/NaOH (by wt.) of 2.0. Additionally, an evaluation of ground alumina versus fine alumina was undertaken to determine the best particle size for Al_2O_3 components. The last phase of the 2"x2" mortar cubes concluded with the completion of the alumina comparison. Representative samples were identified, and the results were examined for use in an upscaled 3"x6" cylinder category.

Casting and testing of 3"x6" cylinders occurred for nine samples selected from the 2"x2" mortar series. The samples were chosen based on the highest compressive strength, and calorimetry reports were used to examine hardening and polymerization trends. Cross-referencing with existing research allowed for data analysis, and a compression zone was determined using ternary diagrams and new target ratios (Provis and Bernal, 2014; Luo et al., 2023; Garcia-Lodeiro et al., 2011). The new mix designs were utilized for the 3"x6" cylinders and were based on the same procedure for mixing RBD components, described in the 2"x2" mortar section.

The batching and tamping of cylinders followed the ASTM Standard C192/C192M (2019). For each batch, three specimens were created for 7-day strength, 28-day strength, and oven-cured strength, resulting in nine samples per mix. Uniaxial compression tests

were conducted for each cylinder series and conformed to ASTM Standard C39/C39M (2021), while calorimetry tests followed ASTM Standard C1753/C1753M (2021). For all 3"x6"cylinders, the following parameters were applied: a grinding machine was used to provide a clean surface before compression tests, length-to-diameter tolerances were checked for size factors, the oven-cured samples were kept inside molds during curing (to prevent microcracks and provide confinement), and ambient-cured samples were placed in sealed containers after de-molding (to avoid excess water loss).

3.2 Results & Analysis

3.2.1 Compressive Strength

Compressive strength is a key characteristic for judging and utilizing concrete and other cementitious materials. It is an essential consideration in the construction industry, used to assess quality and reliability. OPC strength usually falls between 3000 psi and 5000 psi, which serves as the target zone for strength development. Figure 3-2 indicates the compressive strength from specimens created with just NaOH and Na_2SiO_3 as activators. The ambient-cured RBD geopolymer labeled 5M NaOH-2.0 attained a maximum compressive strength of 260 psi, whereas the oven-cured 5M NaOH-2.5 mixture reached a peak of 2420 psi. The 5M NaOH-2.0 label meant that the molarity of NaOH and Na_2SiO_3/NaOH weight ratio was set to 5M and 2.0, respectively. This labeling system was applied to each category and used throughout the rest of this research; for example, 5M NaOH-2.5 signified 5M NaOH molarity and 2.5 Na_2SiO_3/NaOH by weight.
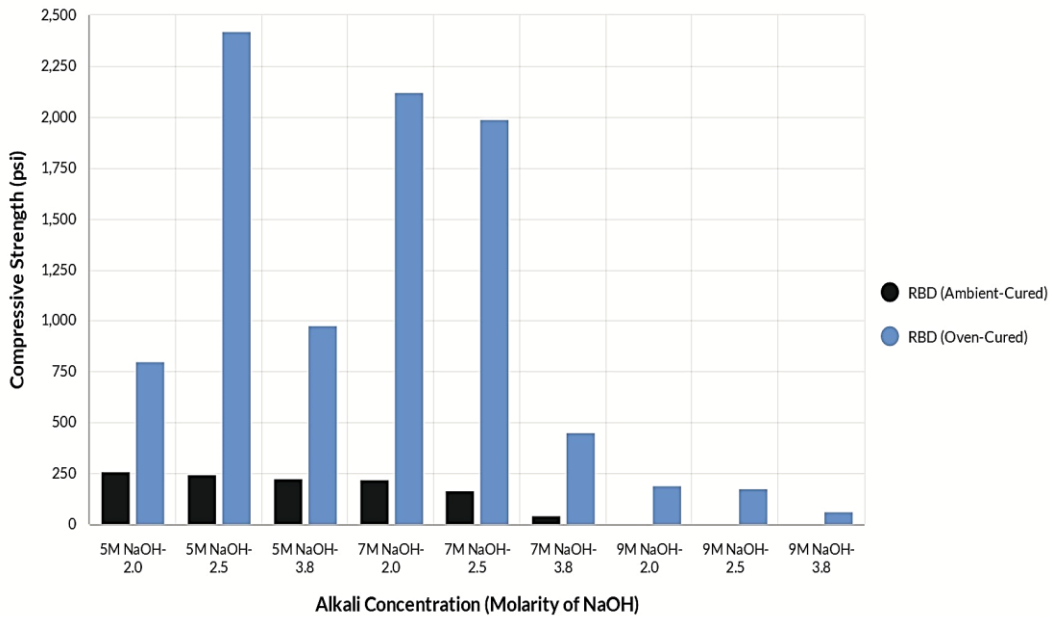
Figure 3-2: Compressive Strength Results for Alkali Only RBD Geopolymer

Robayo-Salazar et al. (2016) and Youssef et al. (2019) reported that for dissolution of an aluminosilicate to occur, an optimal alkali concentration is essential. Excessive alkali concentrations led to salt bleeding and decreased compressive strength, while inadequate concentrations of alkali activators did not suffice to break down the aluminosilicates and initiate dissolution. Therefore, 5M, 7M and 9M NaOH solutions, along with Na_2SiO_3/NaOH of 2.0, 2.5, and 3.81 by weight, were used to remain within this optimum range. Combined with the experimental data, another filter was placed on the alkali activators and the highest compressive strength for ambient-cured samples was found within the following ranges: 5M-7M for NaOH molarity and 2.0-2.5 Na_2SiO_3/NaOH by weight.

The oven-cured samples of 5M NaOH-2.0, 5M NaOH-2.5, 7M NaOH-2.0, and 7M NaOH-2.5 demonstrated an elevated compressive strength threshold. Oven-cured

specimens enabled accelerated RBD geopolymerization and are speculated to have distinct bonding mechanisms compared to the ambient-cured specimens with similar chemical compositions (Robayo-Salazar et al., 2016; Nurruddin et al., 2018). The aim is to reach the same levels as the oven-cured specimens with ambient-cured ones. When these two values substantially deviate, the ambient-cured version may be inhibited due to drying conditions or excessive components. Oven curing supplies additional heat that allows for accelerated polymerization reactions and faster development of strength.

The optimal alkali activator zone was determined using the existing categories; however, 9M NaOH-2.5 was added to guarantee oversaturation. Consequently, the next research phase incorporated five concentrations of the alkali activator: 5M NaOH-2.0, 5M NaOH-2.5, 7M NaOH-2.0, 7M NaOH-2.5, and 9M NaOH-2.5. Three series were tested using the same activators and labeled as the following: hydrated lime series, hydrated lime and limestone series, and hydrated lime, limestone, and alumina series. The RBD geopolymers were separated into three parts to provide a checkpoint toward target ratios. The compressive strengths were evaluated after each series for trends or stagnation.

As shown in Figure 3-3, the addition of hydrated lime to the series yielded a marked increase in strength. The highest compressive strengths were found for ambient-cured 5M NaOH-2.0 and 5M NaOH-2.5 with 6% hydrated lime substitution. The 5M NaOH-2.0 sample had a compressive strength of 2350 psi, and the 5M NaOH-2.5 was 1910 psi. This exceeds Temuujin et al. (2009) suggested limit of 3% hydrated lime substitution for an improved compressive strength. Additional strength properties were achieved for samples containing 2%, 4%, and 6% hydrated lime by substitution without a limit. Calcium

saturation, through hydrated lime, has shown improvement through the 6% substitution window and could be useful for pushing calcium limits during cylinder production.
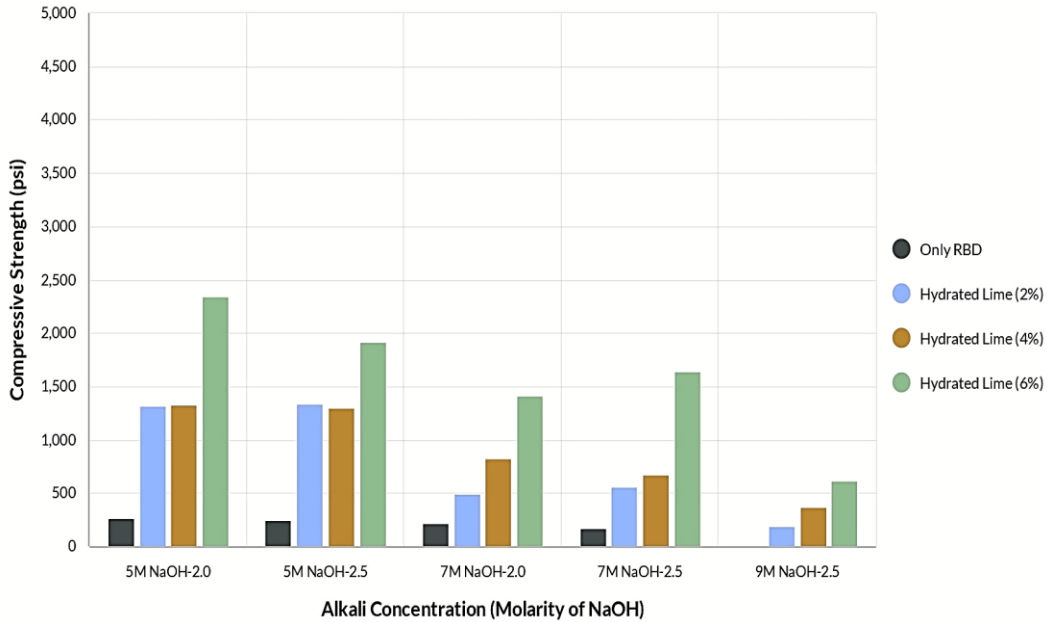
Figure 3-3: Compressive Strength Results for Ambient-Cured RBD Geopolymer With Hydrated Lime Added

Figure 3-4 shows the 6% hydrated lime added by weight for the ambient-cured specimens compared against the oven-cured versions. The highest compressive strength for the ambient-cured model was 2350 psi with sample 5M NaOH-2.0, while the oven-cured model boasted 3160 psi. Also, the 5M NaOH-2.5 category produced samples with an ambient-cured compressive strength of 1910 psi and oven-cured strength of 2730 psi. The hydrated lime model generated closer results to those of the oven-cured samples, resulting in a higher average compressive strength than the alkali-only approach. When the

ambient-cured strengths corresponded to or exceeded those from oven-cured samples, the chosen model can be considered optimized and then used for further evaluations.
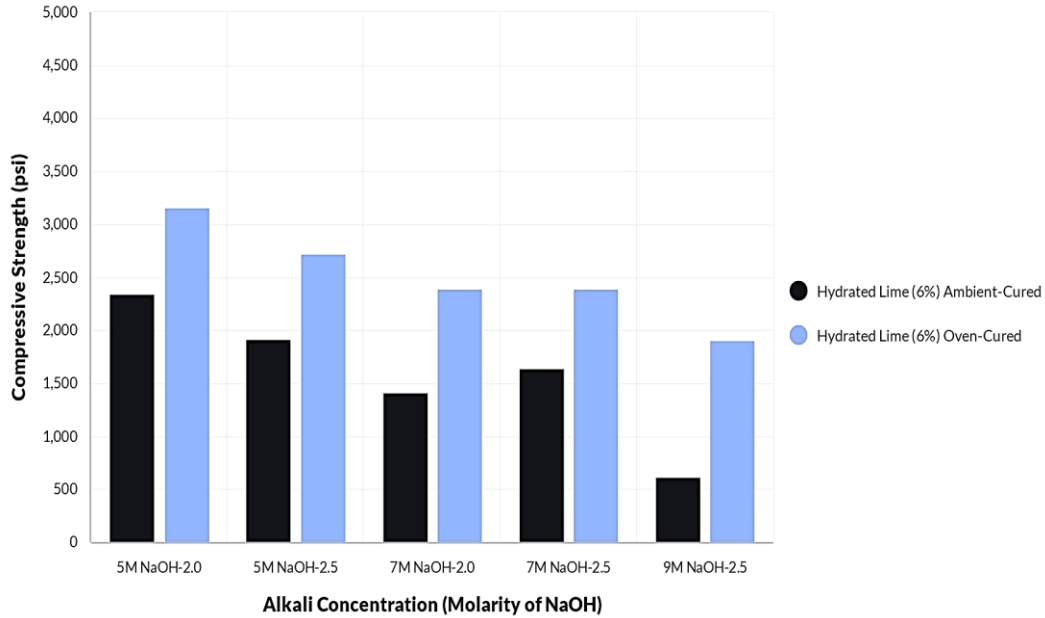
Figure 3-4: Compressive Strength Results for RBD Geopolymer with 6% Hydrated Lime Added and Both Curing Methods

The compressive strength continued to increase with the addition of powdered limestone to the RBD geopolymer matrix. The highest compressive strength for the ambient-cured specimens was seen between 5M NaOH-2.5 and 7M NaOH-2.0 with 12% limestone by weight, shown in Figure 3-5. The maximum compressive strength achieved was 4490 psi for the 5M NaOH-2.5 sample. However, beyond 12% limestone, it had a detrimental effect on the compressive strength. The high target ratio for Ca/Si necessitated limestone series be structured with 12%, 24%, and 36% substitution by weight.
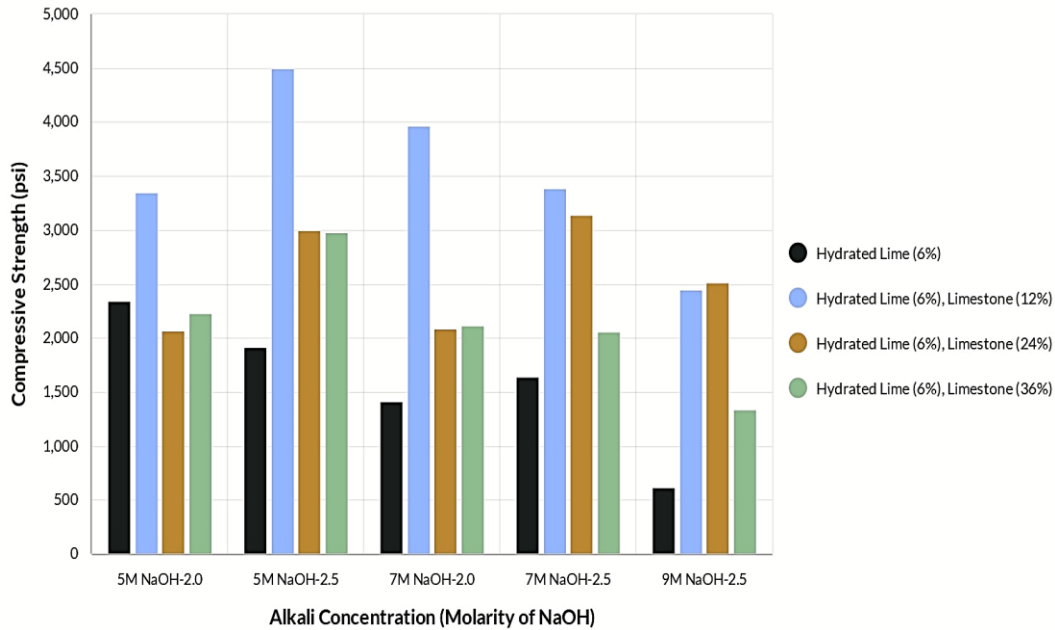
Figure 3-5: Compressive Strength Results for Ambient-Cured RBD Geopolymer with 6% Hydrated Lime and Limestone Added

Based on the compressive strengths in the ambient-cured model, 12% limestone was selected for comparison between the ambient-cured and oven-cured samples. Figure 3-6 depicts 12% limestone added by weight for the ambient-cured specimens against the oven-cured specimens. The highest compressive strength for the ambient-cured model was 4490 psi for the 5M NaOH-2.5 sample. For the oven-cured model, 3640 psi was the highest value under the 7M NaOH-2.5 sample. The hydrated lime and limestone model displayed higher compressive strengths in the ambient-cured samples compared to the oven-cured samples and an overall higher compressive strength than the hydrated lime model.
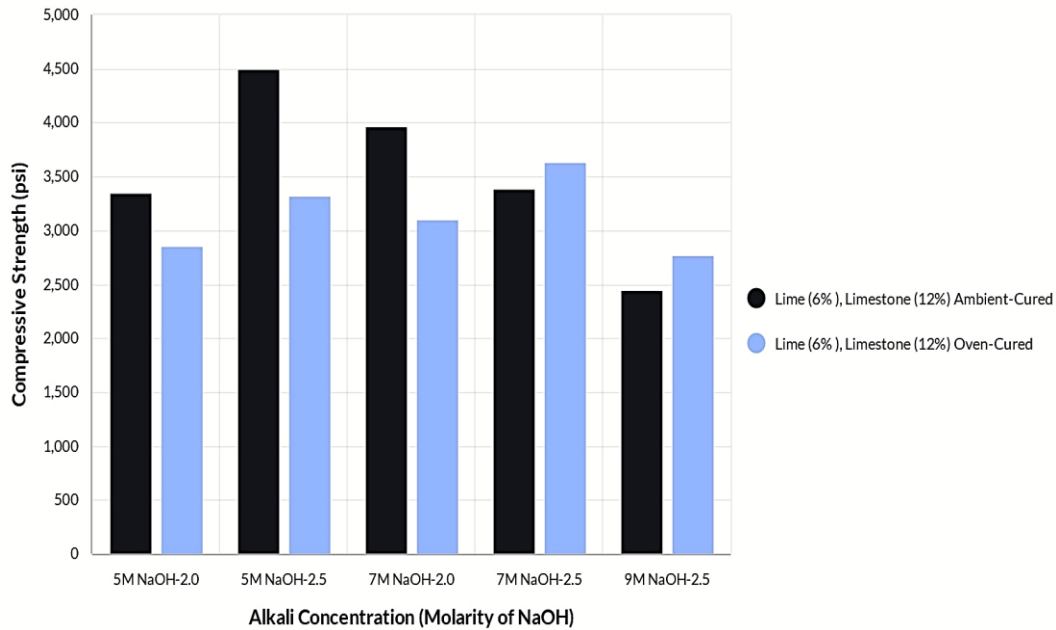
Figure 3-6: Compressive Strength Results for RBD Geopolymer with 12% Limestone Added and Both Curing Methods

The ambient-cured specimens should be verified against their oven-cured counterparts to determine if the limestone series experienced oversaturation of the RBD geopolymer components. For the 12% limestone series, the ambient-cured model surpassed the oven-cured samples for 5M NaOH-2.0, 5M NaOH-2.5, and 7M NaOH-2.0. This mirrored the research of Kalinkin et al. (2020). Kalinkin et al. (2020) investigated powdered limestone incorporation up to a limit of 10%, observing increased compressive strengths across all specimens. It was argued that limestone assists in generating C-A-S-H gels and provides a seeding function for the gels to accumulate. Nonetheless, overabundant limestone concentrations can result in substandard strength performance due to the unutilized filler material, which was noticeable in both curing procedures.

The final phase of the experiment involved combining alumina with 36% powdered limestone and 6% hydrated lime. The compressive strength decreased because of excessive powdered limestone, which adversely impacted the performance of the samples within the limestone series. The low compressive strength was caused by unutilized components in the geopolymer matrix. The powdered limestone could not be fully converted to Ca^{+2} ions and start the seeding process. This prevented the chemical process from proceeding and stagnated the solution. The added alumina works to bridge interlocking calcium layers within C-A-S-H gels or sodium layers in N-A-S-H gels. The aim is to provide additional reaction capacity through bridging of unreacted calcium sources.

The 5M NaOH-2.5 and 7M NaOH-2.0 zones with 0%-10% alumina by weight showed the greatest compressive strength, as shown in Figure 3-7, with the highest being 2980 psi for the 5M NaOH-2.5 with 0% alumina. The second highest was 2640 psi for the same series with 10% alumina. A decrease was detected throughout the alkali series and with each addition of alumina, apart from 10 % alumina. The optimal zone was the 5M NaOH 2.5 series, and results from outside this area were varied.
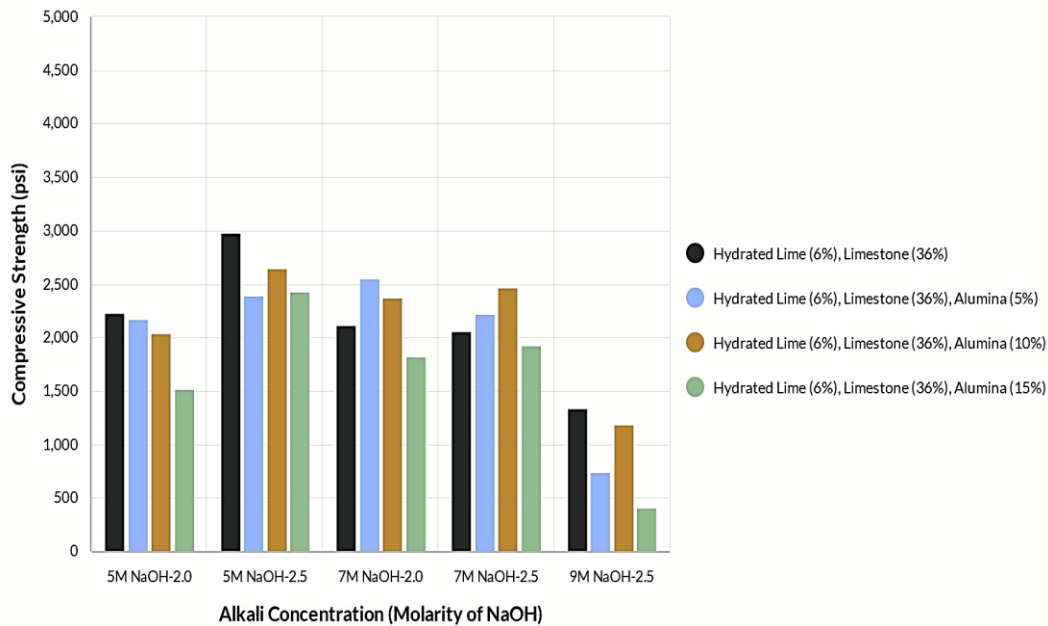
Figure 3-7: Compressive Strength Results for Ambient-Cured RBD Geopolymer with 36% Limestone and Alumina Added

When compared against the oven-cured samples for the alumina series, the results were sporadic, and several categories yielded higher or lower than anticipated outcomes. The 5M NaOH-2.5 samples with no alumina showed the greatest compressive strength; however, when looking at the effects of alumina addition, the 10% alumina had a greater compressive strength than anticipated. Comparing the 5M NaOH-2.5 and 7M NaOH-2.0 range with 10% alumina by weight, oven-cured samples were contrasted to their ambient-cured versions, shown in Figure 3-8. The 5M NaOH-2.5 with 10% alumina ambient-cured sample displayed the highest compressive strength at 2640 psi. The highest compressive strength for the oven-cured sample was 2280 psi recorded from the 7M NaOH-2.5 with 10% alumina.
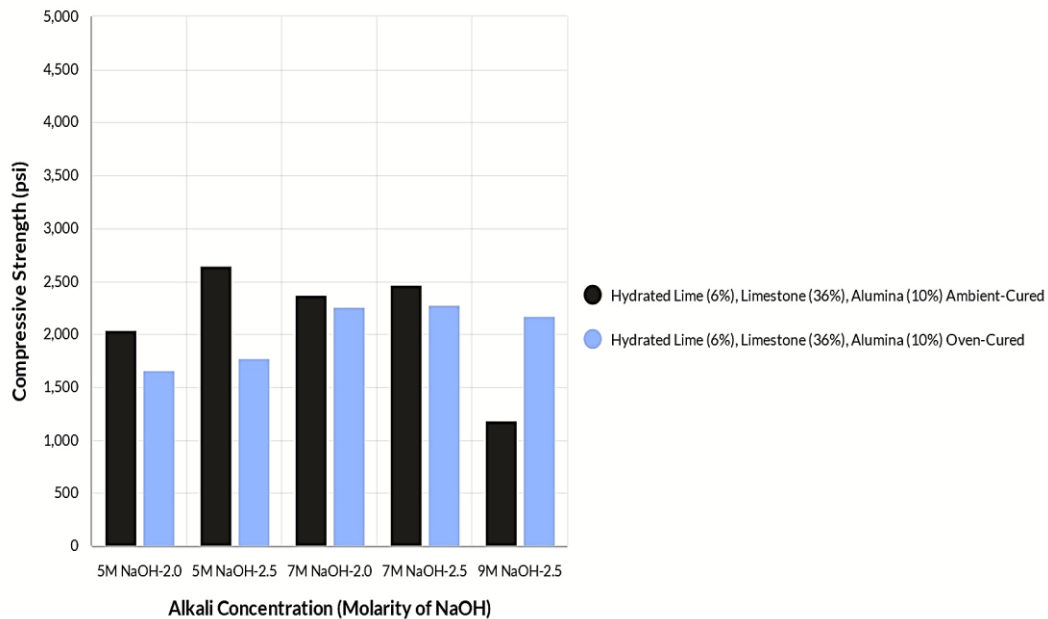
Figure 3-8: Compressive Strength Results for RBD Geopolymer with 10% Alumina Added and Both Curing Methods

The empirical results of the ambient models indicated that, except for the 9M NaOH-2.5 series, the strengths were equal to or better for each series compared. Notably, the alumina series achieved an overall reduction in compressive strength for the maximum strengths observed from the preceding series. This is suggestive of the same oversaturation issue within the geopolymer mixture, witnessed in the 2"x2" mortar cubes. To counteract this, finer particle-size alumina was introduced to increase the bioavailability of alumina. In addition, the powdered limestone was reduced to avoid unreacted limestone. Lowering the limestone addition and ascertaining a finer alumina source should supply more information on their proportional relationship.

The alkali concentrations were narrowed to 5M NaOH-2.0, 5M NaOH-2.5, and 7M NaOH-2.0 to limit iteration. Limestone substitutions were limited to 0%, 6%, and 12%,

with a constant 5% alumina substitution throughout the series. Results of the series are shown in Figure 3-9, with the highest compressive strength of 3760 psi recorded for 5M NaOH-2.5 samples under the hydrated lime (6%), limestone (6%), and coarse alumina (5%) category. However, the fine and coarse alumina samples yielded variable results in different alkali categories and should be reevaluated using average compressive strengths.
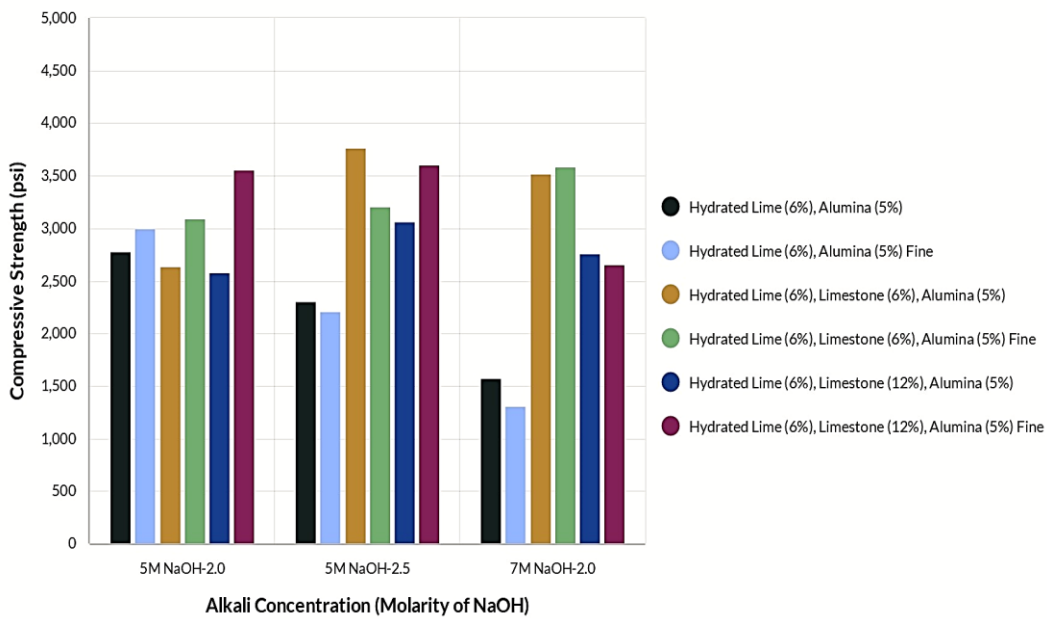
Figure 3-9: Compressive Strength Results for Ambient-Cured RBD Geopolymer with Variable Limestone and 5% Alumina Added

The next highest compressive strength was 3600 psi for hydrated lime (6%), limestone (12%), and fine alumina (5%) series under the same alkali category. This shows a complicated relationship between the amount of calcium, alumina, and silica present, yet the results indicated the hydrated lime (6%), limestone (12%), and fine alumina (5%) series was outperforming the other series for 5M NaOH-2.0 and 5M NaOH-2.5 categories. Figure

3-10 indicates the highest compressive strengths for the hydrated lime (6%), limestone (12%), and fine alumina (5%) series with ambient-cured models compared against oven-cured models. The highest compressive strength for the ambient-cured series was 3600 psi within 5M NaOH-2.5 region. For the oven-cured series, 3340 psi was the highest average compressive strength and was found within the 7M NaOH-2.0 zone.
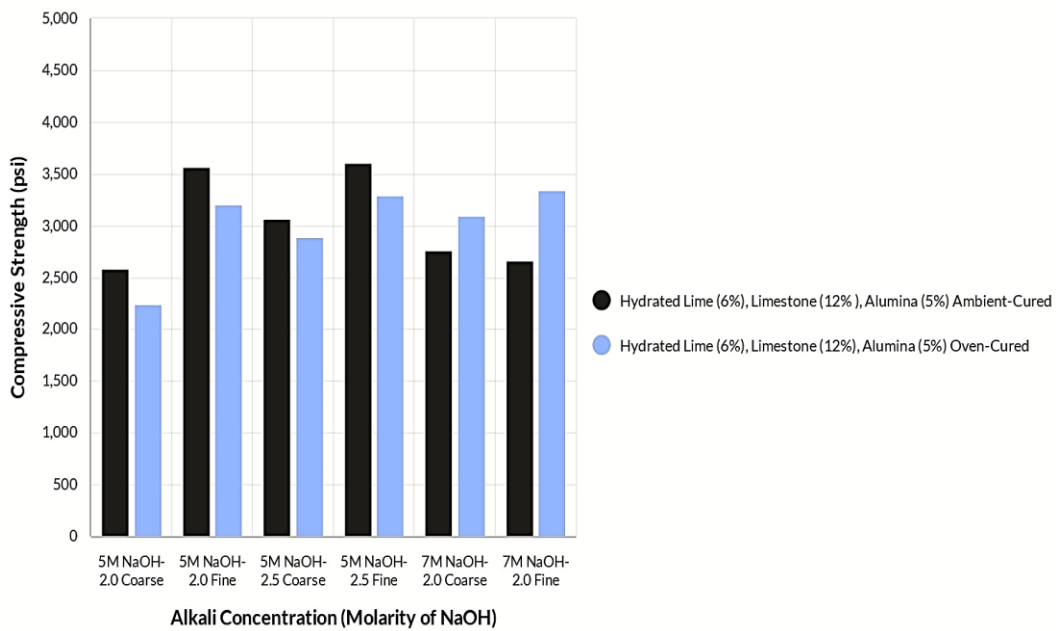
Figure 3-10: Compressive Strength Results for RBD Geopolymer with Both Alumina Particle Sizes and Both Curing Methods

It is essential to analyze the average strengths for each category before selecting specimens. The primary determinant for further selection should be the average compressive strengths within a given series or category. There have been issues with variability due to the introduction of constituents in the past. It is crucial to proceed through each phase with averages for each category and select the most representative samples

46

based on compressive strength. However, compressive strength alone does not necessarily reflect the success of gel production within the RBD geopolymer matrix. Therefore, it is important to identify and address any thermal peaks as an indication of the polymerization and hardening phase using calorimetry.

3.2.2 Calorimetry Peaks

A calorimeter was used to identify thermal peaks for each sample used within the RBD geopolymer matrix. Calorimetry peaks are useful in the determination of the gelation phase. Zhang et al. (2012) and Provis and Bernal (2014) described the geopolymerization process that begins with the dissolution of the aluminosilicate species followed by a reformation of the oxide chains. The oxide chains act as bridging components which then allow for the formation of C-A-S-H, N-A-S-H, or (N, C or C, N)-A-S-H gels via gel nucleation. Finally, polymerization and hardening occur, and compressive strength production can begin.

The calorimeter indicates initial heat production caused by the exothermic reaction of the alkali activators within the geopolymer mix. This is followed by a decrease in temperature, until a second exothermic peak occurs indicating the polymerization and hardening phase. The calorimetry peaks were examined for the following alkali activators: 5M NaOH-2.0, 5M NaOH-2.5, and 7M NaOH-2.0. In addition, the selection was filtered by RBD only and each added raw material. Figure 3-11 shows the calorimetry peaks for the highest compressive strength specimens in each category within the 5M NaOH-2.0 series. Figure 3-12 features the calorimetry peaks for the highest compressive strength

47

specimens in each category within the 5M NaOH-2.5 series. Figure 3-13 presents the

calorimetry peaks for the highest compressive strength specimens in each category within

the 7M NaOH-2.0 series.
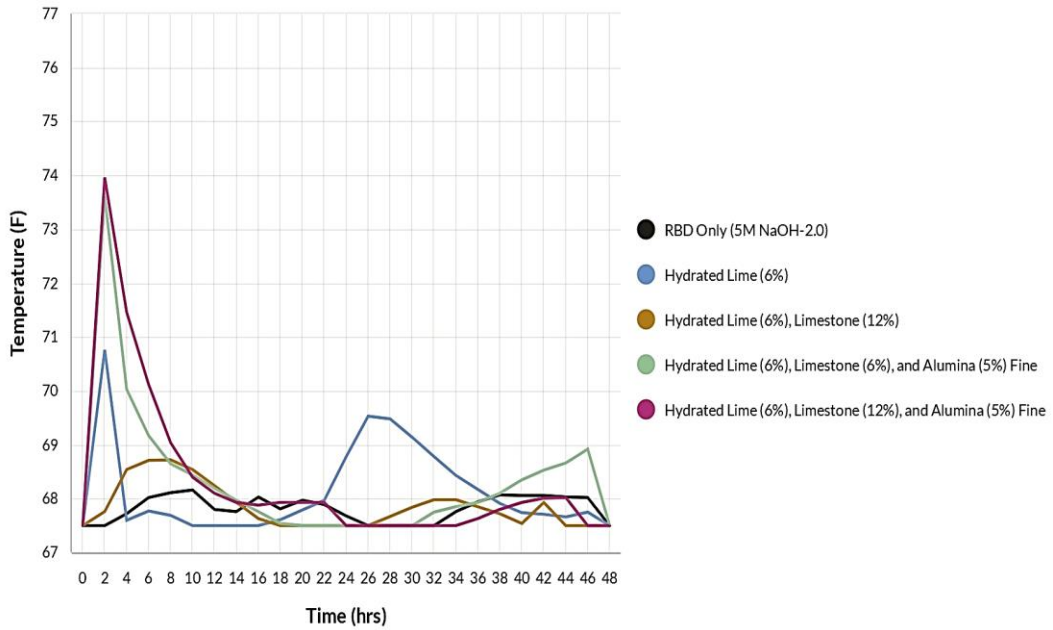
Figure 3-11: Calorimetry Results for 5M NaOH-2.0 Category
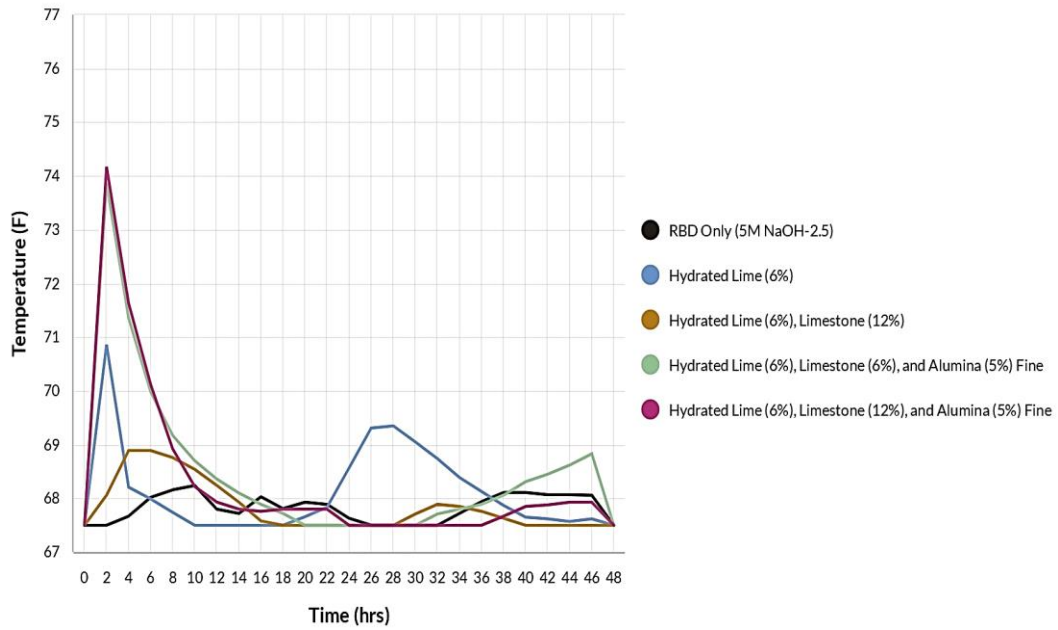
Figure 3-12: Calorimetry Results for 5M NaOH-2.5 Category
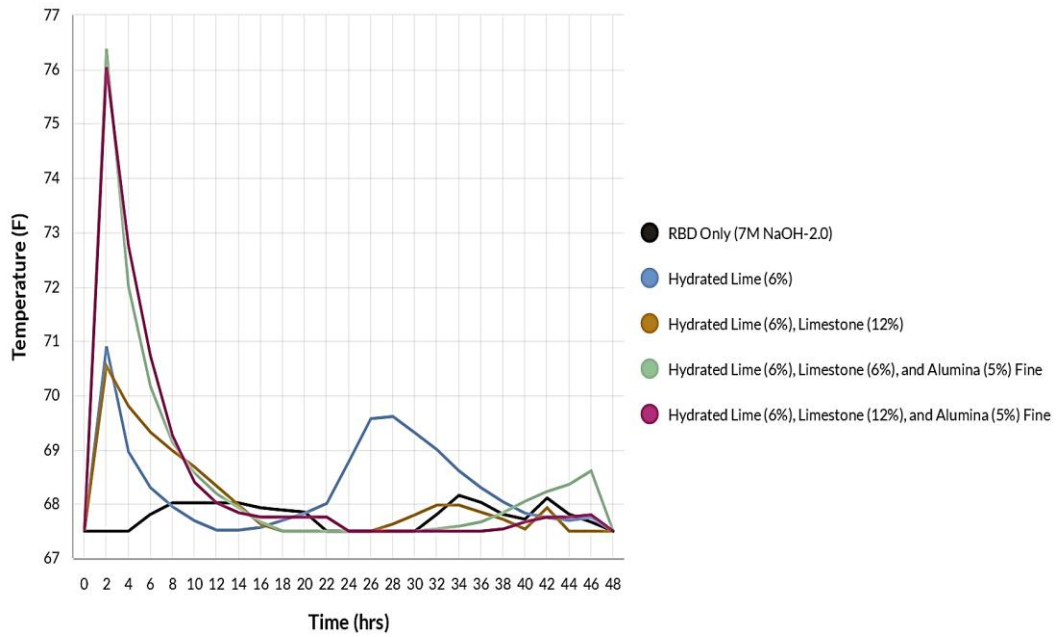
Figure 3-13: Calorimetry Results for 7M NaOH-2.0 Category

49

Initial examination of the data reveals that, except for the RBD-only and hydrated lime (6%) and limestone (12%) series, a notable heat spike can initially be observed. Subsequently, all specimens displayed elevated temperatures over the course of 4-10 hours before declining to ambient levels. Moreover, all samples experienced a secondary heat increase around the 24-hour mark, which signifies polymerization and hardening. Specimens with higher secondary peaks are anticipated to exhibit greater strength, which will be explored in greater detail in the ensuing section. Notably, the hydrated lime (5%) series exhibited a unique pattern of heat development, with its peak occurring at the 32-hour mark and generating more heat than other categories typically did at the 30-hour mark.

Another identified trend can be seen with the difference in the initial heat spikes for each alkali category. The hydrated lime (6%), limestone (6%), and fine alumina (5%) series had an initial temperature of 73.61°F, while the hydrated lime (6%), limestone (12%), and fine alumina (5%) series had an initial temperature of 73.96°F. Both of which are multiple degrees higher than their counterparts. This suggests an initial reaction that is based on the bioavailability of calcium, silica, and alumina. Depending on the saturation levels of each constituent, the initial peak either grew or decreased. The added alumina spiked these initial heat values, while the added limestone, without alumina, reduced the initial heat spike.

Furthermore, each alkali category had a noticeable increase in the initial heat evolution based on the levels of alkalinity. The higher alkalinity of the activators produced higher thermal peaks based on the calorimetry reports. The same hydrated lime (6%), limestone (6%), and fine alumina (5%) series and hydrated lime (6%), limestone (12%), and fine alumina (5%) series under the 5M NaOH-2.5 category produced an increase of 0.25°F and

0.21˚F, respectively. The 7M NaOH-2.0 category showed an increase of 2.77˚F for the hydrated lime (6%), limestone (6%), and fine alumina (5%) series and 2.08˚F for hydrated lime (6%), limestone (12%), and fine alumina (5%) series. The smaller differential in the 5M NaOH-2.0 to the 5M NaOH-2.5 samples can be attributed to the increase in Na_2SiO_3/NaOH ratio by weight. The greater heat release observed for the 5M NaOH-2.5 to the 7M NaOH-2.0 series occurred due to additional NaOH, which produced a higher exothermic reaction when combined with the raw materials.

Calorimetry reports provide insight into the saturation of the RBD geopolymer matrix, as well as the prolongation of the curing window due to an influx of fillers and un-processed ingredients. Secondary peaks, signifying slower reaction times, can be associated with a decreased compressive strength over a 28-day period. Walkey et al. (2016) discussed the promotion of C-A-S-H gel production with higher calcium and lower alumina concentrations. On the other hand, reduced calcium content and higher alumina ratios can have a striking effect on the Ca/Si and Al/Si molar ratios, not to mention the curing time of specimens. Achieving the correct ratios will promote secondary heat development and indicate the beginning of the polymerization and hardening phase.

Provis and Bernal (2014) reinforce the late curing times with their study showing the production of additional C-A-S-H gels when comparing 28-day curing cycles to 180-day curing cycles. Initially, N-A-S-H gels were formed in the alkali-activated geopolymer, then these N-A-S-H gels began to bridge out into (N, C)-A-S-H or (C, N)-A-S-H gels. Available calcium ions will substitute into the N-A-S-H gels, until a saturation limit is reached, and additional compressive strength formation is achieved. The alumina serves as oxide

branches between the calcium chains, yet there can also be unfavorable substitutions of other oxide-bonded metals into the alumina cross-bridging position.

The extent of polymerization and hardening can be determined by combining compressive strength measurements with calorimetry reports. Evaluating the hardening period can reveal if a sample exhibits delayed curing compared to the same series. A correlation between low compressive strength values and stagnant calorimetry results can be used to check the saturation of the matrix. If saturation occurs or a hindrance in the formation of the geopolymer matrix is observed, a slower strength development may follow and be detrimental to the RBD geopolymer.

3.2.3 Selection of Promising RBD Geopolymer Mixtures

Data collected from the compression and calorimetry tests were processed using Microsoft Excel and Mendenhall and Sincich's (2016) guidelines for outlier identification, data enhancement, and statistical averaging. Due to having two samples per mix design for the 2"x2" mortar cubes, data analysis using error plots and outliers was previously unavailable. An evaluation of average compressive strengths was needed to add validity to the selection of promising RBD geopolymer mixtures and move the research forward.

Figure 3-14 shows the average 28-day ambient-cured compressive strength results for all categories, with error plots showing the standard deviation from the average. The 5M NaOH-2.5 mix had the highest average compressive strength of 3490 psi for the hydrated lime and limestone series. The average compressive strength for the same alkali content decreased for the hydrated lime and alumina-added samples to an average of 1520 psi and

2850 psi, respectively. The 5M NaOH-2.0 and 7M NaOH-2.0 alkali concentrations tended to underperform compared to the 5M NaOH-2.5, except for the 5M NaOH-2.0 hydrated lime category. In addition, the standard deviations were generally smaller for the 5M NaOH-2.5 alkali content, with 5M NaOH-2.0 having similar results.
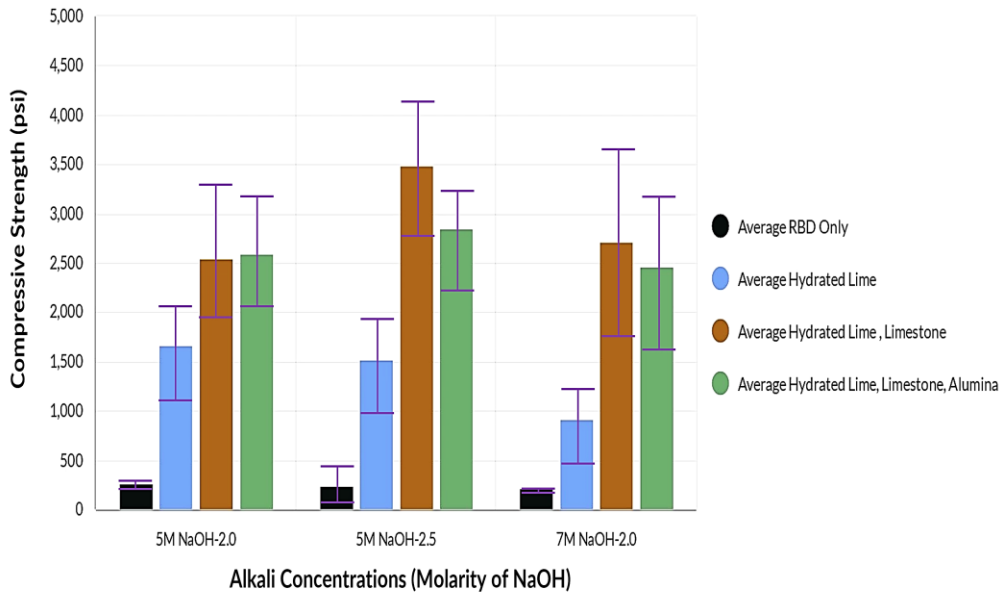
Figure 3-14: Average 28-Day Ambient-Cured Compressive Strengths

An evaluation of the oven-cured counterparts, as illustrated in Figure 3-15, was necessary prior to proceeding with the calorimetry reports. The variability between series diminished for the oven-cured samples because of the mechanisms associated with the oven-curing process, which allowed for the addition of heat and resulted in outcomes that demonstrated minimized deviations from the averages. The expected results should have been higher compressive strengths for the oven-curing process, yet water evaporation and microcracks led to lower-than-expected averages. The 5M NaOH-2.5 mix was second in

line for the highest average 28-day compressive strength at 3280 psi; however, it was still promising when compared against other data points. Because of the ambition for RBD geopolymers to be used via in-situ building, the ambient-curing model was utilized for further analysis and selection.
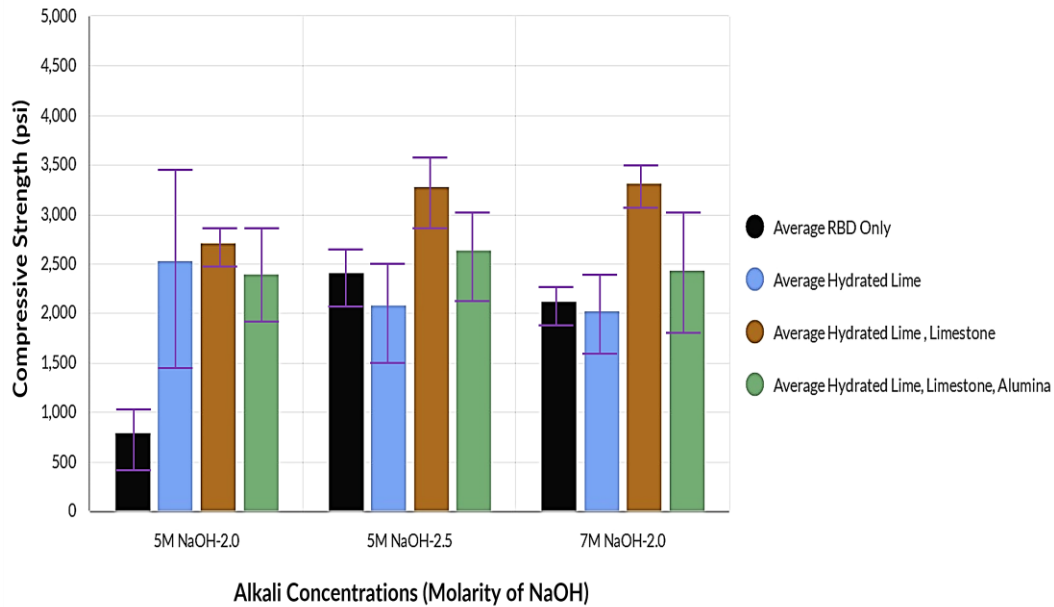
Figure 3-15: Average Oven-Cured Compressive Strengths

Beyond the compressive strength analysis, calorimetry trends can be used to investigate the preferred mix design. To avoid an increase in heat due to alkali concentrations, the 5M NaOH-2.5 category was selected based on the ambient-cured samples and average compressive strengths. The addition of alumina to 5M NaOH-2.5, hydrated lime (6%), limestone (12%), and alumina (0%-10%) samples resulted in an increase in hardening time; a secondary heat evolution was present within 28 hours for the 0% alumina series and 40 hours for the 5% alumina series. Figure 3-16 shows that, while the hardening period

remained 28 hours with the addition of alumina, locally maximum temperatures dropped from 74.17˚F to below 71.00˚F for 5M NaOH-2.5, hydrated lime (6%), limestone (12%), and alumina (0%). The exception was for 5M NaOH-2.5, hydrated lime (6%), limestone (36%), and alumina (15%) samples which had an initial heat spike of 72.16˚F.
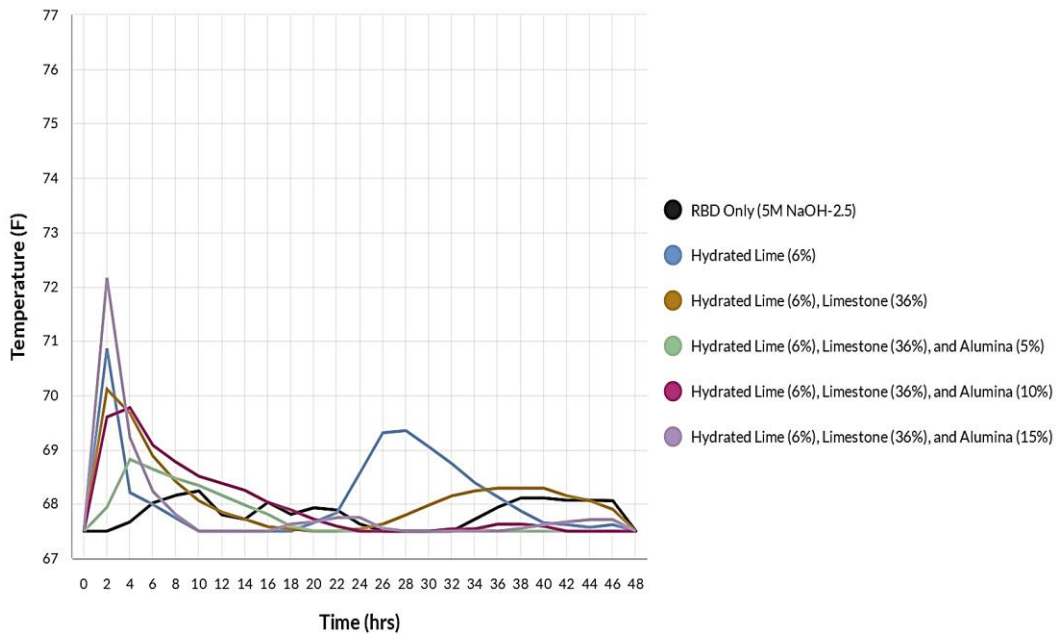
Figure 3-16: Calorimetry Results for 5M NaOH-2.5 Alumina Series

Within the 5M NaOH-2.5 category, the secondary thermal peaks were generally absent or relatively small. The oversaturation limits were reached with 36% limestone and 15% alumina. New maximums needed to be considered for optimal compressive strength. The substitution by weight for limestone was set at 12%, and the alumina was maxed at 10%. Figure 3-17 illustrates the compressive strength difference between 12% and 36% limestone substitution. The highest compressive strength in this range, 4490 psi, was observed for 12% limestone and 0% alumina; the strength decreased to 3600 psi with 5%

alumina addition by weight. Further decreases in compressive strength can be observed with higher limestone and alumina percentages.
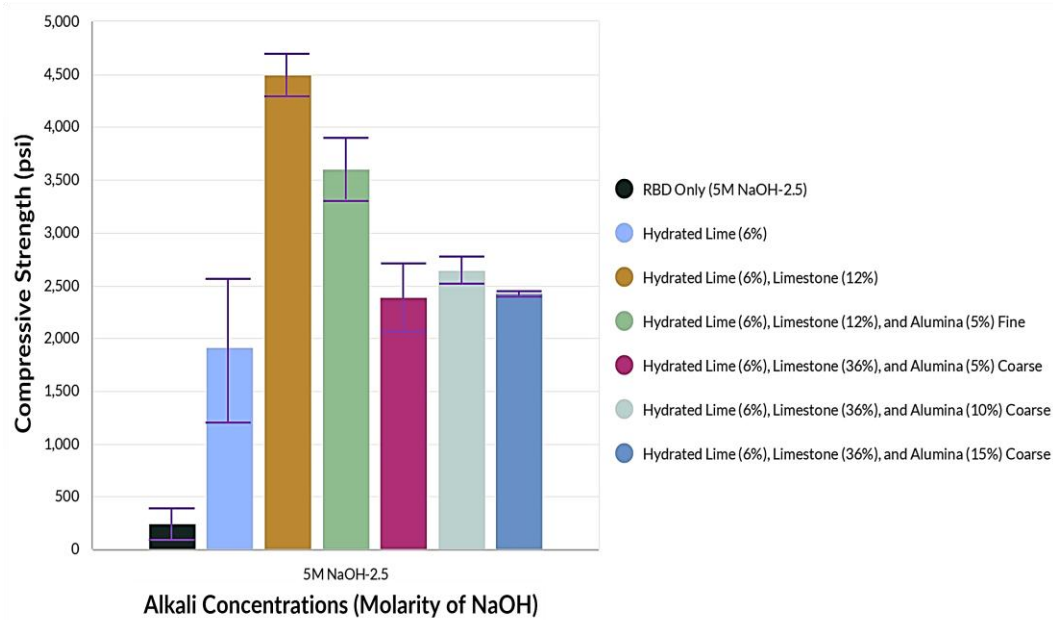
Figure 3-17: Compressive Strength Results for Ambient-Cured RBD Geopolymer With Limestone (0-36%) and Alumina (0-15%) Addition

To better understand the underlying mechanisms in the RBD geopolymer matrix, ternary diagrams were investigated for Ca:Si:Al molar percentages. Figure 3-18 demonstrates the compressive strengths of each specimen within the 5M NaOH-2.5 category, and an overlay provided by Jackson et al. (2017). The Jackson et al. (2017) overlay demonstrates the zone of Ca:Si:Al molar percentages for Ancient Roman concrete sources from various locations. These values were representative of target ratios determining the added raw material for the initial phases of research. The initial goal was to add enough raw materials to the RBD geopolymer matrix to force a conversion onto the target ratios established for C-A-S-H gel production.
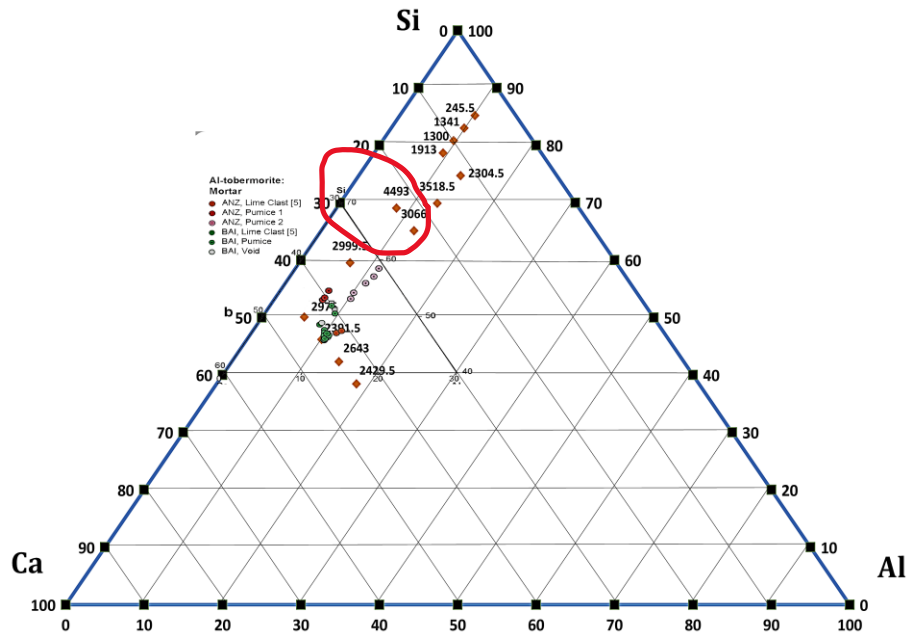
Figure 3-18: Ternary Diagram of Compressive Strengths for 5M NaOH-2.5 Category With Jackson et al. (2017) Overlay

Jackson et al. (2017) reported that the primary gel formations in Ancient Roman concrete of interest were C-S-H and C-A-S-H gels, which were key elements for the strength development and durability of the concrete. It was suggested that the tobermorite-like formations in Ancient Roman concrete were mostly composed of C-A-S-H gels, potentially serving as a factor for the observed strength improvement over time. However, the highest compressive strength values for the 5M NaOH-2.5 category did not adhere to Ancient Roman concrete parameters due to an oversaturation issue with the unreacted components. The highest compression zone was outside the Jackson et al, (2017) overlay, which negated the relationship between compressive strengths and molar ratios from earlier. Garcia-Lodeiro et al. (2011) was used to delve deeper into N-A-S-H and C-A-S-H gel production.

For the final step, deciding where the optimal zone should begin was conducted using multiple ternary diagram overlays. Figure 3-19 indicates that Jackson et al. (2017) and Garcia-Lodeiro et al. (2011) provided useful insights that can be combined with compressive strength results to foster a more in-depth understanding. Specifically, the C-A-S-H production zone of the Ancient Roman concrete, illustrated in Jackson et al. (2017) research, can be stretched to 10%-20% calcium area where (N, C)-A-S-H zone can form according to Garcia-Lodeiro et al. (2011). Moreover, satisfying compatibility between N-A-S-H and C-A-S-H gels with precise Ca:Si:Al molar ratios could explain the high compressive strength level of the 5M NaOH-2.5 category. This suggests compatibility between these two gel chains may have improved the overall strength of the RBD geopolymer.
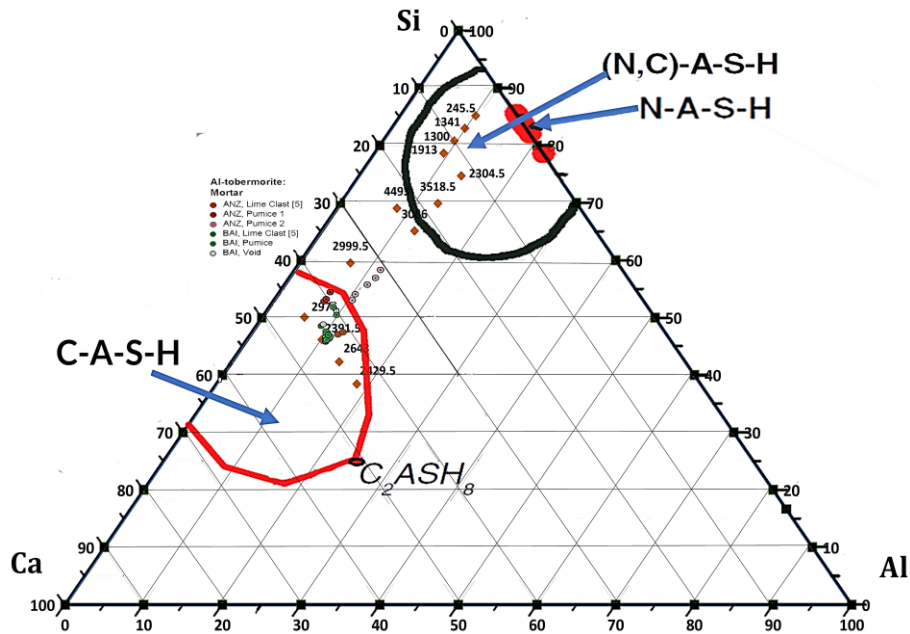
Figure 3-19: Ternary Diagram of Compressive Strengths for 5M NaOH-2.5 Category with Jackson et al. (2017) and Garcia-Lodeiro et al. (2011) Overlay

Chapter 4: Verification of Maximum Compressive Strength Zone

The maximum compressive strength zone for the 2"x2" mortar cubes was found near the (N, C)-A-S-H zone, providing a suitable starting point for the 3"x6" cylinder recipes. The intention was to fully encapsulate the hybrid gel zones by adjusting the components using ternary diagrams. To avoid an excess of unreacted calcium, the limestone content was kept constant, and the hydrated lime was adjusted. Maximum compressive strength was not achieved with hydrated lime, so further testing was warranted. The chosen mix designs consist of the following: 5M NaOH-2.5, hydrated lime (6%-12%), limestone (12%), and alumina (0%-10%).

4.1 Upscaling of Promising Specimens

4.1.1 Scope of Research

Figure 4-1 shows the chosen values for the Ca:Si:Al molar percentages derived from ternary diagrams and experimentation. Table 4-1 indicates the corresponding Ca:Si:Al molar percentages for the 3"x6" cylinder series. Instead of replicating the Ca, Si, or Al molar ratios from Ancient Roman concrete for C-A-S-H production, the new target values for the 3"x6" cylinder category are based on hybrid gel compatibility. This led to a hypothesized outcome of either a calcium-dominant hybrid gel, (C, N)-A-S-H, or a sodium-dominant version, (N, C)-A-S-H (Garcia-Lodeiro et al., 2011; Luo et al., 2023). The target zone reflected an area between both hybrid gels and suspected gel production zones, allowing for either hybrid gel or a combination of them.
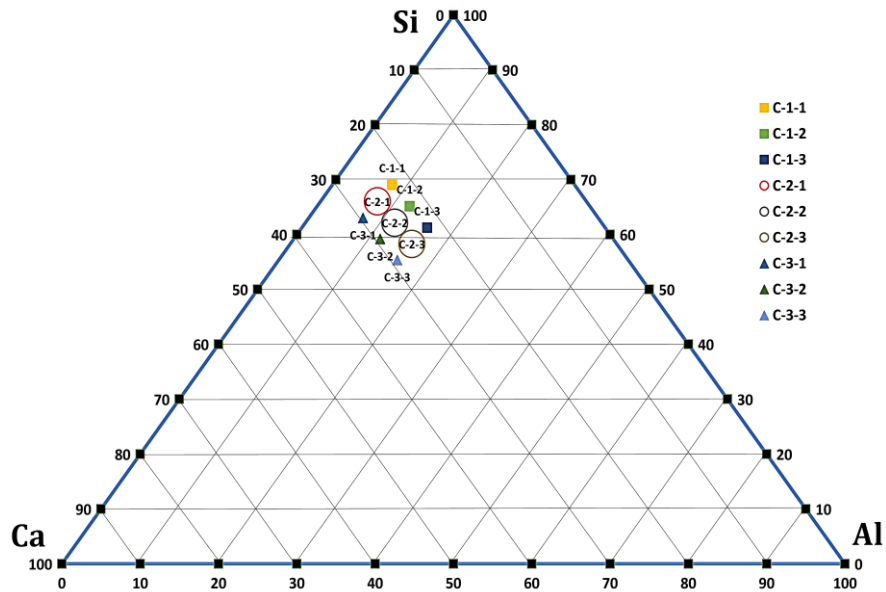
Figure 4-1: Ternary Diagram of Final RBD Geopolymer Cylinders

Table 4-1: Ca:Si:Al Molar Percentages for 3"x6" Cylinder Series

Sample	Ca (% mole)	Si (% mole)	Al (% mole)
C-1-1	23	69	8
C-1-2	23	65	12
C-1-3	23	61	16
C-2-1	26	66	8
C-2-2	26	62	12
C-2-3	26	58	16
C-3-1	30	62	8
C-3-2	30	58	12
C-3-3	30	54	16

Each set of 3"x6" cylinders was labeled based on the amount of hydrated lime and alumina added. A continuous calcium tangent for the three-cylinder series was followed, with the increase within each row accounting for the additional alumina. An example is C-1-1, containing hydrated lime (6%), limestone (12%), and alumina (0%). C-1-2 has

hydrated lime (6%), limestone (12%), and alumina (5%); C-1-3 has hydrated lime (6%), limestone (12%), and alumina (10%). This generated a 23% calcium content tangent for C-1, increasing to 26% for C-2 and 30% for C-3. The alumina tangent was set at 8%, then increased to 12% and 16% for each series.

Adjustments made to the RBD geopolymer 2"x2" mortar regimen were based on content values representing the entirety of the RBD geopolymer mixture, and the coarse alumina was changed to fine alumina. The Ca:Si:Al molar percentages were adapted to a whole content approach, which allowed for the use of ternary diagrams with target zones. In addition, Activated Alumina 14x28 mesh by USAlab, course alumina, was replaced by Martoxid MR-32 from Huber Engineering Materials, fine alumina. Preliminary experimentation showed fine alumina as the more efficient choice and was adopted as the primary alumina source. NaOH and "water glass" solutions of 5M and 2.5 Na_2SiO_3/NaOH by weight, respectively, were determined to be the most effective alkali combination for the tested RBD geopolymers. The NaOH solution was prepared 24 hours before batching then allowed to rest at room temperature. After the solids were mechanically mixed in a Hobart mixer, the "water glass" and NaOH solutions were added following the prescribed routine. Testing procedures were then performed based on previous testing paradigms.

4.1.2 Suggested Location of Maximum Compressive Zone

Figure 4-2 shows a ternary diagram displaying four zones: one where N-A-S-H chains are dominant, another exhibiting (N, C)-A-S-H formation, a third responsible for (C, N)-A-S-H formation, and fourth corresponding to traditional C-A-S-H generation (Garcia-

Lodeiro et al., 2011; Luo et al., 2023). The hypothesized maximum compression zone was situated between the (N, C)-A-S-H and (C, N)-A-S-H regions, which is consistent with Luo et al.'s (2023) findings that the two chains lock together under sufficient Na_2O concentrations. These chains have been able to contribute to higher compressive strength by working together to reinforce the RBD geopolymer matrix.

With the combination of these two hybrid gel chains, the RBD geopolymer mixture can be optimized without oversaturating the components with excess calcium products. The samples along series C-1 contained hydrated lime (6%) and started at alumina (0%), then increased to alumina (10%). The C-2 series contained hydrated lime (9%) with the same increasing alumina content (0%-10%). Series C-3 had hydrated lime (12%) with alumina ranging from 0% to 10%.
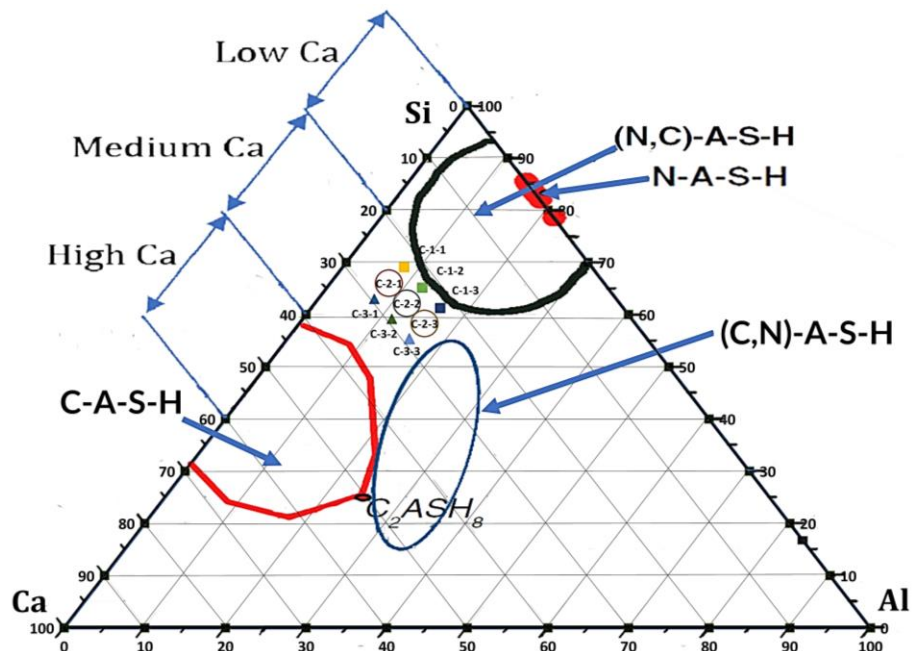
Figure 4-2: Ternary Diagram of RBD Geopolymer Cylinders in Comparison to Predicted Gel-Chain Zones (Garcia-Lodeiro et al., 2011; Luo et al., 2023)

4.2 Results and Analysis

4.2.1 Correlation of Compressive Strength and Calorimetry Peaks

Compressive strengths and calorimetry readings were examined in the 2"x2" mortar section to identify patterns in the RBD geopolymer components. An initial spike of heat generation was often followed by a secondary peak, suggesting dissolution of aluminosilicate species in the beginning, and then hardening at the end. The interval between these points determined curing times and potential oversaturation of the sample. Stagnation of the components could be inferred from these correlations, aiding in optimizing the RBD geopolymer formula.

Figure 4-3 shows the calorimetry data for cylinders C-1-1 through C-1-3, while Figure 4-4 indicates the compressive strengths for the same cylinders with 7-day strength, 28-day strength, and oven-cured strength. C-1-3 had the lowest initial heat spike at 74.99˚F compared to C-1-1 at 76.52˚F and C-1-2 at 76.64˚F. However, the secondary peak for C-1-3 started sooner than the C-1-1 and C-1-2 at the 24-hour mark instead of 28 hours past. The secondary heat evolution for C-1-3 also crested the highest at 67.97˚F versus 67.93˚F for C-1-1 and 67.89˚F for C-1-2. C-1-3 had the highest compressive strength for 7-day ambient-cured at 1000 psi. C-1-3 also had the greatest oven-cured strength at 4520 psi. C-1-2 was the highest for the 28-day ambient-cured at 3070 psi.
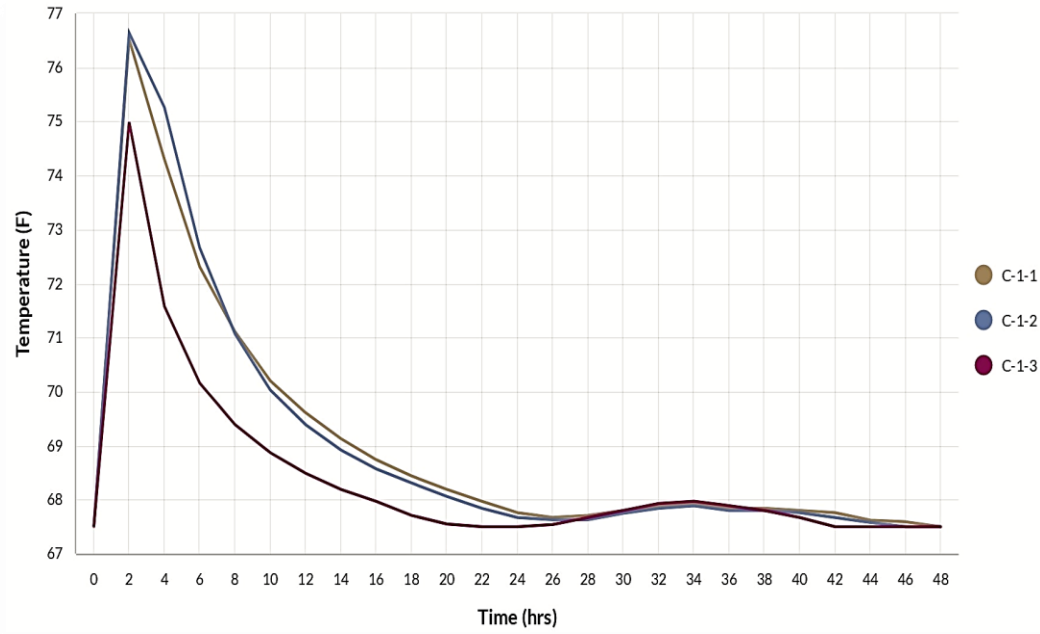
Figure 4-3: Calorimetry Results for C-1-1 through C-1-3
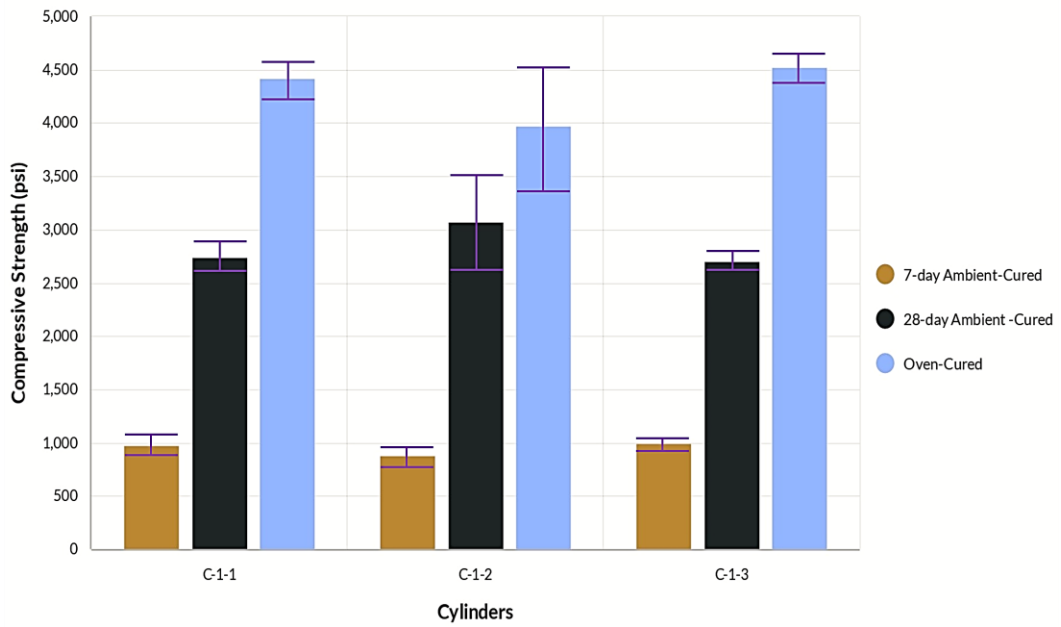
Figure 4-4: Compressive Strengths for C-1-1 through C-1-3

The C-1 series posed a challenging question regarding which cylinder should be the series representative. C-1-2 had the highest compressive strength over a 28-day period, which is the primary strength indicator for structural use. However, C-1-3 showed higher strength results at 7 days and after oven curing compared to C-1-2. A calorimetry report showed a more energetic secondary peak and a lower initial spike for C-1-3, which could help to explain these trends. It is also noted that the location of the secondary peak and the length of each peak are important to strength development and duration of curing. The 28-day strengths can be stalled or lower due to the hour location of secondary heat evolutions, and oven-cured strengths have been higher when the amplitude of the secondary peak is higher.

Figure 4-5 presents the calorimetry reports for series C-2, while Figure 4-6 displays their corresponding compressive strengths. The most substantial thermal spike was generated by C-2-1 at 75.82°F, followed by C-2-2 at 70.55°F and C-2-3 at 72.88°F. C-2-2 and C-2-3 exhibited prolonged initial heat evolution of approximately 12 hours before dropping to ambient then increasing for the second peak around the 26-hour mark. The secondary peak registered 68.46°F for C-2-2 and 68.01°F for C-2-3.
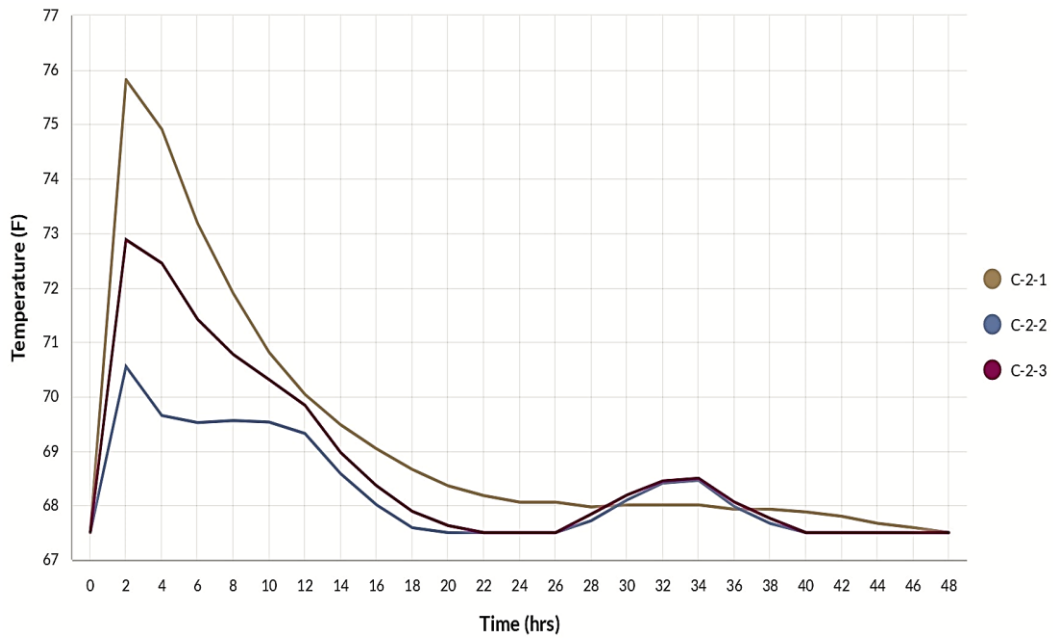
Figure 4-5: Calorimetry Results for C-2-1 through C-2-3
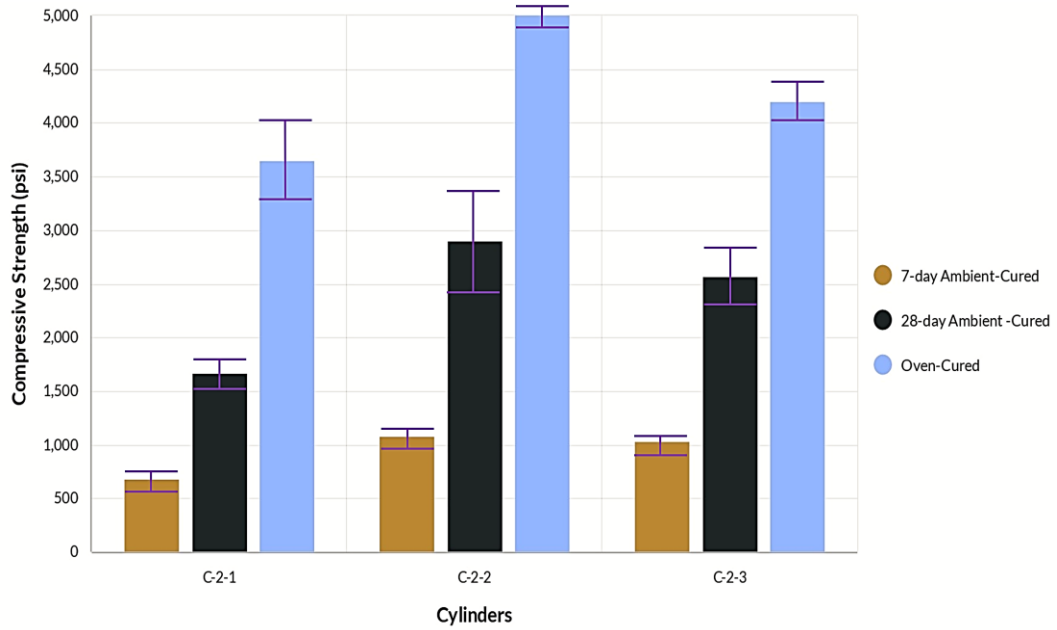
Figure 4-6: Compressive Strengths for C-2-1 through C-2-3

Sample C-2-2 also produced the highest 7-day, 28-day, and oven-cured strengths at 1080 psi, 2900 psi, and 5080 psi, respectively. Sample C-2-1 reported lower compressive strength values at 680 psi for 7-day strength, 1670 psi for 28-day strength, and 3650 psi for oven-cured strength. C-2-3 compressive strengths were 1040 psi for 7-day strength, 2570 psi for 28-day strength, and 4200 psi for oven-cured strength. C-2-1 had the highest heat development in phase one yet performed poorly in each strength category. This suggests fully reacted RBD with prominent dissolution, but the samples were oversaturated in calcium components.

In addition, insufficient alumina to facilitate interlocking sites for the calcium compounds would deteriorate the RBD geopolymer system. In contrast, C-2-2 had the lowest initial heat and suggested the dissolution phase was incomplete. The unreacted RBD present led to a reduced compressive strength for 7-day or 28-day. However, the second thermal peak was indicative of a successful hardening and polymerization stage. This resulted in the oven-cured strength sample exhibiting the highest compressive strength.

C-2-3 exhibited an excess of alumina and decreased temperature during the dissolution phase. C-2-3 and C-2-2 had superior compressive strengths than C-2-1 despite the smaller intensity of their initial peaks. The initial heat spike is not a reliable predictor of strength generation, while the secondary peak is more reliable at predicting compressive strength production in RBD geopolymer applications. There is a countervailing relationship between dissolution and hardening for 7-day and 28-day samples, while oven-cured samples experience greater heat to enable maximum dissolution rate and avoid the same complications as the ambient-cured specimens.

For the last series, Figure 4-7 shows the calorimetry reports for C-3-1, C-3-2, and C-3-3, while Figure 4-8 contains the compressive strengths. The initial heat spikes were lower overall for this series compared to the others. The highest thermal peak came from sample C-3-1 at 70.33˚F, which was 5.49˚F lower than C-2-1 and 6.31˚F below C-1-2. The C-3 series experienced extended initial thermal peaks for all samples. The exothermic reaction caused by dissolution occurred well into the 10-hour window and then dissipated around the 16-hour mark. The secondary peak developed later than the other series at the 30-hour mark compared to the 26-hour mark for C-2 and the 28-hour mark for C-3.
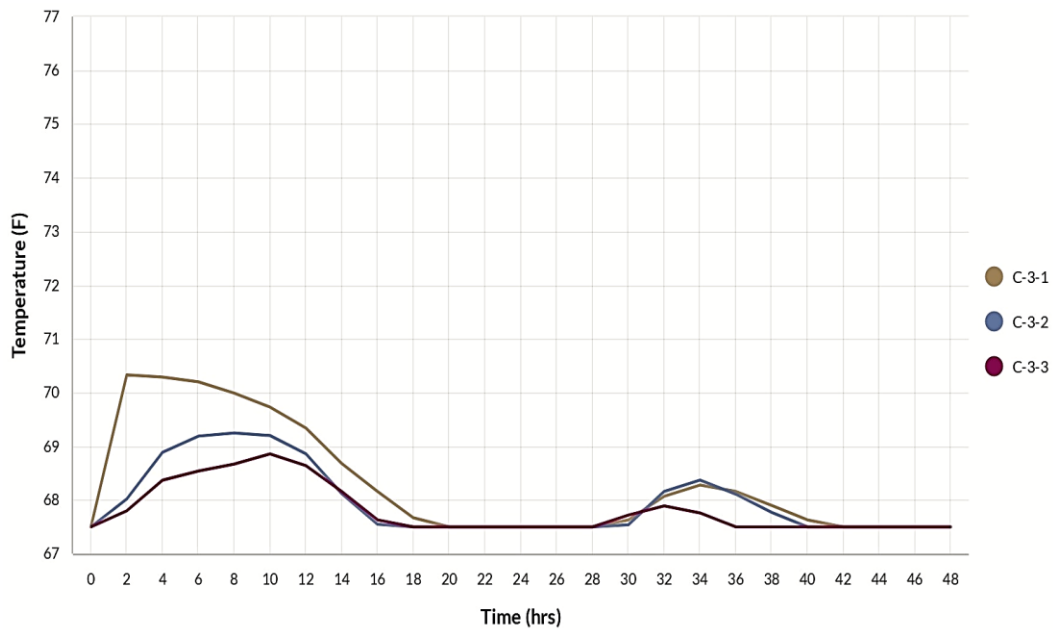
Figure 4-7: Calorimetry Results for C-3-1 through C-3-3
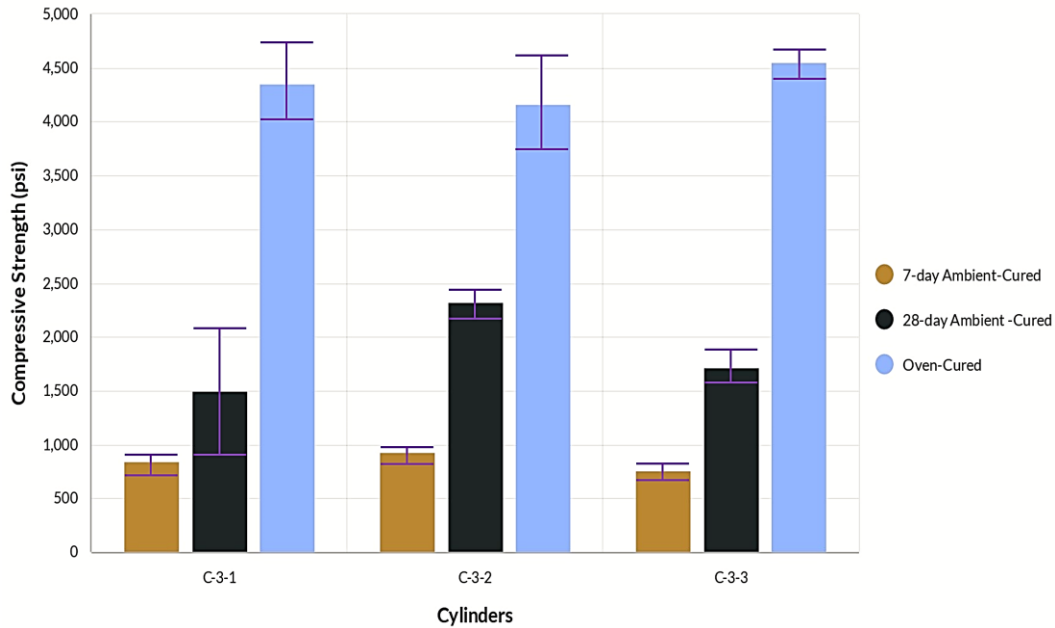
Figure 4-8: Compressive Strengths for C-3-1 through C-3-3

Sample C-3-1 reported a 7-day strength of 850 psi, a 28-day strength of 1500 psi, and an oven-cured strength of 4360 psi. Sample C-3-2 produced a 7-day strength of 930 psi, 28-day strength of 2320 psi, and oven-cured strength of 4170 psi. Sample C-3-3 strength tests resulted in a 7-day 760 psi, 28-day strength of 1710 psi, and oven-cured strength of 4550 psi. Sample C-3-2 had the highest compressive strengths at 7 days and 28 days, yet the oven-cured strength was greatest in C-3-3.

By comparing compressive strengths and calorimetry results, the unusual compressive strength behavior was examined and rationalized. The third sample in each series had the highest alumina and developed secondary heat evolution windows before the other samples, apart from C-2-2. C-2-2 showed a secondary heat spike similar to C-1-3, C-2-3, and C-3-3, with the activation window beginning around the 26-hour or 28-hour mark. An equilibrium shift may have taken place, with saturation limits being reached for each

respective series. To gain a more comprehensive view, the best samples from each series were compared against their calorimetry reports.

The data from each series was selected using 28-day strength trends, as opposed to 7-day strength or oven-cured strength. This was done to get an ambient-cured sample suitable for structural use. The 28-day compressive strength is the industry standard for evaluating the quality of concrete and was chosen as the best metric for obtaining a complete analysis without additional iterations. Figures 4-9 and 4-10 provide calorimetry and compressive strength results for samples C-1-2, C-2-2, and C-3-2 from each series, respectively.
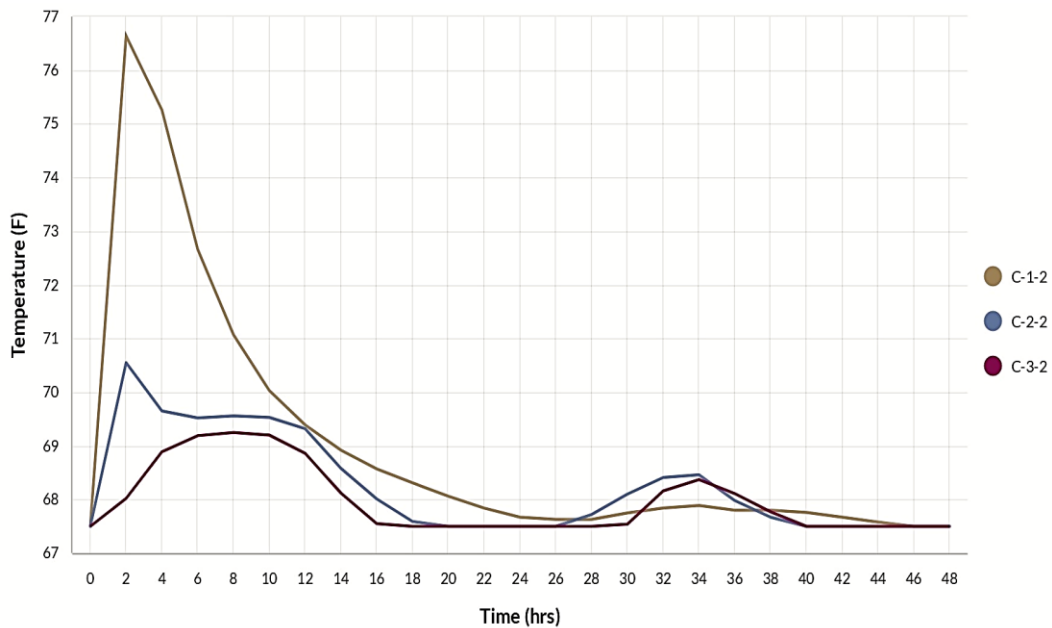
Figure 4-9: Calorimetry Results for C-1-2, C-2-2, and C-3-2
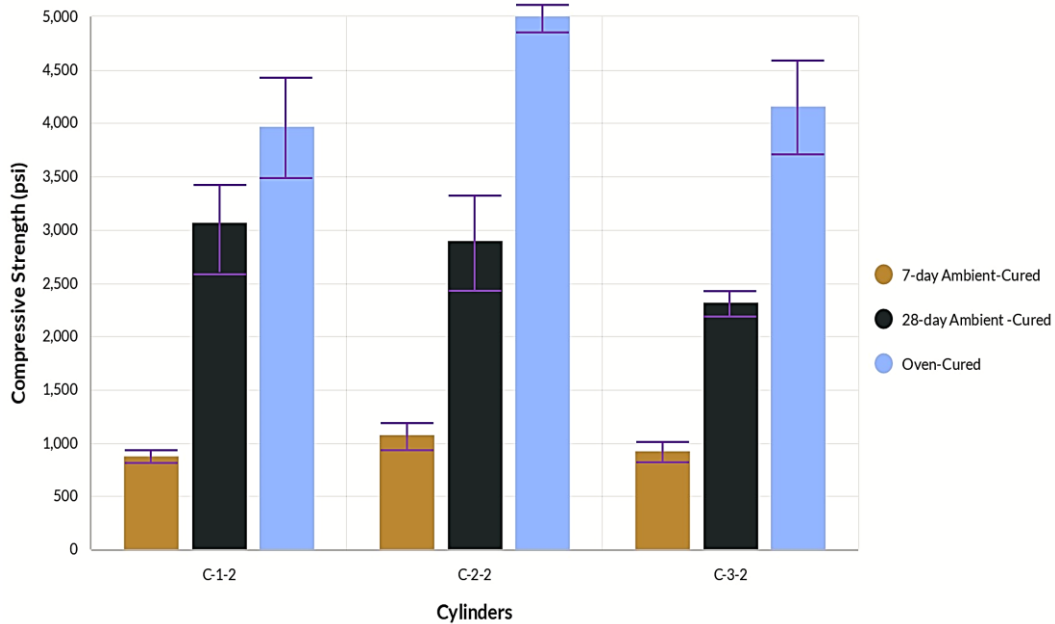
Figure 4-10: Compressive Strengths for C-1-2, C-2-2, and C-3-2

The highest temperature spike was for C-1-2 at 76.67°F compared to C-2-2 at 70.55°F and C-3-2 at 68.02°F. This represented a temperature difference of 6.12°F for C-1-2 to C-2-2 and 8.65°F for C-1-2 to C-3-2. The significant temperature differential can be attributed to the difference in dissolution of the aluminosilicate species, as mentioned earlier. The C-1-2 sample was experiencing a higher degree of dissolution compared to the others due to the lack of added components. The unreacted alumina and hydrated lime tended to stall the dissolution phase and even prolong it at times.

The 28-day compressive strengths also showed this trend with decreasing compressive strengths for each series with additional constituents. C-1-2 started with a compressive strength of 3070 psi, then reached 2900 psi for C-2-2, and finally lowered to 2320 psi for C-3-2. Due to the second sample from each series being chosen, the alumina content was

constant throughout. The only changing variable was the amount of hydrated lime, which never reached a maximum concentration limit during the 2"x2" mortar tests.

Even with a 28-day strength being the primary measure of success, Sample C-2-2 had the greatest 7-day strength and oven-cured strength compared to the other samples. The 7-day strength is generally provided by N-A-S-H gels and is more prominent with a greater degree of polymerization and hardening. Initial heat spikes for C-2-2 and C-3-2 were lower than C-1-2; however, they presented higher 7-day strengths. The calorimetry reports suggest that an extended heat production contributes to the greater 7-day strength more effectively than a higher initial heat spike. The results showed that C-2-2 and C-3-2 had 7-day strengths at 1080 psi and 930 psi, respectively, while C-1-2 had a lower 7-day strength at 880 psi.

The oven-cured versions provided a fully reacted by-product by increasing the thermal environment and accelerating the geopolymerization process to finality. C-2-2 produced the highest oven-cured compressive strength at 5080 psi compared to C-1-2 at 3980 psi and C-3-2 at 4170 psi. This represents a 1170 psi increase for C-2-2 over C-1-2 and a 920 psi increase over C-3-2. An equilibrium shift can be seen in sample C-2-2, providing a baseline for further examination. Ca:Si:Al contents were examined against the compressive strengths to help verify these observations.

4.2.2 Analysis of Compressive Strength Vs. Ternary Diagrams

To validate cylinder data and analyze additional trends, ternary diagrams were used to display Ca:Si:Al molar percentages in correlation to their compressive strength results.

The ternary diagram approach was employed to analyze the quantities of Ca:Si:Al contents that contributed to geopolymerization. The calorimetry recordings guided trends of stagnation and oversaturation in the chemical processes, whereas the ternary diagrams served as a component guide for determining which hybrid gels were most likely present. Figure 4-11 illustrates the ternary diagram of the RBD geopolymer mixtures and their 7-day compressive strengths. It is observable that the two highest compressive strengths exist in series C-2 along the same calcium tangent. Additionally, 7-day compressive strength diminishes with increased or decreased calcium tangent, except for sample C-2-1.
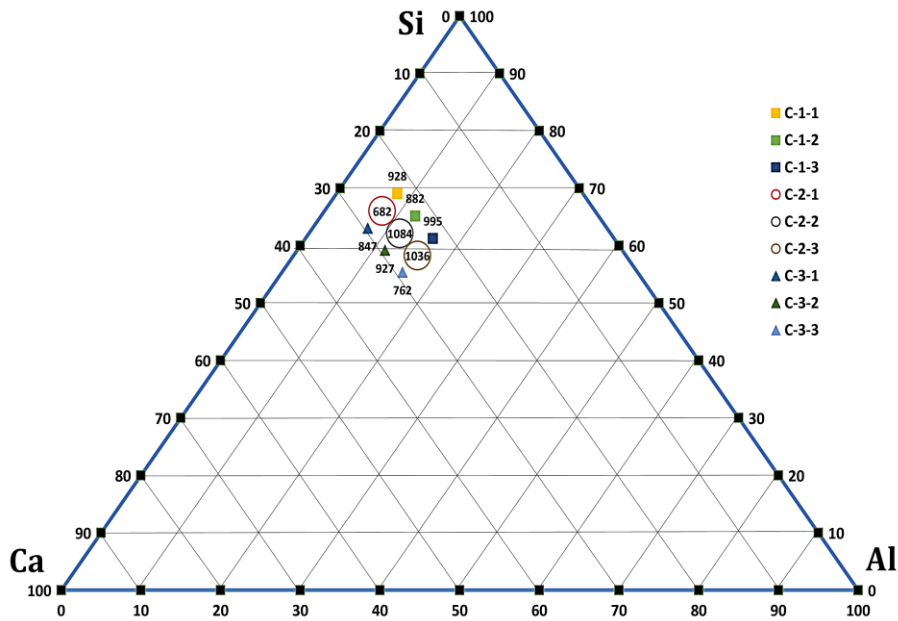
Figure 4-11: Ternary Diagram With 7-Day Compressive Strength Values

It was observed that the Ca:Si:Al molar percentages intended to produce a zone where (N, C)-A-S-H and (C, N)-A-S-H gels were compatible and would result in the highest compressive strength for the 2"x2" mortar category. A shift in the ratios to either the N-A-

S-H or C-A-S-H regions was seen to produce lower compressive strengths. The 2"x2" mortar category showed an area situated between both N-A-S-H and C-A-S-H zones, allowing for (N, C)-A-S-H and (C, N)-A-S-H gels to form upon activation with an alkali environment. This zone was liable to produce higher compressive strengths because of the geopolymerization processes and possible compatibility of the two hybrid gels (Luo et al., 2023).

In addition, the differing reaction times between C-A-S-H and N-A-S-H gels typically led to early strength development with faster reaction times under dominant C-A-S-H production. The N-A-S-H gels form more slowly over time and normally begin forming only after the Ca saturation has been depleted or the substitutions slowed (Wang et al., 2019). The C-1 series, which was closer to the (N, C)-A-S-H and N-A-S-H zones, and the C-3 series, which was at the edge of the (C, N)-A-S-H and C-A-S-H areas, both produced lower compressive strengths than the C-2 series in the middle. This supports the idea of (N, C)-A-S-H and (C, N)-A-S-H compatibility, at least within the 7-day curing samples. In addition, the maximum alumina content seemed to be along the 12% Al content tangent as the samples tended to decrease in compressive strength on either side of the line. This suggests a dual planar solution for using ternary diagrams and locating the maximum compressive zone.

Figure 4-12 shows the ternary diagram for 28-day compressive strengths. C-1-2 demonstrated the highest compressive strength, followed by C-2-2. Compared to the 7-day strength, the 28-day compressive strength trends changed. The 12% Al content tangent still demonstrated a greater strength than 8% and 16% Al variants; however, samples along the

23% Ca content tangent yielded better results for the dual planar model, correlating to series C-1.
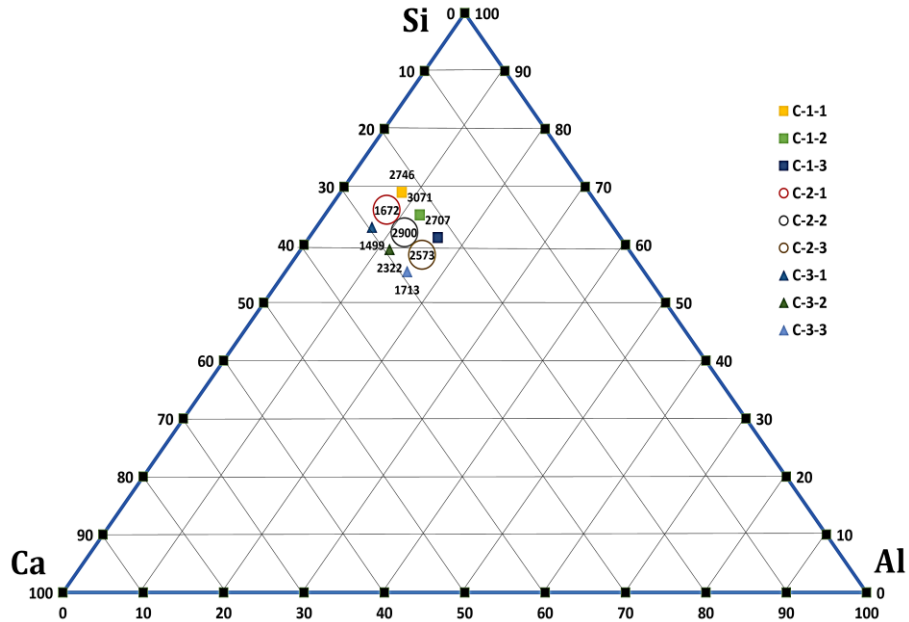
Figure 4-12: Ternary Diagram With 28-Day Compressive Strength Values

For the C-1 series, the samples were closer to the (N, C)-A-S-H region and produced the highest compressive strengths along the 23% Ca tangent. This is a mostly Na-dominant zone corresponding to later strength development. The higher compressive strengths for the C-1 series at 23% Ca content compared to the others at 26% Ca and 30% Ca was indicative of Wang et al.'s (2019) observations. The 7-day strengths indicated the C-2 series as the strongest Ca tangent line for early strength production, while the 28-day results indicated the C-2 series for optimum strength development. These results pointed to promising trends within the RBD geopolymer matrix, yet the rates of Ca substitution, reaction of all components, and prolonged curing times are still slightly unpredictable.

Provis and Bernal (2014) reported the process for the formation of hybrid gels that could take up to 180 days to form with ambient curing. The inclusion of calcium in N-A-S-H gel networks or sodium in C-A-S-H gel networks were discussed as potential alternatives to achieve the desired composition. This process can fluctuate in either direction depending on calcium saturation levels. While the exact timeframe for this process remains somewhat unknown, compressive strengths produced after 28 days of ambient curing may be higher due to increased chain compatibility and conversion.

Stabilization of gel interactions at 28 days produced the highest compressive strength samples closer to the (N, C)-A-S-H, while 7-day stabilization was found to be nearer to the (C, N)-A-S-H region. The 7-day samples displayed an optimal Ca tangent for C-2 and suggested (N, C)-A-S-H and (C, N)-A-S-H compatibilities are early stages, then switching to a more (N, C)-A-S-H dominant phase. This is counterintuitive to Provis and Bernal's (2014) observations and can be better explained with oven-cured specimens.

For an accurate assessment, oven-cured samples were evaluated for their capability to catalyze geopolymerization when exposed to elevated temperatures. Variations in concentrations, gel compatibility, and conversion could be bypassed by hastening the RBD geopolymer mixtures. Figure 4-13 displays the ternary diagram for oven-cured samples and their corresponding compressive strengths. The oven-cured samples did not demonstrate a dual planar trend. The stronger samples were scattered across each series. The highest compressive strength was observed at C-2-2, followed by C-3-3 on the 30% Ca and 16% Al content tangents. Moreover, the third highest compressive strength for C-1-3 could be found along the 16% Al content tangent. Should C-2-2 be absent, the tendency

76

for the oven-cured samples would have been in line with the 16% Al content tangent as opposed to the 12% Al content tangent utilized for 7-day and 28-day values.
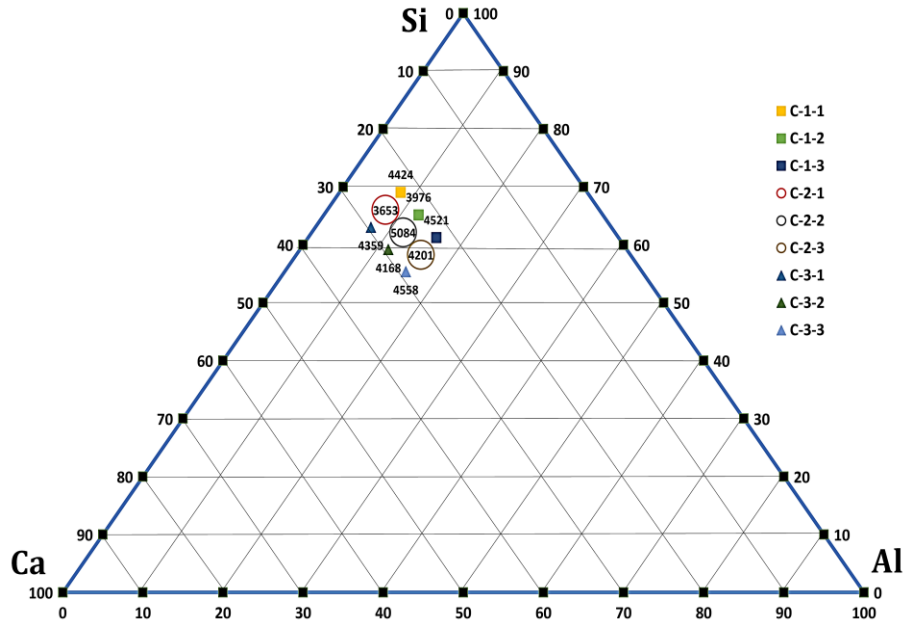
Figure 4-13: Ternary Diagram With Oven-Cured Compressive Strengths

Oven-cured samples enabled full utilization of the components in the RBD geopolymer mixtures, leading to comparative results between 7-day and 28-day strength data. The 7-day results featured stronger samples along the 26% Ca and 12% Al content lines, while the 28-day window showed sluggish strength development from its preceding stage. It is likely that strength development would continue under the slower reactive N-A-S-H-based chains. The calcium-rich environment, encouraging substitution and rearrangement, was never fully developed; however, only the 28-day curing limit was tested. The oven curing process accelerated geopolymerization, yet the anticipated results were not achieved.

The Ca-tangent displayed the highest compressive strengths, except for sample C-2-2. The Na-dominant chains responsible for late-stage strength development were overridden by the accelerated curing process, disrupting the (N, C)-A-S-H and (C, N)-A-S-H compatibility zone along series C-2. This caused an alteration of oven-cured compressive strength outcomes, resulting in better performance for samples near the C-A-S-H dominant zone. To help justify unreacted material in the RBD geopolymer mixtures, the 7-day and 28-day ambient-cured specimens were investigated against their oven-cured versions. The aim was to verify curing penetration into the inner cores.

4.2.3 Visual Examination of Promising RBD Geopolymer Mixtures

Calorimetry results, compressive strength tests, and ternary diagrams provided avenues of empirical validation for optimized RBD geopolymer blends. Beyond these tests, a simple visual inspection can help to determine if the RBD geopolymer mixtures were still curing. Figure 4-14, Figure 4-15, and Figure 4-16 show series C-1 after uniaxial compression tests for 7-day ambient-cured, 28-day ambient-cured, and oven-cured samples, respectively.
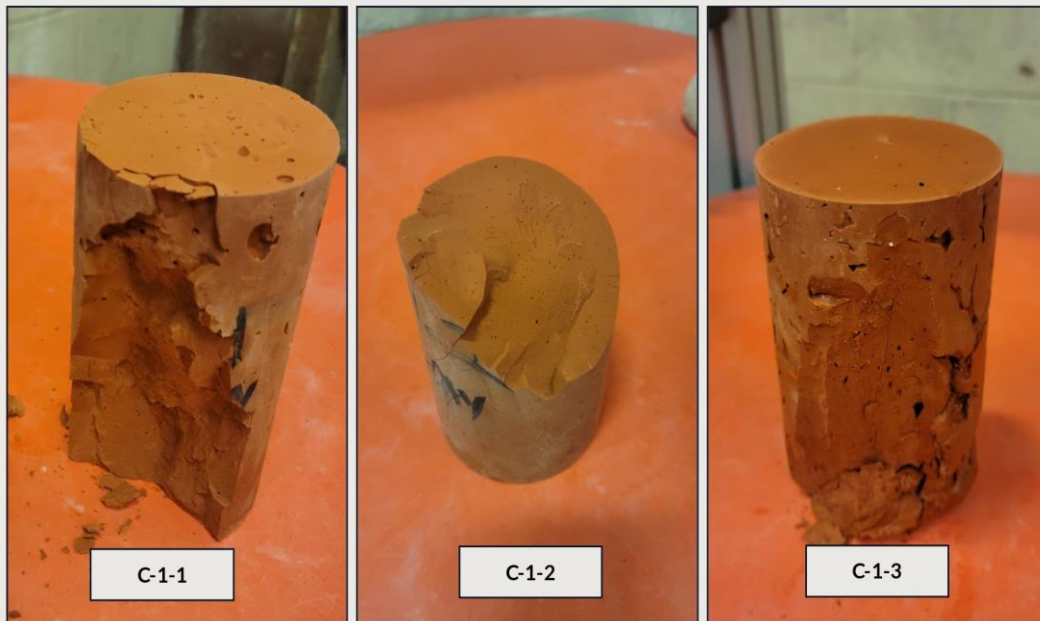
Figure 4-14: Images of 7-Day Ambient-Cured C-1 Series
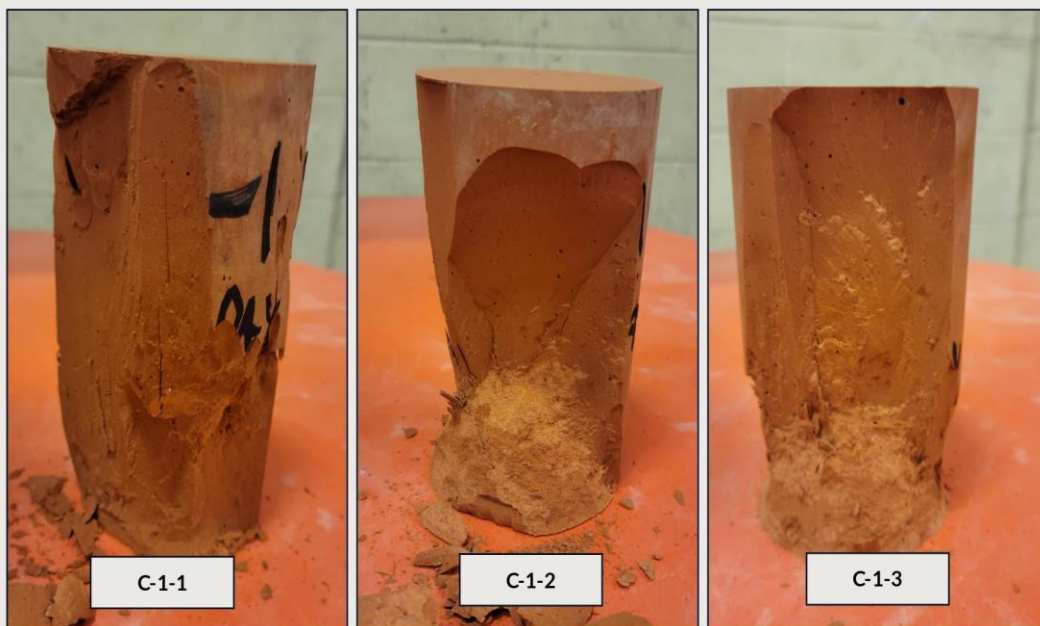
Figure 4-15: Images of 28-Day Ambient-Cured C-1 Series
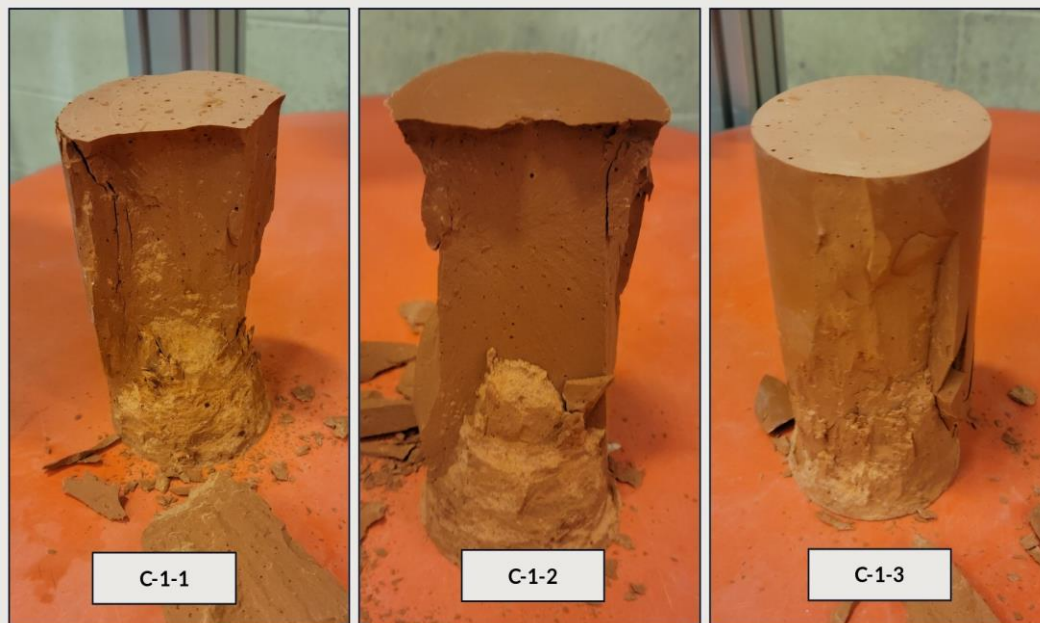
Figure 4-16: Images of Oven-Cured C-1 Series

It is evident from the images that the material that has yet to dry features a deeper shade of red, whereas the material that has already hardened displays a lighter hue. The 7-day samples of C-1 predominantly feature an inner core of dark red. Meanwhile, the 28-day samples depict a transition from dark red to a lighter tint as drying further penetrates the core. The oven-cured strength points to even more drying around the inner cores. Compared to the levels seen in 7-day and oven-cured samples, the 28-day samples still had a way to go in terms of development; in this regard, the inner cores were characterized as "wet." The 7-day samples constituted an extreme example of wetness, while the oven-cured samples represented its antithesis. The 28-day samples were between these two boundaries, with most of the inner cores still needing additional curing time.

Figure 4-17, Figure 4-18, and Figure 4-19 show the 7-day ambient-cured, 28-day ambient-cured, and oven-cured images for series C-2, respectively. These samples showed

the same drying spectrum from 7-day strength to oven-cured strength. The 7-day strength specimens were the least developed, and the oven-cured category served as the most developed. The 28-day samples for C-2 showed less drying penetration than those from series C-1, attesting to a lack of full-strength development. The underdeveloped inner cores of the specimens indicated stagnation within the RBD geopolymer mixture, which shows in the decreased 28-day compressive strengths for C-2 compared to C-1.
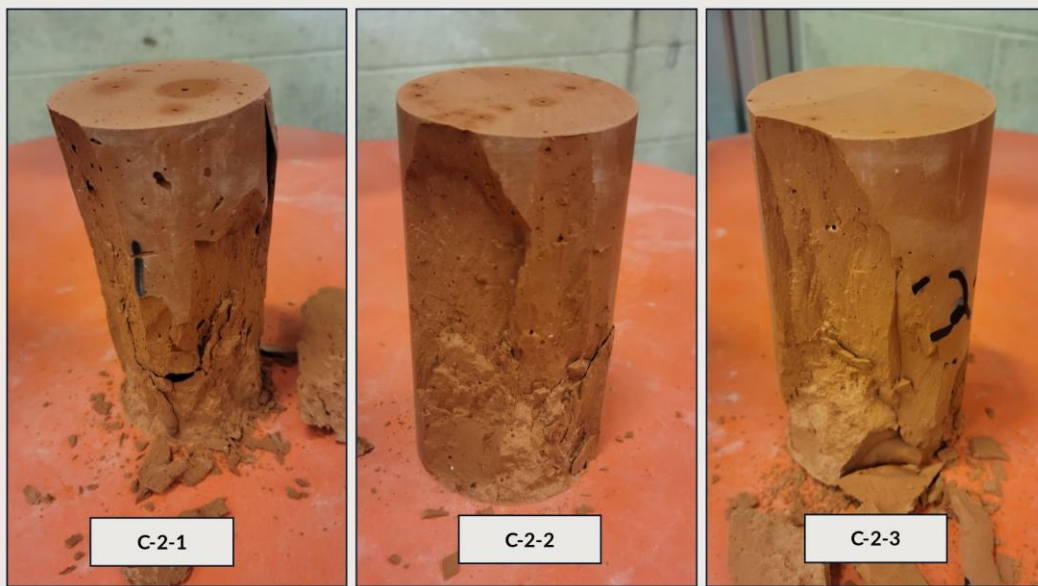
Figure 4-17: Images of 7-Day Ambient-Cured C-2 Series
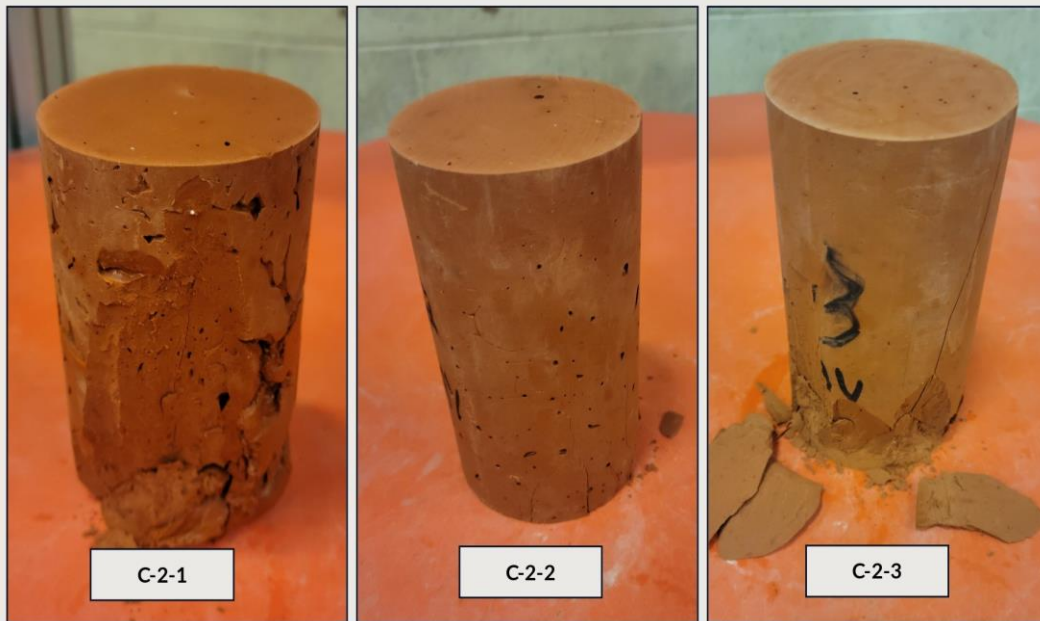
Figure 4-18: Images of 28-Day Ambient-Cured C-2 Series
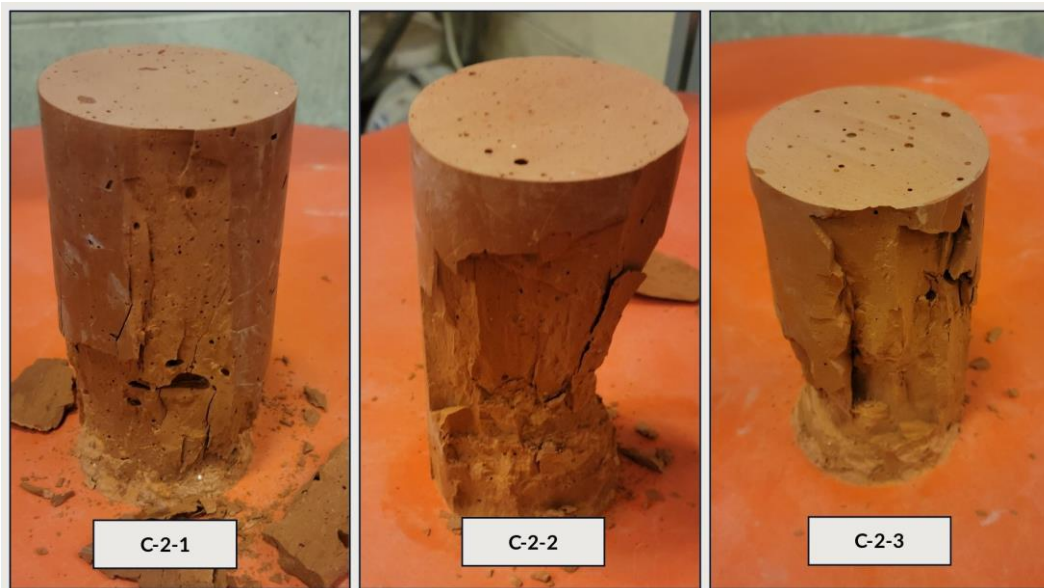
Figure 4-19: Images of Oven-Cured C-2 Series

The 7-day ambient-cured samples for series C-3 are shown in Figure 4-20, along with the 28-day samples in Figure 4-21, and the oven-cured samples in Figure 4-22. The pattern of decreasing curing penetration can be seen for C-3 compared to C-2 and C-1. The compressive strengths were also the lowest in each category for series C-3, except for the oven-cured samples. The oven-cured samples produced higher compressive strengths than C-1 and C-2, with C-2-2 being another exception.

The observed decrease in compressive strengths for each series and corresponding calorimetry results mimicked wetness levels in the samples. The increased wetness indicated oversaturation limits corresponding to falling 7-day and 28-day compressive strengths with plateaued calorimetry peaks. Excessive calcium and alumina components seemed to stall the curing process for these categories while increasing the compressive strengths for the oven-cured category. Visual inspection was adequate for determining the relative dryness of the samples, yet microscopic imaging would be necessary for the identification of unreacted portions within the RBD geopolymer matrix. This was outside the scope of this research, causing assumptions to be based on unmagnified visual analysis.
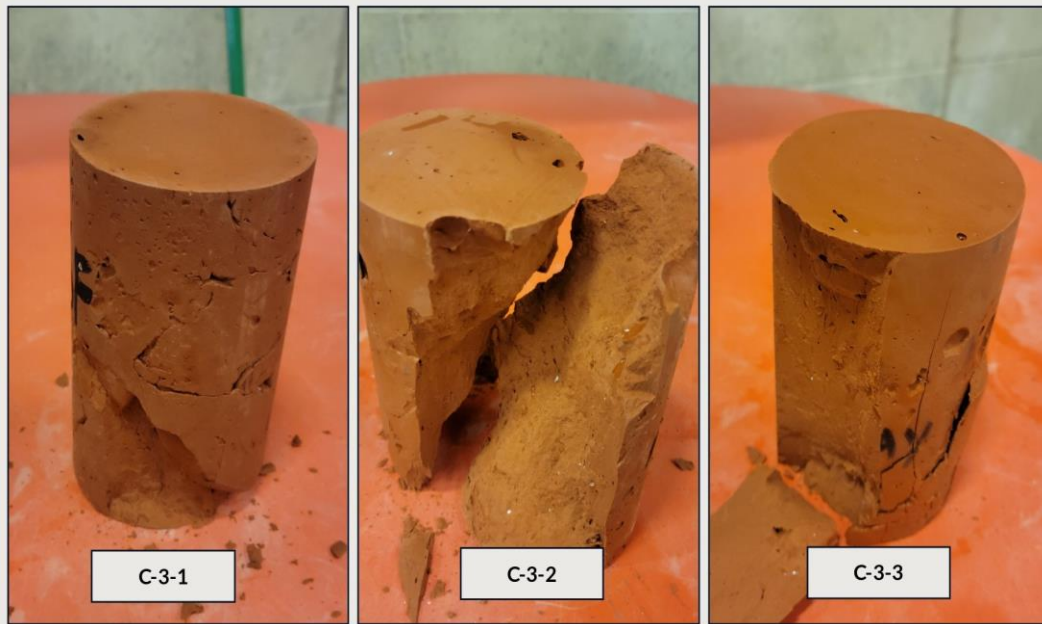
Figure 4-20: Images of 7-Day Ambient-Cured C-3 Series
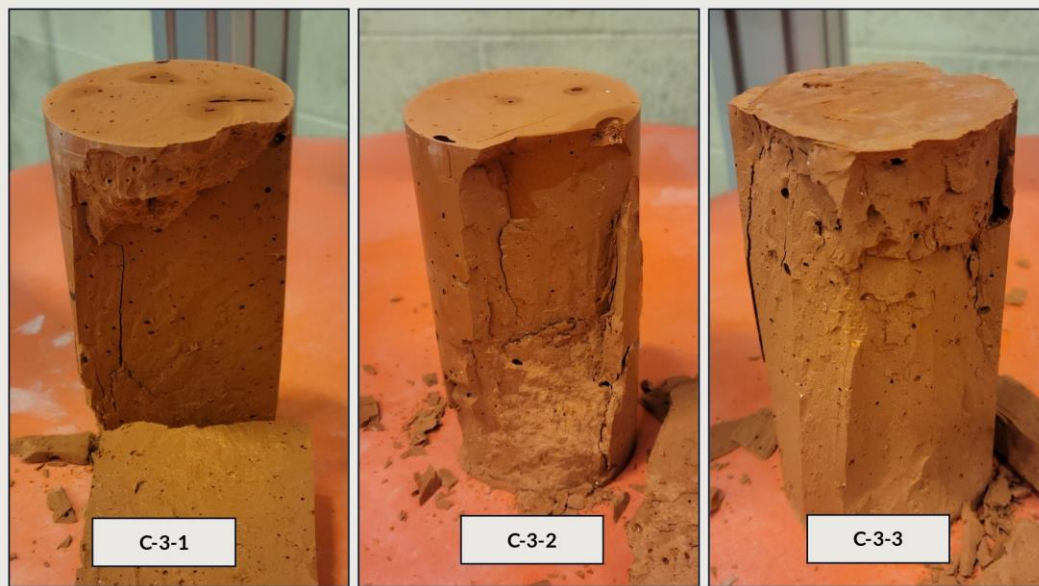
Figure 4-21: Images of 28-Day Ambient-Cured C-3 Series
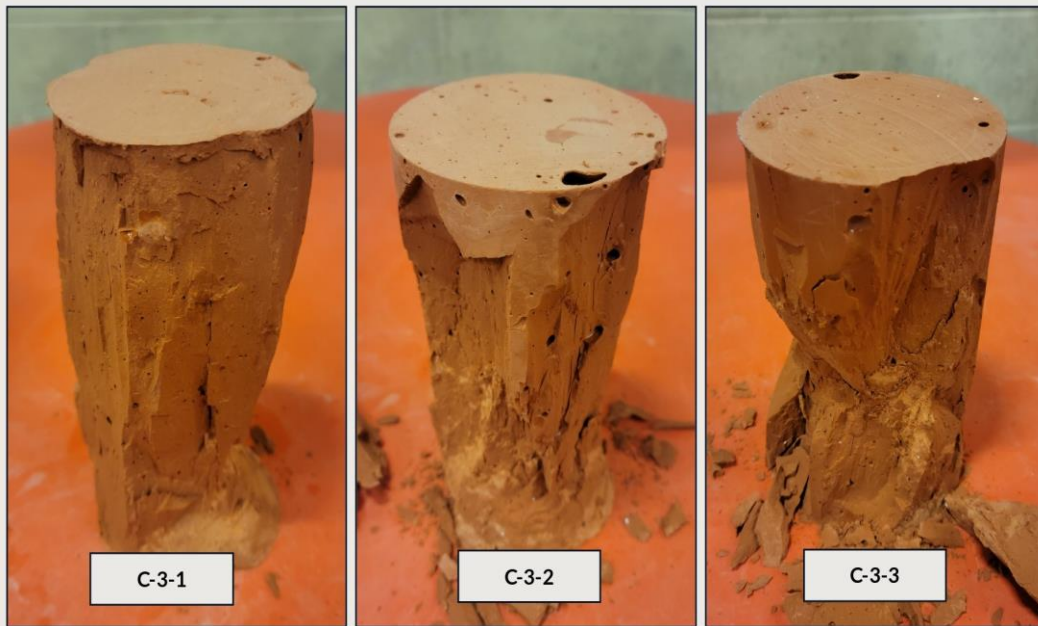
Figure 4-22: Images of Oven-Cured C-3 Series

Chapter 5: Conclusions and Recommendations

The original approach to the maximum compressive strength zone was based on Ancient Roman concrete. The tobermorite-like structures in the Ancient Roman concrete made it an ideal target for molar ratios. The lime clast sites in the hydrologic mortar produced C-A-S-H sites not seen in modern-day concrete. These C-A-S-H gels were hypothesized to produce additional strength over time and were thought to be the main mechanism behind Ancient Roman concrete's strength (Jackson et al., 2013; Jackson et al., 2017).

Empirical results from the 2"x2" mortar series revealed a maximum compressive strength zone outside the C-A-S-H or N-A-S-H region, instead located in the hybrid gel region. Garcia-Lodeiro et al. (2011) and Luo et al. (2023) offered valuable insights into theoretical hybrid gel production zones, which were integrated with ternary diagrams to direct the 3"x6" cylinder series. Visual inspections, calorimetry results, and compressive strength tests allowed for a discussion on gel formation within the specimens.

Unmagnified visual inspections were used, and validation of gel production was conducted using justified approaches and sound judgment. The 3"x6" cylinders' compressive strengths were based on 7-day ambient-cured, 28-day ambient-cured, and oven-cured conditions. Due to the retarding nature of excessive hydrated lime or alumina, the specimens displayed varying degrees of drying penetration, correlating to higher or lower compressive strengths with plateaued calorimetry heat spikes.

5.1 Conclusions

The following conclusions were determined based on the results and observations laid out in this report; a more in-depth discussion follows the list below:

- Sample C-2-2 outperformed the others in 2 out of 3 categories and was considered optimized.

- Compatibility in (N, C)-A-S-H and (C, N)-A-S-H gels was most likely responsible for increased strength properties.

- Unreacted RBD seemed to be the main cause of lower than expected 28-day compressive strengths.

- Sample C-1-2 and C-2-2 were at or near the optimized 28-day compressive strength goal (3000 psi) set by ACI Standard 318-19 (2019).

5.1.1 N-A-S-H, C-A-S-H, and Hybrid Gel Discussion

N-A-S-H, C-A-S-H, and hybrid gel production were assumed based on the ternary diagrams provided by Garcia-Lodeiro et al. (2011) and Luo et al. (2023). The ternary overlays allowed for a visual representation of production zones and boundary limits. These zones were used to explain which gel formation was occurring within the RBD geopolymer mixture and were integral for identifying changes in compressive strengths. N-A-S-H and C-A-S-H gel production was at the extremes of the ternary diagrams and were not reached in this research. The hybrid zones of (N, C)-A-S-H and (C, N)-A-S-H gel production became the areas of interest after the 2"x2" mortar series. Ternary diagrams for

these specimens showed the highest 28-day compressive strength values near the (N, C)-A-S-H region.

The (N, C)-A-S-H region was used as the upper boundary, with alumina contents shifting between specimens. This boundary zone then spreads out to a lower limit representing the edge of the (C, N)-A-S-H zone. Results from the 3"x6" cylinder series showed a maximum compressive strength for 7 days, for the C-2 series with 26% Ca. The second highest 7-day compressive strengths were found in the C-1 series, at 23% Ca, closer to the (N, C)-A-S-H zone. The Na-dominant hybrid gel for the C-1 series was hypothesized by Wang et al.'s (2019) to produce lower initial compressive strength due to the nature of Na-dominant chains leading to late-stage strength or Ca-dominant interactions causing earlier strength development. It was noted that (N, C)-A-S-H gels followed closer to N-A-S-H gel trends, while (C, N)-A-S-H gels trended with C-A-S-H gel behavior. Conclusions were made based on these underlying principles.

The 7-day samples for C-3 produced the lowest compressive strengths, even though it was closest to the C-A-S-H region. There was an increase in compressive strengths from C-1 to C-2, then an equilibrium shift occurred. The samples for the 7-day C-3 series reached an oversaturation limit compared to the others. This explained the increasing strengths along the Ca tangent from C-1 to C-2, maximizing in the C-2 series, then decreasing with further addition of Ca components. Also, the alumina content stalled the RBD geopolymer matrix and reduced the 7-day compressive strengths along the 8% or 16% Al tangent, except for the C-1 series. Within Series C-1, an opposite trend occurred, leading to higher 7-day compressive strengths for C-1 departing from the center 12% Al

tangent. Regardless, the strength results and calorimetry data indicated the 26% Ca and 12% Al contents as the optimized location for hybrid gel compatibility within the 7-day ambient curing window.

The 28-day samples displayed higher compressive strengths for the C-1 Series, suggesting there was enough time for N-A-S-H chains to start forming. The Si took longer than Ca to substitute into the gel chains during precipitation. This precipitation period proceeded based on the Ca concentrations after dissolution and continued through the 28-day ambient curing window. After the concentrations of Ca reduced, N-A-S-H gels began to form, and long-term strength development began (Luo et al., 2023).

Analysis of the 28-day compressive strength results revealed that Series C-1 had the highest value compared to C-2 or C-3. Further investigation demonstrated that the 23% Ca content tangent produced the highest strength, along with the 12% Al tangent being the optimum Al content. The specimens closest to the (N, C)-A-S-H region also exhibited better compressive strength than those nearer to the (C, N)-A-S-H zone. This illustrates that a longer curing period enabled the formation of a Na-dominant hybrid gel in contrast to the 7-day observations. In addition, those located farther away from the (N, C)-A-S-H zone lacked sufficient curing time to fully benefit from the available components, leading to weaker 7-day compressive strengths. The balanced mechanism within the hybrid gel system allowed for (N, C)-A-S-H gels to be formed without interference from C-A-S-H chains, thereby enhancing compressive strengths in the C-1 series.

Oven-cured samples demonstrated an increase in gel production when exposed to higher temperatures during the curing process. The compressive strength results for each

specimen varied, with C-2-2 being the strongest. Both C-1 and C-3 showed similar results and trends when compared. The oven-cured compressive strengths for specimens in C-1 were not substantially different than those in C-3. However, the 8% Al content tangent of the C-2 series showed a lower oven-cured compressive strength compared to the other series. The oven-cured compressive strengths of C-2-3 were comparable to those of C-1-3 and C-3-3, indicating similar compressive strength results for both (N, C)-A-S-H and (C, N)-A-S-H samples. However, there was a zone in the center of the oven-cured samples with abnormal strength characteristics, which warranted further investigation.

Sample C-2-2, with a dual planar tangent of 26% Ca and 12% Al content, displayed the best compressive strength results after 7-day ambient curing. Despite this, the 23% Ca and 12% Al content tangents for C-1-2 achieved a higher strength result after 28 days. The oven-cured samples bypassed the usual formation processes, leading to higher compressive strengths and accelerated gel formation behavior. The additional heat promoted fast strength development in the oven-cured samples and exhibited an increase in compressive strengths for the C-2 series. Luo et al. (2023) suggested the (N, C)-A-S-H and (C, N)-A-S-H gels can wrap around each other, forming stronger binder agents compared to individual parts. Sample C-2-2 achieved the highest oven-cured compressive strength during testing, suggesting hybrid gel compatibility as a viable explanation.

5.1.2 28-Day Compressive Strength Feasibility

The N-A-S-H, C-A-S-H, and hybrid gel chains remained in fluctuation during the 28-day curing window. Upon formation of Ca-dominant gel chains, there was a corresponding

reduction in available Ca components, especially when the rate of dissolution was surpassed by precipitation. Walkey et al. (2016) observed that hybrid gels tended to be limited with alumina cross-linking, prompting the production of N-A-S-H gels with lower Ca and higher Al levels. As Ca levels became less saturated, (N, C)-A-S-H and N-A-S-H mechanisms were enabled, allowing for later-stage strength development.

The later stage strength development and hybrid gel finalization exceeded the 7-day ambient curing window and was underdeveloped by the 28-day compressive strength tests. Oven curing of the samples hastened this process and enabled strength development within a 24-hour period at 150 ˚F. This prompted the geopolymerization process and circumvented the typical complications in hybrid gel formations. Shown in Table 5-1, samples C-1-2, C-2-2, and C-3-2 were selected for optimized 7-day, 28-day, and oven-cured strength conditions. C-1-2 had the highest 28-day compressive strength with the lowest 7-day and oven-cured strengths. C-2-2 had 170 psi lower 28-day compressive strength than C-1-2, yet there was a 1110 psi increase for the oven-cured compressive results. For the same readings in the ambient and oven curing categories, additional time is needed for the curing process, or augmented heat is necessary during batching.

Table 5-1: Comparative Review of Representative Samples

Sample	7-Day Strength (psi)	28-day Strength (psi)	Oven-Cured Strength (psi)
C-1-2	880	3070	3980
C-2-2	1080	2900	5080
C-3-2	930	2320	4170

The visual inspections revealed that the 28-day ambient-cured samples had not completely dried internally within the 28-day curing window (visually observable as internal "wetness" of the samples after compressive testing). The 28-day curing duration is the industry norm and was the focus of this RBD geopolymer research. In addition, the 28-day curing window was established by ACI Standard 318-19 (2019), along with the minimum compressive strength of 3000 psi shown in Table 5-1. The aim was to achieve a 3000 psi benchmark to cover additional categories outside the General category for minimum f'_c limits. The 2500 psi limit was set as the lower boundary, while the 3000-psi mark established the desired threshold.

Table 5-2: Limits for f'_c (ACI Standard 318-19, 2019)

Application	Minimum f'_c, psi
General	2500
Foundations for structures assigned to SDC A, B, or C	2500
Foundations for Residential and Utility use and occupancy classification with stud bearing wall construction two stories or less assigned to SDC D, E, or F	2500
Foundations for structures assigned to SDC D, E, or F other than Residential and Utility use and occupancy classification with stud bearing wall construction two stories or less	3000
Special moment frames Special structural walls with Grade 60 or 80 reinforcement	3000

The results of the analysis demonstrated that the compressive strength decreased gradually as the gel zones moved away from (N, C)-A-S-H while under 28-day ambient conditions. Sample C-1-2 reached the 3000 psi mark, while the other samples fell short. Nonetheless, the oven-cured versions exhibited higher compressive strengths due to the

combination of both hybrid gels through an accelerated geopolymerization process. This implied that a 28-day ambient curing cycle was inadequate, and that the initial heat production was lacking. The 2500 psi lower boundary was achieved in C-1-2 and C-2-2, yet only one specimen met the desired 3000 psi benchmark.

Provis and Bernal (2014) and Walkey et al. (2016) noticed a significant alteration in the crystalline structure of their geopolymer beyond the 28-day ambient curing period, with some changes occurring up to 180 days. This prolonged curing duration was understood to be a result of the reactivity of the aluminosilicate material, as well as the alkali concentrations and constituent availability. Consequently, these discoveries explained the underperforming compressive strength performance of the 28-day samples, including the "wetness" levels identified through visual inspections. With the assistance of the calorimetry results, it is possible to infer stagnation of elements or an excessive amount of Ca or Al within the RBD geopolymer mixture.

The 28-day curing window was lacking for low-reactive aluminosilicate sources, such as RBD. The added components displayed higher bioavailability than the RBD, yet saturation issues slowed the curing process as the gel chains were forming and adjusting. The ability of the RBD geopolymer matrix to continue building gel chains was evident, along with increased compressive strength from hybrid chain compatibility. Further research is needed to verify 28-day feasibility and accelerate ambient curing to satisfy a 28-day curing window.

5.2 Recommendations

The following recommendations were determined based on the results and observations laid out in this report; a more in-depth discussion follows the list below:

- The use of ground-granulated blast furnace slag, fly ash, or ordinary Portland cement for a highly reactive calcium source.

- Extension of the 28-day ambient curing window and exploration of the hybrid gel theory to allow for additional strength production throughout the RBD geopolymer lifecycle.

5.2.1 Base Material Recommendations

The low-reactive nature of the RBD can be improved with the addition of a highly bioavailable calcium source. The increased dissolution rate will produce additional heat and drive the geopolymerization process more quickly. Materials like ground granulated blast furnace slag (GGBFS), fly ash, and ordinary Portland cement (OPC) could be used to improve strength conditions and gel production. These materials will provide C-A-S-H gel production, which will cannibalize the available Ca content from the initial precipitation phase and allow long-term strength development through N-A-S-H gels to proceed more efficiently (Provis and Bernal, 2014).

It is recommended to replace limestone with GGBFS or fly ash as the calcium source in the RBD geopolymer mix. The goal is to avoid the use of OPC and satisfy the environmental aspect of this research. The 6% hydrated lime content should remain fixed; however, the alumina content needs to be adjusted depending on the material chosen. Fly

ash provides additional bioavailable calcium and alumina simultaneously, while GGBFS requires extra alumina to be added for optimal chain formation. The selection of alumina content will differ depending on the material used; a calcium-forward approach must be taken for GGBFS, while fly ash would require an alumina-forward approach. Ultimately, the best material to use for further research depends on its availability and compatibility with the RBD geopolymer matrix.

5.2.2 Ambient Curing Window Recommendations

With observations and research indicating a strength development window outside the 28-day window, further research should investigate the 56-day, 84-day, and 112-day curing windows to verify the limits of compressive strength production. This continued pattern of compressive strength increase has been shown in geopolymers and Ancient Roman concrete. C-A-S-H gel creation, found in hydraulic cement in contact with seawater, was shown by Jackson et al. (2013) to also produce long-term durability and increased strength over time. Combined with N-A-S-H gels' late-stage compressive strength development, there can be notable long-term potential for RBD geopolymer mixtures cured past the 28-day window.

The implications suggest that 28-day samples of RBD geopolymer mixture with around 3000 psi, such as C-1-2 or C-2-2, would have continued strength increases after the 28-day window. Therefore, RBD geopolymers have shown the potential to support the minimum concrete strength of 2500 psi and could continue developing strength over time. Late-stage strength may conflict with the maximum limits established in the ACI Standard

318-19 (2019), and additional measures will need to be taken to adjust for the possibilities. For now, the replacement of OPC with a low-reactive aluminosilicate, such as RBD, has proven viable for general construction. Additional research is needed for structural applications, flexural strength, gel formation verification, and environmental safety.

References

ACI Standard 318-19, 2019, "Building Code Requirements for Structural Concrete; Commentary on Building Code Requirements for Structural Concrete," <u>American Concrete Institute</u>, Farmington Hills, MI, pp. 355-369.

ASTM Standard C39/C39M, 2021, "Standard Test Method for Compressive Strength of Cylindrical Concrete Specimens," <u>ASTM International</u>, West Conshohocken, PA.

ASTM Standard C109/C109M, 2021, "Standard Test Method for Compressive Strength of Hydraulic Cement Mortars (Using 2-in. or [50 mm] Cube Specimens)," <u>ASTM International</u>, West Conshohocken, PA.

ASTM Standard C192/C192M, 2019, "Standard Practice for Making and Curing Concrete Test Specimens in the Laboratory," <u>ASTM International</u>, West Conshohocken, PA.

ASTM Standard C305, 2020, "Standard Practice for Mechanical Mixing of Hydraulic Cement Pastes and Mortars of Plastic Consistency," <u>ASTM International</u>, West Conshohocken, PA.

ASTM Standard C1753/C1753M, 2021, "Standard Practice for Evaluating Early Hydration of Hydraulic Cementitious Mixtures Using Thermal Measurements," <u>ASTM International</u>, West Conshohocken, PA.

Davidovits, J., <u>Geopolymer: Chemistry and Applications</u>, 5th ed., Institut Géopolymère, Saint-Quentin, France, 2020, pp. 3-7, 152-157, 185, 190-193, 200, 201, 219, 221-231, 239, 243-245.

Firdous, R., and Stephan, D., "Effect of Silica Modulus on the Geopolymerization Activity of Natural Pozzolans," <u>Construction & Building Materials</u>, Vol. 219, 2019, pp. 31–43.

Garcia-Lodeiro, I., Palomo, A., Fernandez-Jimenez, A., and Macphee, D.E., "Compatibility Studies between N-A-S-H and C-A-S-H Gels: Study in the Ternary Diagram Na_2O-CaO-Al_2O_3-SiO_2-H_2O," <u>Cement and Concrete Research</u>, Vol. 41, No. 9, 2011, pp. 923–931.

Jackson, M.D., Moon, J., Gotti, E., Taylor, R., Chae, S.R., Kunz, M., Emwas, A., Meral, C., Guttmann, P., Levitz, P., Wenk, H., and Monteiro, P.J.M., "Material and Elastic Properties of Al-tobermorite in Ancient Roman Seawater Concrete," <u>Journal of the American Ceramic Society</u>, Vol. 96, No. 8, 2013, pp. 2598–2606.

Jackson, M.D., Mulcahy, S.R., Heng, C., Yao, L., Qinfei, L., Cappelletti, P., and Wenk, H., "Phillipsite and Al-tobermorite Mineral Cements Produced Through Low-Temperature Water-Rock Reactions in Roman Marine Concrete," <u>The American Mineralogist</u>, Vol. 102, No. 7, 2017, pp. 1435–1450.

Kalinkin, A.M., Gurevich, B.I., Myshenkov, M.S., Chislov, M.V., Kalinkina, E.V., Zvereva, I.A., Cherkezova-Zheleva, Z., Paneva, D., and Petkova, V., "Synthesis of Fly Ash-Based Geopolymers: Effect of Calcite Addition and Mechanical Activation," <u>Minerals (Basel)</u>, Vol. 10, No. 9, 2020, pp. 827.

Luo, Y., Brouwers, H., & Yu, Q., "Understanding the Gel Compatibility and Thermal Behavior of Alkali-Activated Class F Fly Ash/Ladle Slag: The Underlying Role of Ca Availability," <u>Cement and Concrete Research</u>, Vol. 170, 2023.

Mendenhall, W., and Sincich, T., "Estimation Using Confidence Intervals," <u>Statistics for Engineering and the Sciences</u>, 4th ed., CRC Press, Boca Raton, FL, 2016, pp. 288-367.

Nurruddin, M.F., Haruna, S., Mohammed, B.S., and Sha´aban, I.G., "Methods of Curing Geopolymer Concrete: A Review," <u>International Journal of Advanced and Applied Sciences</u>, Vol. 5, No. 1, 2018, pp. 31–36.

Provis, J., and Bernal, S., "Geopolymers and Related Alkali-Activated Materials," <u>Annual Review of Materials Research</u>, Vol. 44, No. 1, 2014, pp. 299–327.

Richardson, I.G., and Groves, G.W., "The Incorporation of Minor and Trace Elements into Calcium Silicate Hydrate (C-S-H) Gel in Hardened Cement Pastes," <u>Cement and Concrete Research</u>, Vol. 23, No. 1, 1993, pp. 131–138.

Robayo-Salazar, R.A., Mulford, A., Munera, J., and De-Gutiérrez, R.M., "Alternative Cements Based on Alkali-Activated Red Clay Brick Waste," <u>Construction & Building Materials</u>, Vol. 128, 2016, pp. 163–169.

Robayo-Salazar, R.A., Mejia-Arcila, J.M., and De-Gutierrez, R.M., "Eco-Efficient Alkali-Activated Cement Based on Red Clay Brick Wastes Suitable for the Manufacturing of Building Materials," <u>Journal of Cleaner Production</u>, Vol. 166, 2017, pp. 242–252.

Scrivener, K.L., John, V.M., and Gartner, E.M., "Eco-Efficient Cements: Potential Economically Viable Solutions for a Low-CO2 Cement-Based Materials Industry," <u>Cement and Concrete Research</u>, Vol. 114, 2018, pp. 2–26.

Taylor, H.F.W., "Proposed Structure for Calcium Silicate Hydrate Gel," <u>Journal of the American Ceramic Society</u>, Vol. 69, No. 6, 1986, pp. 464–467.

Tchakoute, K.H., Elimbi, A., Mbey, J.A., Ngally Sabouang, C.J., Njopwouo, D., "The Effect of Adding Alumina-Oxide to Metakaolin and Volcanic Ash on Geopolymer

Products: A Comparative Study," <u>Construction & Building Materials</u>, Vol. 35, 2012, pp. 960–969.

Temuujin, J., Van Riessen, A., and Williams, R., "Influence of Calcium Compounds on the Mechanical Properties of Fly Ash Geopolymer Pastes," <u>Journal of Hazardous Materials</u>, Vol. 167, 2009, pp. 82-88

Youssef, N., Rabenantoandro, A.Z., Dakhli, Z., Chapiseau, C., Waendendries, F., Hage Chehade, F., and Lafhaj, Z., "Reuse of Waste Bricks: A New Generation of Geopolymer Bricks," <u>SN Applied Sciences</u>, Vol. 1, 2019.

Walkley, B., San Nicolas, R., Sani, M., Rees, G., Hanna, J., Van Deventer, J., and Provis, J., "Phase Evolution of C-(N)-A-S-H/N-A-S-H Gel Blends Investigated Via Alkali-Activation of Synthetic Calcium Aluminosilicate Precursors," <u>Cement and Concrete Research</u>, Vol. 89, 2016, pp. 120-135.

Wang, Y., Alrefaei, Y., and Dai, J., "Silico-Aluminophosphate and Alkali-Aluminosilicate Geopolymers: A Comparative Review," <u>Frontiers in Materials</u>, Vol. 6, 2019.

Wong, C., Mo, K., Yap, S., Alengaram, U., and Ling, T., "Potential Use of Brick Waste as Alternate Concrete-Making Materials: A Review," <u>Journal of Cleaner Production</u>, Vol. 195, 2018, pp. 226-239.

Zhang, Z., Provis, J., Wang, H., Bullen, F., and Reid, A., "Quantitative Kinetic and Structural Analysis of Geopolymers; Part 2: Thermodynamics of Sodium Silicate Activation of Metakaolin," <u>Thermochimica Acta</u>, Vol. 565, 2013, pp. 163-171.

Appendix A – RBD Geopolymer Results for 2"x2" Mortar Cubes

Targets	Test 1	Test 2	Test 3	Test 4	Test 5
Sodium Silicate / NaOH Molar Ratio	3.81	3.05	2.00	3.81	3.05
Sodium Oxide/Silica Molar Ratio Op = 0.12	0.15	0.17	0.19	0.21	0.23
Ca/Si Molar Ratio Op = 0.8-1.2, max = 2.25	0.06	0.06	0.06	0.06	0.06
Ca/(Si+Al) Molar Ratio Op = 0.74-0.9	0.05	0.05	0.05	0.05	0.05
Si/Al Molar Ratio Op = 5.8-6.5 (2.0 for Phillipsite)	8.8	8.9	9.2	9.0	9.1
Al/Ca Molar Ratio Max = 0.15-0.25	1.83	1.83	1.83	1.83	1.83
Silica Modulus Op = 0.6-1.1 (From Solution only)	0.52	0.60	0.76	0.52	0.60
Sodium Silicate / NaOH Ratio by Weight	2.00	2.50	3.81	2.00	2.50
Alumina/Silica Molar Ratio, Max = 0.43	0.11	0.11	0.11	0.11	0.11
Compressive Strength 28 Days (psi) Ambient Dry	262	246	227	220	169
Compressive Strength (psi) Oven Dry	801	2421	979	2122	1991

Figure A-1: Molar Ratios and Compressive Strengths for Test 1-5

Targets	Test 6	Test 7	Test 8	Test 9
Sodium Silicate / NaOH Molar Ratio	2.00	3.81	3.05	2.00
Sodium Oxide/Silica Molar Ratio Op = 0.12	0.26	0.27	0.28	0.32
Ca/Si Molar Ratio Op = 0.8-1.2, max = 2.25	0.06	0.06	0.06	0.05
Ca/(Si+Al) Molar Ratio Op = 0.74-0.9	0.05	0.05	0.05	0.05
Si/Al Molar Ratio Op = 5.8-6.5 (2.0 for Phillipsite)	9.6	9.2	9.4	9.9
Al/Ca Molar Ratio Max = 0.15-0.25	1.83	1.83	1.83	1.83
Silica Modulus Op = 0.6-1.1 (From Solution only)	0.76	0.52	0.60	0.76
Sodium Silicate / NaOH Ratio by Weight	3.81	2.00	2.50	3.81
Alumina/Silica Molar Ratio, Max = 0.43	0.10	0.11	0.11	0.10
Compressive Strength 28 Days (psi) Ambient Dry	44	0	0	0
Compressive Strength (psi) Oven Dry	454	192	175	65

Figure A-2: Molar Ratios and Compressive Strengths for Test 6-9

Targets	Test L1	Test L2	Test L3	Test L4	Test L5
Sodium Silicate / NaOH Molar Ratio	3.81	3.05	3.81	3.05	3.05
Sodium Oxide/Silica Molar Ratio Op = 0.12	0.16	0.17	0.22	0.23	0.29
Ca/Si Molar Ratio Op = 0.8-1.2, max = 2.25	0.09	0.09	0.09	0.09	0.09
Ca/(Si+Al) Molar Ratio Op = 0.74-0.9	0.08	0.08	0.08	0.07	0.07
Si/Al Molar Ratio Op = 5.8-6.5 (2.0 for Phillipsite)	8.8	8.9	9.0	9.2	9.4
Al/Ca Molar Ratio Max = 0.15-0.25	1.21	1.21	1.21	1.21	1.21
Silica Modulus Op = 0.6-1.1 (From Solution only)	0.52	0.60	0.52	0.60	0.60
Sodium Silicate / NaOH Ratio by Weight	2.00	2.50	2.00	2.50	2.50
Alumina/Silica Molar Ratio, Max = 0.43	0.11	0.11	0.11	0.11	0.11
Compressive Strength 28 Days (psi) Ambient Dry	1318	1341	497	561	186
Compressive Strength (psi) Oven Dry	1304	1555	2151	2118	1390

Figure A-3: Molar Ratios and Compressive Strengths for Test L1-L5

Targets	Test L6	Test L7	Test L8	Test L9	Test L10
Sodium Silicate / NaOH Molar Ratio	3.81	3.05	3.81	3.05	3.05
Sodium Oxide/Silica Molar Ratio Op = 0.12	0.16	0.17	0.22	0.23	0.29
Ca/Si Molar Ratio Op = 0.8-1.2, max = 2.25	0.13	0.13	0.12	0.12	0.12
Ca/(Si+Al) Molar Ratio Op = 0.74-0.9	0.10	0.10	0.10	0.10	0.10
Si/Al Molar Ratio Op = 5.8-6.5 (2.0 for Phillipsite)	8.8	8.9	9.0	9.2	9.4
Al/Ca Molar Ratio Max = 0.15-0.25	0.89	0.89	0.89	0.89	0.89
Silica Modulus Op = 0.6-1.1 (From Solution only)	0.52	0.60	0.52	0.60	0.60
Sodium Silicate / NaOH Ratio by Weight	2.00	2.50	2.00	2.50	2.50
Alumina/Silica Molar Ratio, Max = 0.43	0.11	0.11	0.11	0.11	0.11
Compressive Strength 28 Days (psi) Ambient Dry	1333	1300	830	674	366
Compressive Strength (psi) Oven Dry	3132	1981	1541	1984	2132

Figure A-4: Molar Ratios and Compressive Strengths for Test L6-L10

Targets	Test L11	Test L12	Test L13	Test L14	Test L15
Sodium Silicate / NaOH Molar Ratio	3.81	3.05	3.81	3.05	3.05
Sodium Oxide/Silica Molar Ratio Op = 0.12	0.16	0.18	0.22	0.24	0.30
Ca/Si Molar Ratio Op = 0.8-1.2, max = 2.25	0.16	0.16	0.16	0.16	0.15
Ca/(Si+Al) Molar Ratio Op = 0.74-0.9	0.13	0.13	0.13	0.13	0.12
Si/Al Molar Ratio Op = 5.8-6.5 (2.0 for Phillipsite)	8.8	8.9	9.0	9.2	9.4
Al/Ca Molar Ratio Max = 0.15-0.25	0.70	0.70	0.70	0.70	0.70
Silica Modulus Op = 0.6-1.1 (From Solution only)	0.52	0.60	0.52	0.60	0.60
Sodium Silicate / NaOH Ratio by Weight	2.00	2.50	2.00	2.50	2.50
Alumina/Silica Molar Ratio, Max = 0.43	0.11	0.11	0.11	0.11	0.11
Compressive Strength 28 Days (psi) Ambient Dry	2346	1913	1415	1646	615
Compressive Strength (psi) Oven Dry	3160	2725	2392	2394	1911

Figure A-5: Molar Ratios and Compressive Strengths for Test L11-L15

Targets	Test LL1	Test LL2	Test LL3	Test LL4	Test LL5
Sodium Silicate / NaOH Molar Ratio	3.81	3.05	3.81	3.05	3.05
Sodium Oxide/Silica Molar Ratio Op = 0.12	0.19	0.20	0.25	0.27	0.34
Ca/Si Molar Ratio Op = 0.8-1.2, max = 2.25	0.34	0.34	0.33	0.33	0.32
Ca/(Si+Al) Molar Ratio Op = 0.74-0.9	0.28	0.28	0.27	0.27	0.26
Si/Al Molar Ratio Op = 5.8-6.5 (2.0 for Phillipsite)	8.9	9.0	9.1	9.3	9.6
Al/Ca Molar Ratio Max = 0.15-0.25	0.33	0.33	0.33	0.33	0.33
Silica Modulus Op = 0.6-1.1 (From Solution only)	0.52	0.60	0.52	0.60	0.60
Sodium Silicate / NaOH Ratio by Weight	2.00	2.50	2.00	2.50	2.50
Alumina/Silica Molar Ratio, Max = 0.43	0.11	0.11	0.11	0.11	0.10
Compressive Strength 28 Days (psi) Ambient Dry	3345	4493	3966	3387	2450
Compressive Strength (psi) Oven Dry	2858	3325	3100.5	3636.5	2770

Figure A-6: Molar Ratios and Compressive Strengths for Test LL1-LL5

Targets	Test LL6	Test LL7	Test LL8	Test LL9	Test LL10
Sodium Silicate / NaOH Molar Ratio	3.81	3.05	3.81	3.05	3.05
Sodium Oxide/Silica Molar Ratio Op = 0.12	0.22	0.23	0.29	0.31	0.39
Ca/Si Molar Ratio Op = 0.8-1.2, max = 2.25	0.58	0.57	0.56	0.55	0.53
Ca/(Si+Al) Molar Ratio Op = 0.74-0.9	0.48	0.47	0.46	0.45	0.44
Si/Al Molar Ratio Op = 5.8-6.5 (2.0 for Phillipsite)	9.0	9.2	9.3	9.5	9.8
Al/Ca Molar Ratio Max = 0.15-0.25	0.19	0.19	0.19	0.19	0.19
Silica Modulus Op = 0.6-1.1 (From Solution only)	0.52	0.60	0.52	0.60	0.60
Sodium Silicate / NaOH Ratio by Weight	2.00	2.50	2.00	2.50	2.50
Alumina/Silica Molar Ratio, Max = 0.43	0.11	0.11	0.11	0.11	0.10
Compressive Strength 28 Days (psi) Ambient Dry	2065	3000	2086	3137	2512
Compressive Strength (psi) Oven Dry	2672	3572	3670	3926	2129

Figure A-7: Molar Ratios and Compressive Strengths for Test LL6-LL10

Targets	Test LL11	Test LL12	Test LL13	Test LL14	Test LL15
Sodium Silicate / NaOH Molar Ratio	3.81	3.05	3.81	3.05	3.05
Sodium Oxide/Silica Molar Ratio Op = 0.12	0.26	0.27	0.35	0.37	0.45
Ca/Si Molar Ratio Op = 0.8-1.2, max = 2.25	0.91	0.89	0.88	0.85	0.82
Ca/(Si+Al) Molar Ratio Op = 0.74-0.9	0.75	0.73	0.72	0.71	0.68
Si/Al Molar Ratio Op = 5.8-6.5 (2.0 for Phillipsite)	9.1	9.3	9.4	9.7	10.1
Al/Ca Molar Ratio Max = 0.15-0.25	0.12	0.12	0.12	0.12	0.12
Silica Modulus Op = 0.6-1.1 (From Solution only)	0.52	0.60	0.52	0.60	0.60
Sodium Silicate / NaOH Ratio by Weight	2.00	2.50	2.00	2.50	2.50
Alumina/Silica Molar Ratio, Max = 0.43	0.11	0.11	0.11	0.10	0.10
Compressive Strength 28 Days (psi) Ambient Dry	2234	2976	2117	2063	1339
Compressive Strength (psi) Oven Dry	2634	2950	3178	3305	1872

Figure A-8: Molar Ratios and Compressive Strengths for Test LL11-LL15

Targets	Test LLA1	Test LLA2	Test LLA3	Test LLA4	Test LLA5
Sodium Silicate / NaOH Molar Ratio	3.81	3.05	3.81	3.05	3.05
Sodium Oxide/Silica Molar Ratio Op = 0.12	0.28	0.30	0.38	0.40	0.49
Ca/Si Molar Ratio Op = 0.8-1.2, max = 2.25	0.98	0.96	0.94	0.92	0.88
Ca/(Si+Al) Molar Ratio Op = 0.74-0.9	0.69	0.68	0.67	0.66	0.64
Si/Al Molar Ratio Op = 5.8-6.5 (2.0 for Phillipsite)	4.7	4.8	4.9	5.1	5.3
Al/Ca Molar Ratio Max = 0.15-0.25	0.22	0.22	0.22	0.22	0.22
Silica Modulus Op = 0.6-1.1 (From Solution only)	0.52	0.60	0.52	0.60	0.60
Sodium Silicate / NaOH Ratio by Weight	2.00	2.50	2.00	2.50	2.50
Alumina/Silica Molar Ratio, Max = 0.43	0.21	0.21	0.20	0.20	0.19
Compressive Strength 28 Days (psi) Ambient Dry	2176	2392	2553	2221	742
Compressive Strength (psi) Oven Dry	1688	2248	2109	3385	1555

Figure A-9: Molar Ratios and Compressive Strengths for Test LLA1-LLA5

Targets	Test LLA6	Test LLA7	Test LLA8	Test LLA9	Test LLA10
Sodium Silicate / NaOH Molar Ratio	3.81	3.05	3.81	3.05	3.05
Sodium Oxide/Silica Molar Ratio Op = 0.12	0.30	0.32	0.41	0.43	0.53
Ca/Si Molar Ratio Op = 0.8-1.2, max = 2.25	1.07	1.04	1.02	0.99	0.94
Ca/(Si+Al) Molar Ratio Op = 0.74-0.9	0.64	0.63	0.63	0.61	0.59
Si/Al Molar Ratio Op = 5.8-6.5 (2.0 for Phillipsite)	3.0	3.1	3.1	3.3	3.4
Al/Ca Molar Ratio Max = 0.15-0.25	0.31	0.31	0.31	0.31	0.31
Silica Modulus Op = 0.6-1.1 (From Solution only)	0.52	0.60	0.52	0.60	0.60
Sodium Silicate / NaOH Ratio by Weight	2.00	2.50	2.00	2.50	2.50
Alumina/Silica Molar Ratio, Max = 0.43	0.33	0.32	0.32	0.31	0.29
Compressive Strength 28 Days (psi) Ambient Dry	2038	2643	2377	2470	1186
Compressive Strength (psi) Oven Dry	1717	2046	1880	2372	1657

Figure A-10: Molar Ratios and Compressive Strengths for Test LLA6-LLA10

Targets	Test LLA11	Test LLA12	Test LLA13	Test LLA14	Test LLA15
Sodium Silicate / NaOH Molar Ratio	3.81	3.05	3.81	3.05	3.05
Sodium Oxide/Silica Molar Ratio Op = 0.12	0.34	0.35	0.45	0.47	0.57
Ca/Si Molar Ratio Op = 0.8-1.2, max = 2.25	1.17	1.14	1.12	1.08	1.02
Ca/(Si+Al) Molar Ratio Op = 0.74-0.9	0.60	0.59	0.58	0.57	0.56
Si/Al Molar Ratio Op = 5.8-6.5 (2.0 for Phillipsite)	2.1	2.2	2.2	2.3	2.4
Al/Ca Molar Ratio Max = 0.15-0.25	0.41	0.41	0.41	0.41	0.41
Silica Modulus Op = 0.6-1.1 (From Solution only)	0.52	0.60	0.52	0.60	0.60
Sodium Silicate / NaOH Ratio by Weight	2.00	2.50	2.00	2.50	2.50
Alumina/Silica Molar Ratio, Max = 0.43	0.48	0.46	0.46	0.44	0.42
Compressive Strength 28 Days (psi) Ambient Dry	1514	2430	1820	1928	405
Compressive Strength (psi) Oven Dry	1778	2260	2278	2174	1889

Figure A-11: Molar Ratios and Compressive Strengths for Test LLA11-LLA15

Targets	Test LLAO 1	Test LLAO 1-F	Test LLAO 2	Test LLAO 2-F	Test LLAO 3
Sodium Silicate / NaOH Molar Ratio	3.81	3.81	3.05	3.05	3.81
Sodium Oxide/Silica Molar Ratio Op = 0.12	0.17	0.17	0.18	0.18	0.24
Ca/Si Molar Ratio Op = 0.8-1.2, max = 2.25	0.17	0.17	0.16	0.16	0.16
Ca/(Si+Al) Molar Ratio Op = 0.74-0.9	0.12	0.12	0.12	0.12	0.12
Si/Al Molar Ratio Op = 5.8-6.5 (2.0 for Phillipsite)	5.7	5.7	5.7	5.7	5.8
Al/Ca Molar Ratio Max = 0.15-0.25	1.06	1.06	1.06	1.06	1.06
Silica Modulus Op= 0.6-1.1 (From Solution only)	0.52	0.52	0.60	0.60	0.52
Sodium Silicate / NaOH Ratio by Weight	2.00	2.00	2.50	2.50	2.00
Alumina/Silica Molar Ratio, Max=0.43	0.18	0.18	0.17	0.17	0.17
Compressive Strength 28 Days (psi) Ambient Dry	2779	2994	2305	2208	1575
Compressive Strength (psi) Oven Dry	2857	2463	2678	2222	1973

Figure A-12: Molar Ratios and Compressive Strengths for Test LLAO1-LLAO3

Targets	Test LLAO 3-F	Test LLAO 4	Test LLAO 4-F	Test LLAO 5	Test LLAO 5-F
Sodium Silicate / NaOH Molar Ratio	3.81	3.81	3.81	3.05	3.05
Sodium Oxide/Silica Molar Ratio Op = 0.12	0.24	0.18	0.18	0.20	0.20
Ca/Si Molar Ratio Op = 0.8-1.2, max = 2.25	0.16	0.26	0.26	0.25	0.25
Ca/(Si+Al) Molar Ratio Op = 0.74-0.9	0.12	0.19	0.19	0.19	0.19
Si/Al Molar Ratio Op = 5.8-6.5 (2.0 for Phillipsite)	5.8	5.5	5.5	5.6	5.6
Al/Ca Molar Ratio Max = 0.15-0.25	1.06	0.70	0.70	0.70	0.70
Silica Modulus Op= 0.6-1.1 (From Solution only)	0.52	0.52	0.52	0.60	0.60
Sodium Silicate / NaOH Ratio by Weight	2.00	2.00	2.00	2.50	2.50
Alumina/Silica Molar Ratio, Max=0.43	0.17	0.18	0.18	0.18	0.18
Compressive Strength 28 Days (psi) Ambient Dry	1313	2641	3203	3519	3096
Compressive Strength (psi) Oven Dry	1388	2986	3128	2867	2714

Figure A-13: Molar Ratios and Compressive Strengths for Test LLAO3F-LLAO5F

Targets	Test LLAO 6	Test LLAO 6-F	Test LLAO 7	Test LLAO 7-F	Test LLAO 8
Sodium Silicate / NaOH Molar Ratio	3.81	3.81	3.81	3.81	3.05
Sodium Oxide/Silica Molar Ratio Op = 0.12	0.25	0.25	0.20	0.20	0.21
Ca/Si Molar Ratio Op = 0.8-1.2, max = 2.25	0.25	0.25	0.36	0.36	0.35
Ca/(Si+Al) Molar Ratio Op = 0.74-0.9	0.19	0.19	0.26	0.26	0.26
Si/Al Molar Ratio Op = 5.8-6.5 (2.0 for Phillipsite)	5.7	5.7	5.4	5.4	5.5
Al/Ca Molar Ratio Max = 0.15-0.25	0.70	0.70	0.51	0.51	0.51
Silica Modulus Op= 0.6-1.1 (From Solution only)	0.52	0.52	0.52	0.52	0.60
Sodium Silicate / NaOH Ratio by Weight	2.00	2.00	2.00	2.00	2.50
Alumina/Silica Molar Ratio, Max=0.43	0.18	0.18	0.18	0.18	0.18
Compressive Strength 28 Days (psi) Ambient Dry	3763	3582	2582	3562	3066
Compressive Strength (psi) Oven Dry	3000	2983	2242	3207	2885

Figure A-14: Molar Ratios and Compressive Strengths for Test LLAO6-LLAO8

Targets	Test LLAO 8-F	Test LLAO 9	Test LLAO 9-F
Sodium Silicate / NaOH Molar Ratio	3.05	3.81	3.81
Sodium Oxide/Silica Molar Ratio Op = 0.12	0.21	0.27	0.27
Ca/Si Molar Ratio Op = 0.8-1.2, max = 2.25	0.35	0.35	0.35
Ca/(Si+Al) Molar Ratio Op = 0.74-0.9	0.26	0.26	0.26
Si/Al Molar Ratio Op = 5.8-6.5 (2.0 for Phillipsite)	5.5	5.6	5.6
Al/Ca Molar Ratio Max = 0.15-0.25	0.51	0.51	0.51
Silica Modulus Op= 0.6-1.1 (From Solution only)	0.60	0.52	0.52
Sodium Silicate / NaOH Ratio by Weight	2.50	2.00	2.00
Alumina/Silica Molar Ratio, Max=0.43	0.18	0.18	0.18
Compressive Strength 28 Days (psi) Ambient Dry	3603	2764	2659
Compressive Strength (psi) Oven Dry	3288	3095	3340

Figure A-15: Molar Ratios and Compressive Strengths for Test LLAO8F-LLAO9F
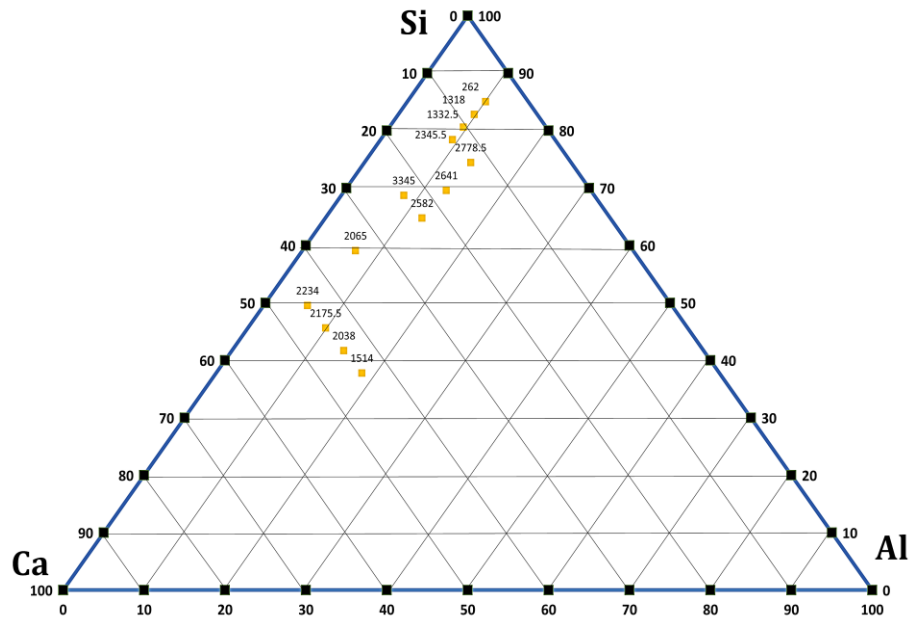
Figure A-16: Ternary Diagram of 28-Day Compressive Strengths for 5M NaOH-2.0 Series
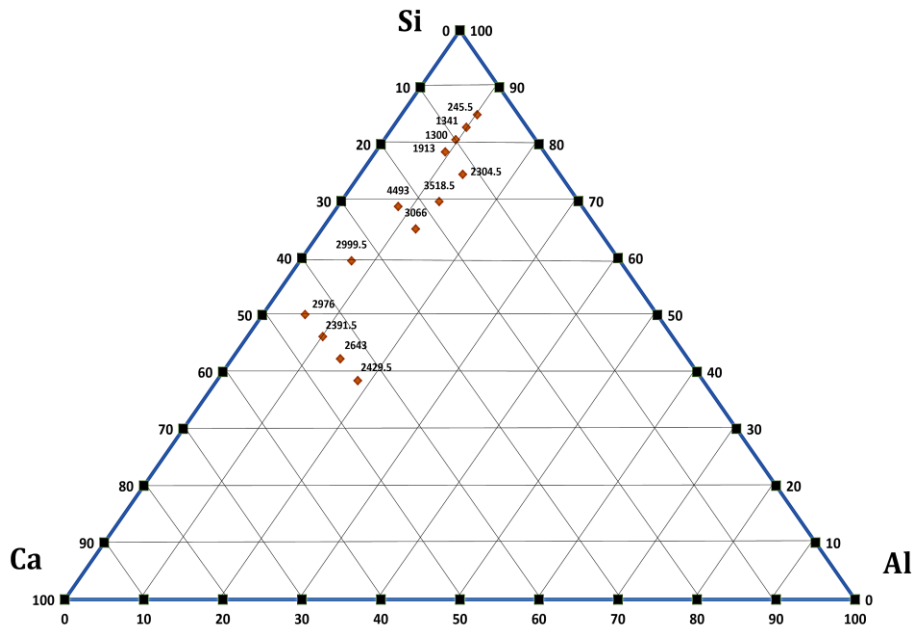
Figure A-17: Ternary Diagram of 28-Day Compressive Strengths for 5M NaOH-2.5 Series
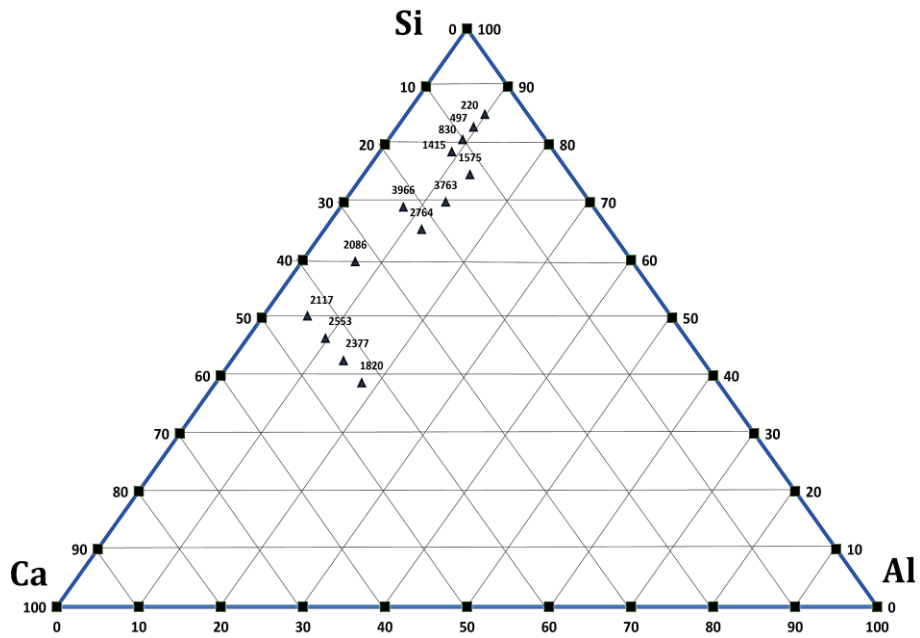
Figure A-18: Ternary Diagram of 28-Day Compressive Strengths for 7M NaOH-2.0 Series
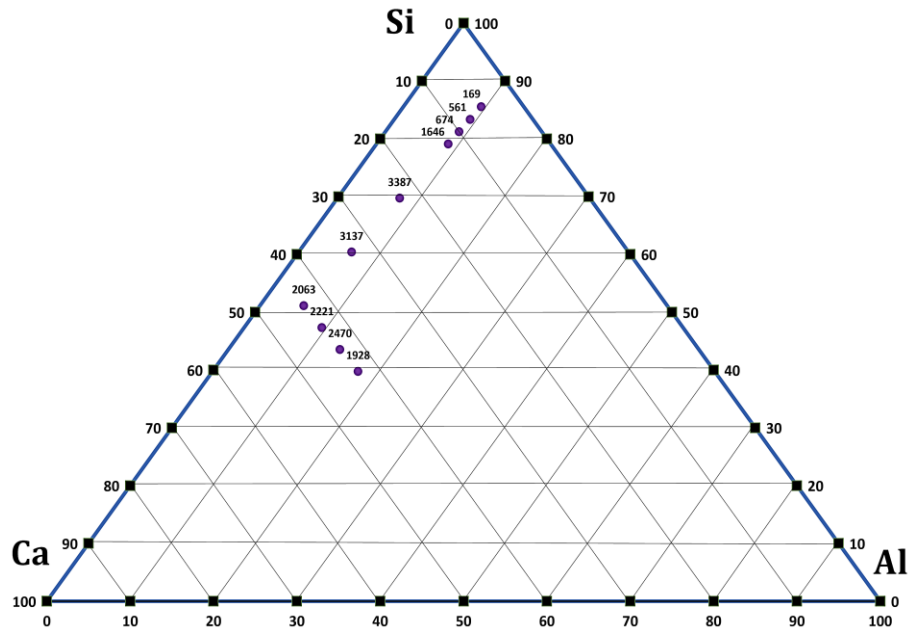
Figure A-19: Ternary Diagram of 28-Day Compressive Strengths for 7M NaOH-2.5
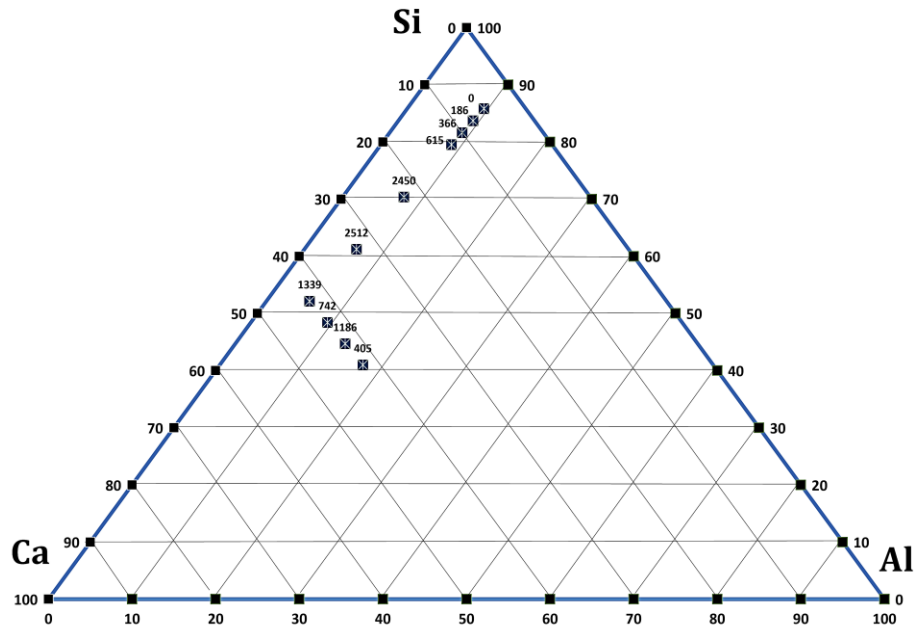
Figure A-20: Ternary Diagram of 28-Day Compressive Strengths for 9M NaOH-2.5

Appendix B – RBD Geopolymer Results for 3"x6" Cylinders

Targets	Test C-1-1	Test C-1-2	Test C-1-3
Sodium Silicate / NaOH Molar Ratio	3.05	3.05	3.05
Sodium Oxide/Silica Molar Ratio Op = 0.12	0.16	0.17	0.18
Ca/Si Molar Ratio Op = 0.8-1.2, max = 2.25	0.34	0.35	0.37
Ca/(Si+Al) Molar Ratio Op = 0.74-0.9	0.28	0.26	0.24
Si/Al Molar Ratio Op = 5.8-6.5 (2.0 for Phillipsite)	9.0	5.5	3.8
Al/Ca Molar Ratio Max = 0.15-0.25	0.33	0.51	0.70
Silica Modulus Op= 0.6-1.1 (From Solution only)	0.76	0.76	0.76
Sodium Silicate / NaOH Ratio by Weight	2.50	2.50	2.50
Alumina/Silica Molar Ratio, Max=0.43	0.11	0.18	0.26

	Test C-1-1	Test C-1-2	Test C-1-3
Compressive Strength 7 Days (psi) Ambient Dry	928	882	995
Compressive Strength 28 Days (psi) Ambient Dry	2746	3071	2707
Compressive Strength (psi) Oven Dry	4424	3976	4521

Figure B-1: Molar Ratios and Compressive Strengths for C-1 Series (3"x6" Cylinders)

Targets	Test C-2-1	Test C-2-2	Test C-2-3
Sodium Silicate / NaOH Molar Ratio	3.05	3.05	3.05
Sodium Oxide/Silica Molar Ratio Op = 0.12	0.16	0.17	0.18
Ca/Si Molar Ratio Op = 0.8-1.2, max = 2.25	0.40	0.43	0.45
Ca/(Si+Al) Molar Ratio Op = 0.74-0.9	0.33	0.31	0.29
Si/Al Molar Ratio Op = 5.8-6.5 (2.0 for Phillipsite)	9.1	5.4	3.7
Al/Ca Molar Ratio Max = 0.15-0.25	0.27	0.43	0.60
Silica Modulus Op= 0.6-1.1 (From Solution only)	0.76	0.76	0.76
Sodium Silicate / NaOH Ratio by Weight	2.50	2.50	2.50
Alumina/Silica Molar Ratio, Max=0.43	0.11	0.18	0.27

	Test C-2-1	Test C-2-2	Test C-2-3
Compressive Strength 7 Days (psi) Ambient Dry	682	1084	1036
Compressive Strength 28 Days (psi) Ambient Dry	1672	2900	2573
Compressive Strength (psi) Oven Dry	3653	5084	4201

Figure B-2: Molar Ratios and Compressive Strengths for C-2 Series (3"x6" Cylinders)

Targets	Test C-3-1	Test C-3-2	Test C-3-3
Sodium Silicate / NaOH Molar Ratio	3.05	3.05	3.05
Sodium Oxide/Silica Molar Ratio Op = 0.12	0.17	0.18	0.19
Ca/Si Molar Ratio Op = 0.8-1.2, max = 2.25	0.48	0.50	0.53
Ca/(Si+Al) Molar Ratio Op = 0.74-0.9	0.39	0.37	0.34
Si/Al Molar Ratio Op = 5.8-6.5 (2.0 for Phillipsite)	9.1	5.4	3.7
Al/Ca Molar Ratio Max = 0.15-0.25	0.23	0.37	0.51
Silica Modulus Op= 0.6-1.1 (From Solution only)	0.76	0.76	0.76
Sodium Silicate / NaOH Ratio by Weight	2.50	2.50	2.50
Alumina/Silica Molar Ratio, Max=0.43	0.11	0.19	0.27
Compressive Strength 7 Days (psi) Ambient Dry	847	927	762
Compressive Strength 28 Days (psi) Ambient Dry	1498	2322	1713
Compressive Strength (psi) Oven Dry	4359	4168	4558

Figure B-3: Molar Ratios and Compressive Strengths for C-3 Series

(3"x6" Cylinders)
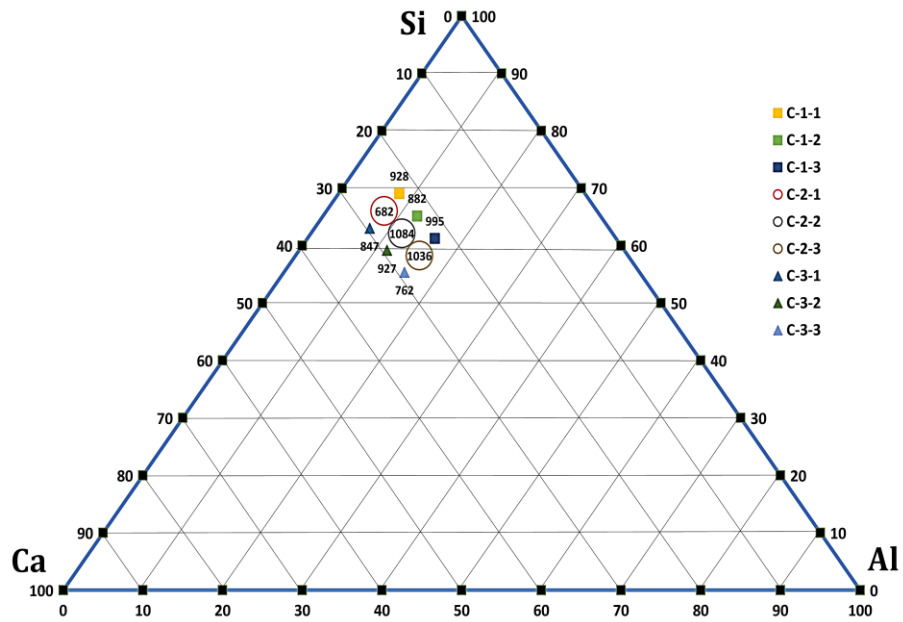
Figure B-4: Ternary Diagram of 7-Day Compressive Strengths
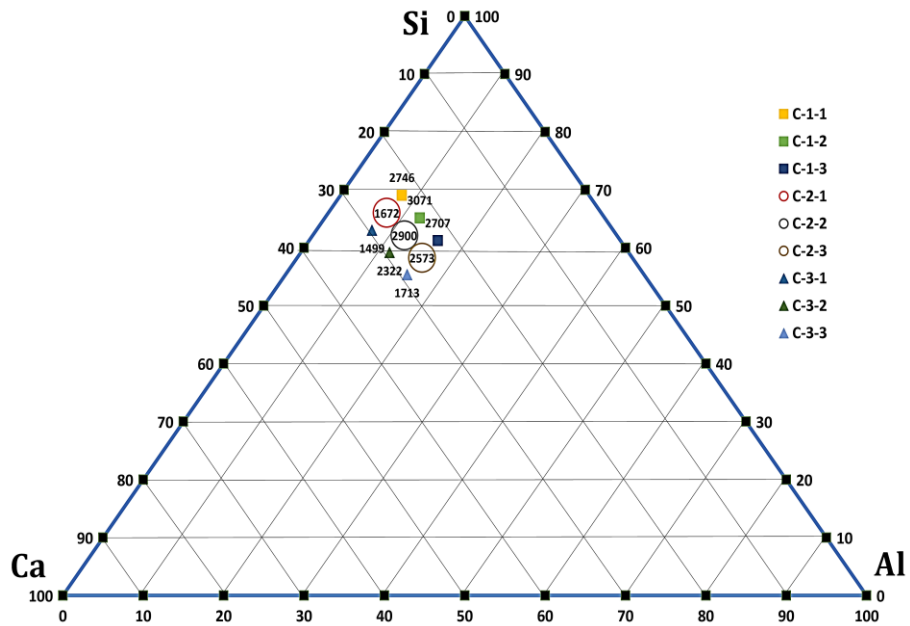
(3"x6" Cylinders)

**Figure B-5: Ternary Diagram of 28-Day Compressive Strengths
(3"x6" Cylinders)**
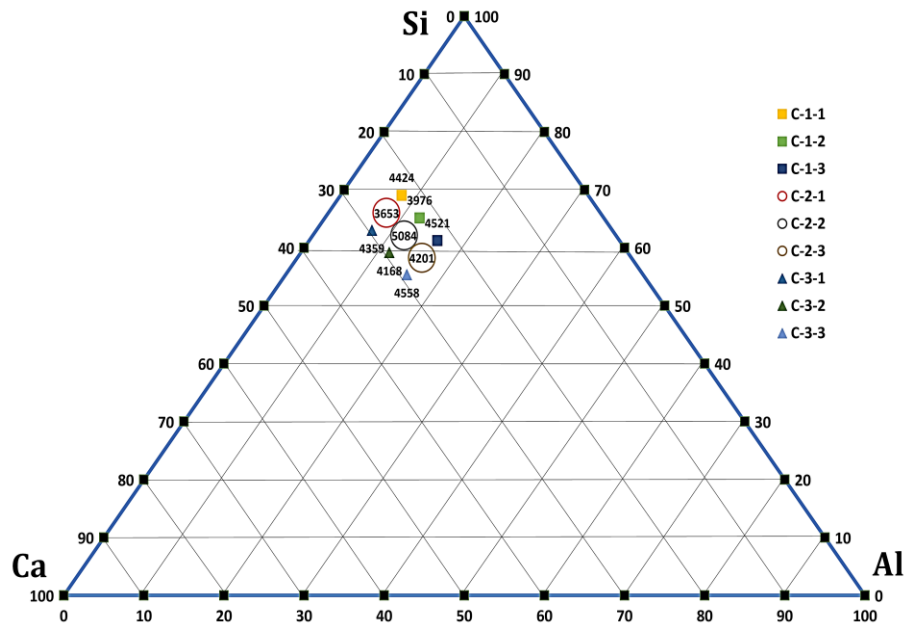
Figure B-6: Ternary Diagram of Oven-Cured Compressive Strengths (3"x6" Cylinders

Appendix C – Photos of RBD Geopolymer Cubes
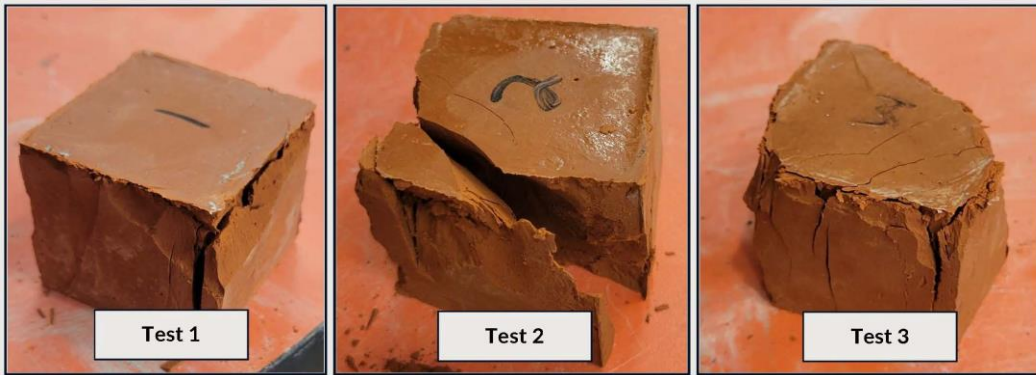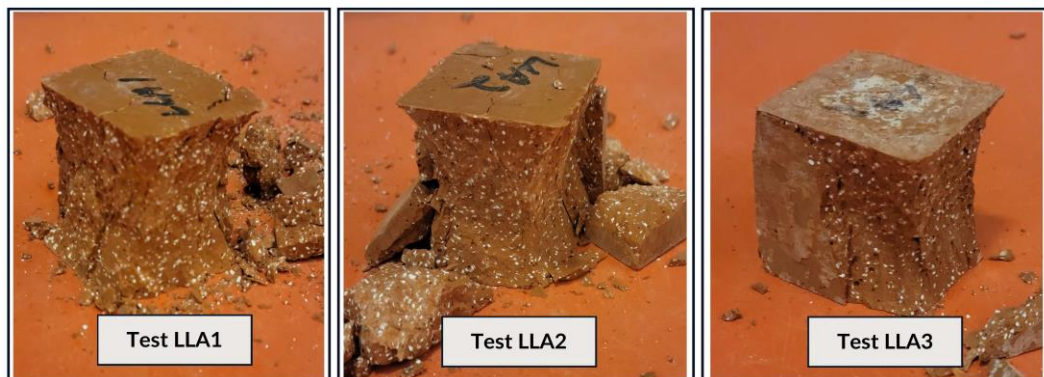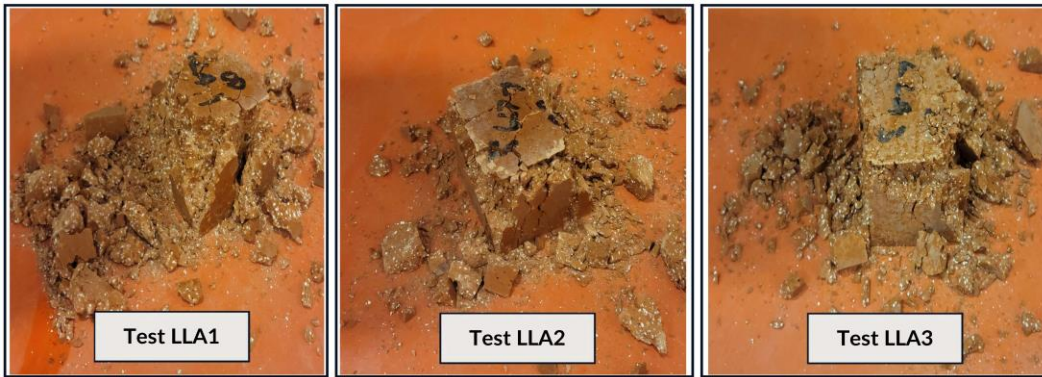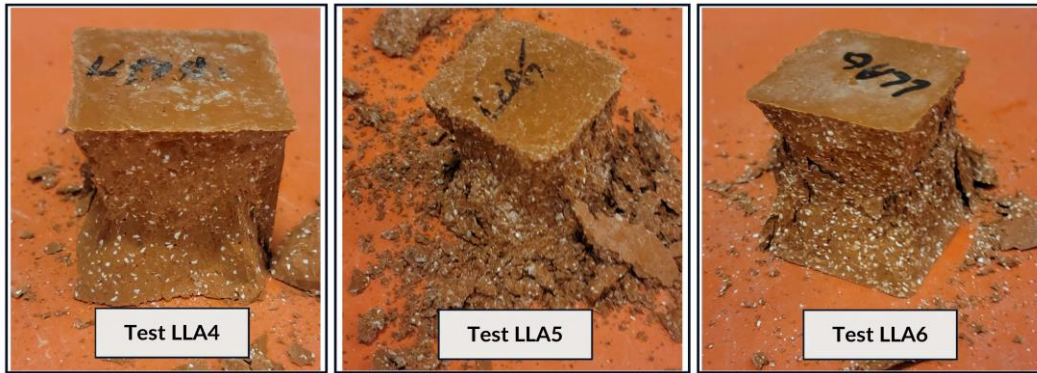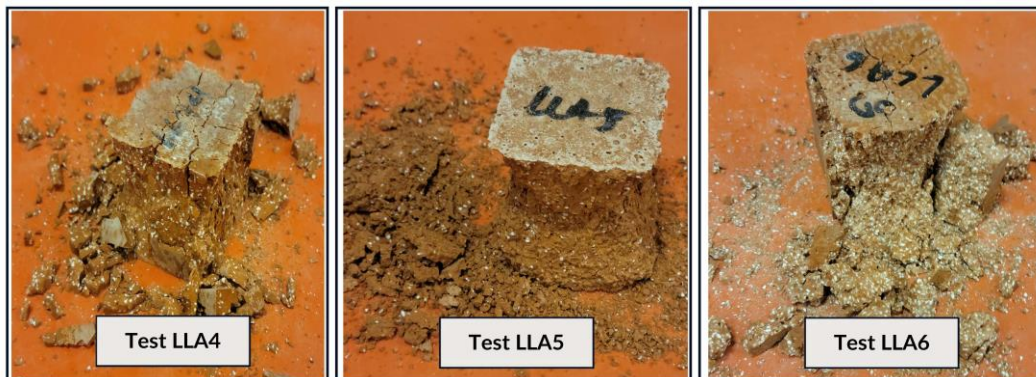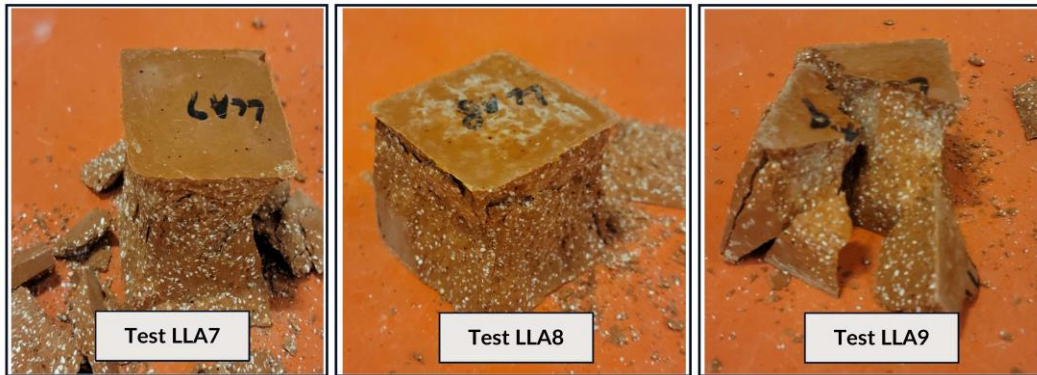
Figure C-1: Images of 28-day Ambient Curing for Tests 1-3
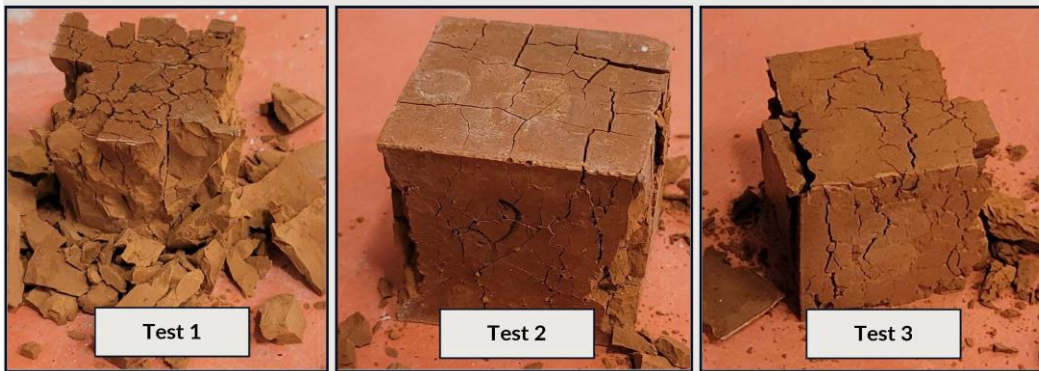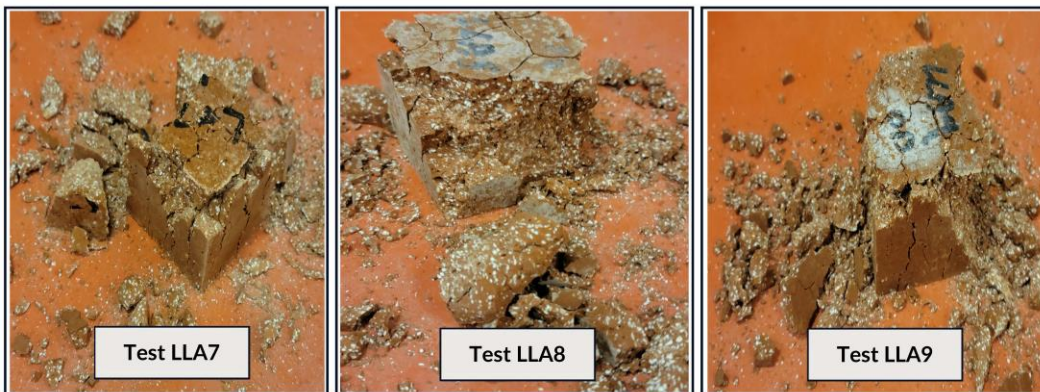

Figure C-2: Images of Oven Curing for Tests 1-3
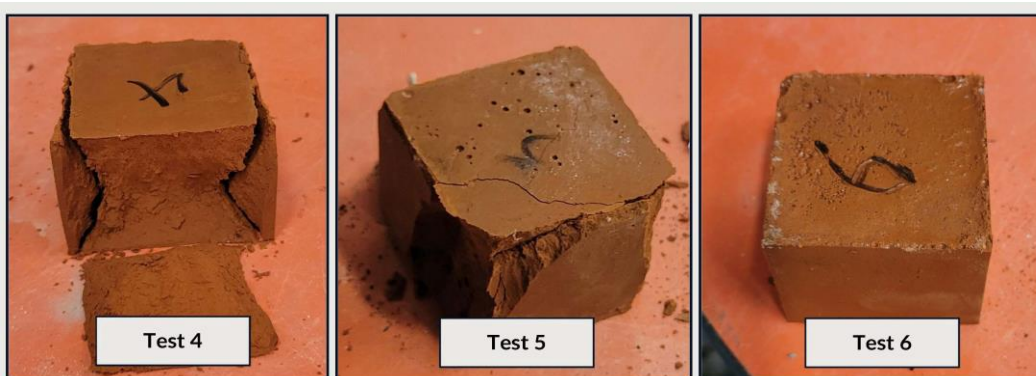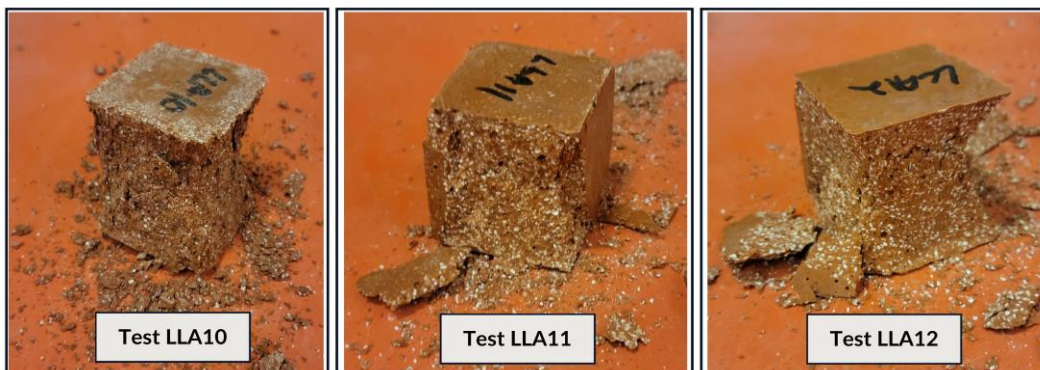

Figure C-3: Images of 28-day Ambient Curing for Tests 4-6
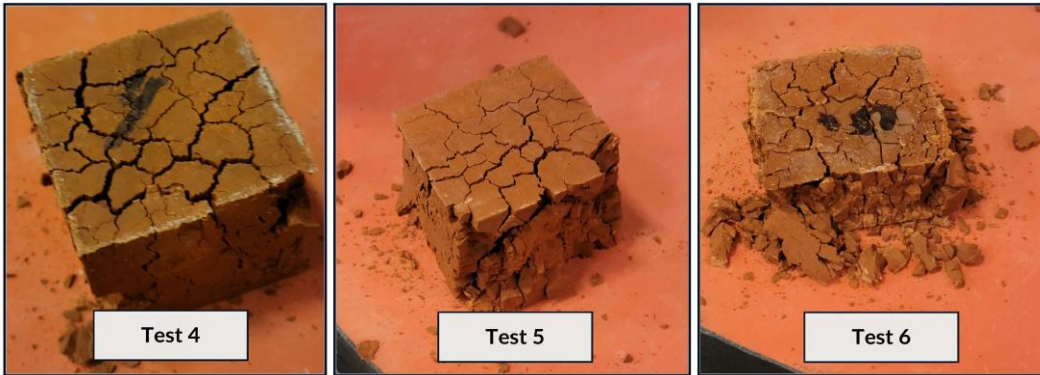
Figure C-4: Images of Oven Curing for Tests 4-6
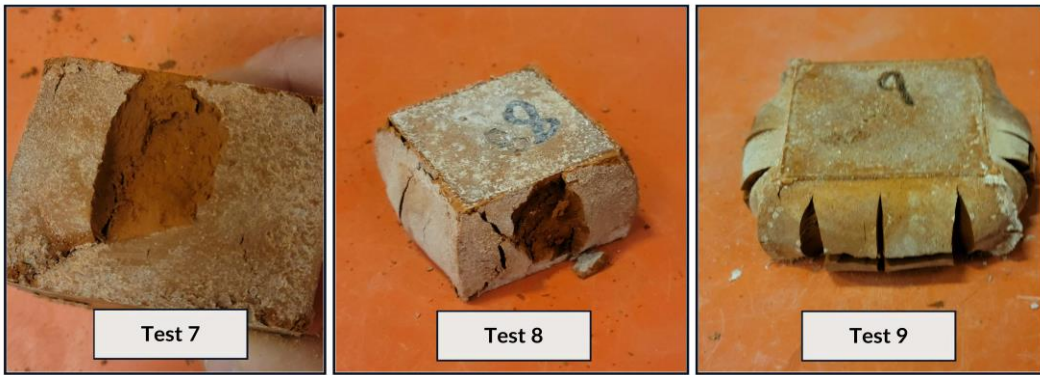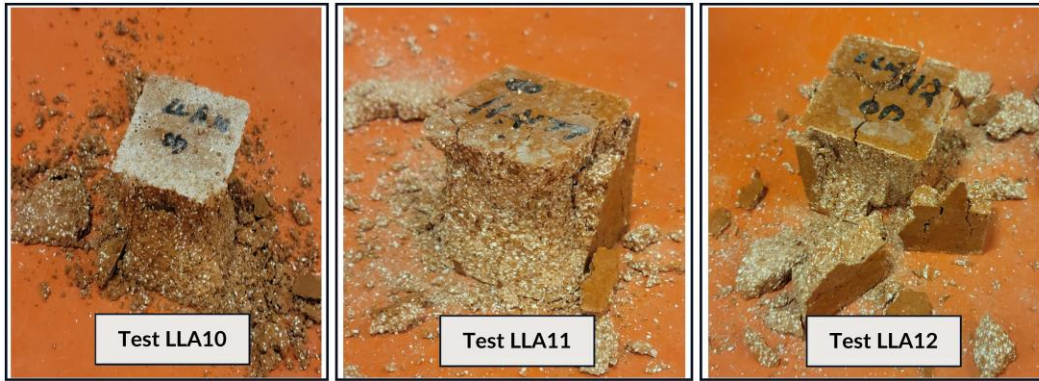

Figure C-5: Images of 28-day Ambient Curing for Tests 7-9

Figure C-6: Images of Oven Curing for Tests 7-9
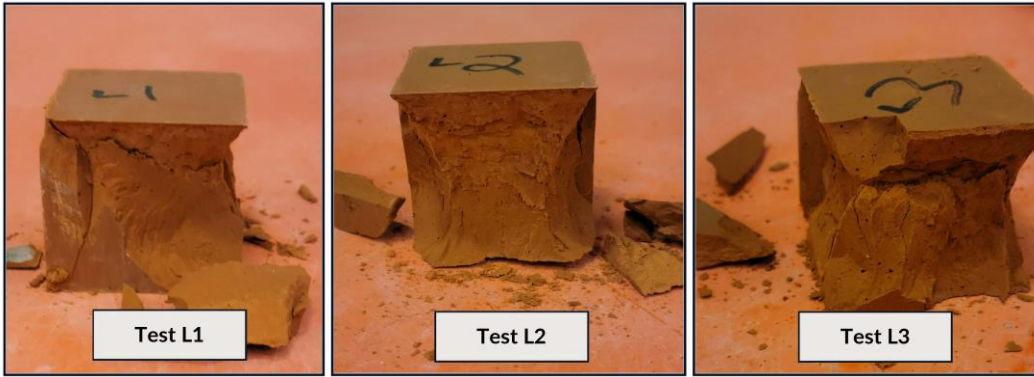
Figure C-7: Images of 28-day Ambient Curing for Tests L1-L3
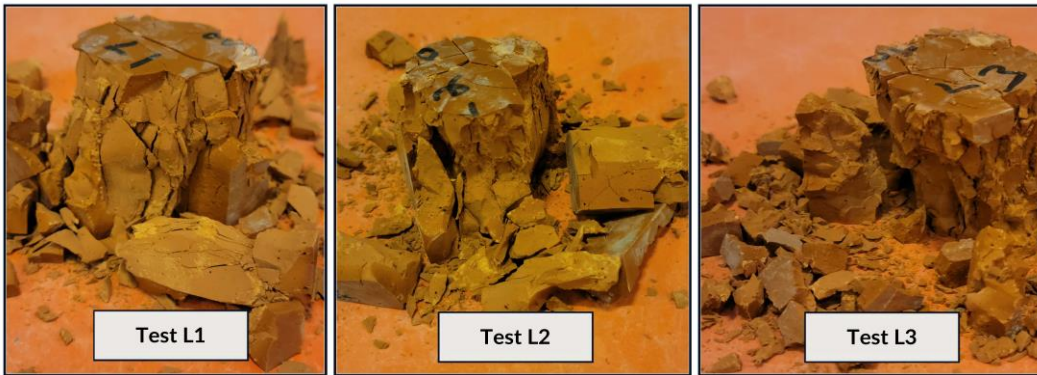
Figure C-8: Images of Oven Curing for Tests L1-L3
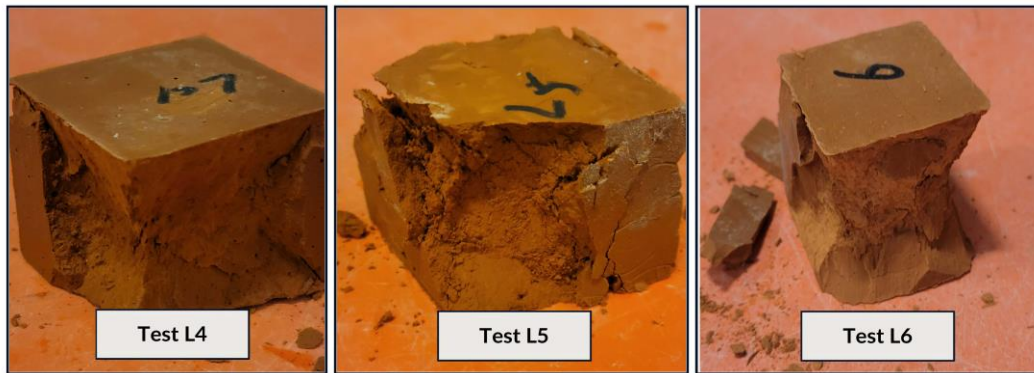
Figure C-9: Images of 28-day Ambient Curing for Tests L4-L6

120
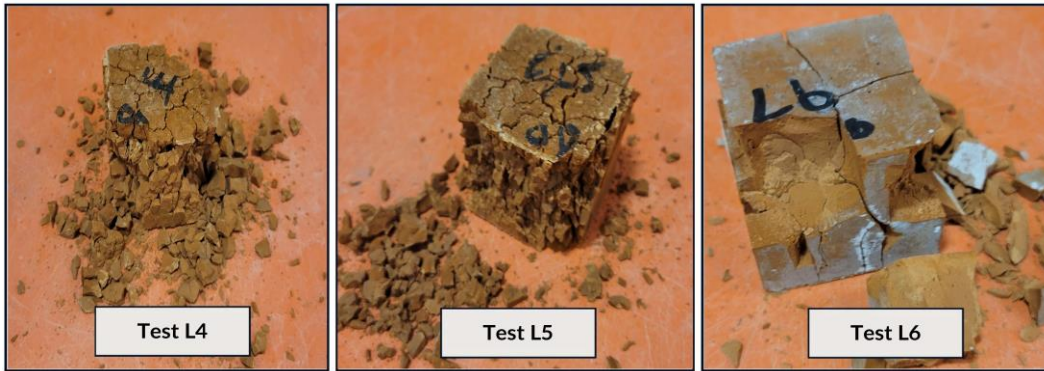
Figure C-10: Images of Oven Curing for Tests L4-L6
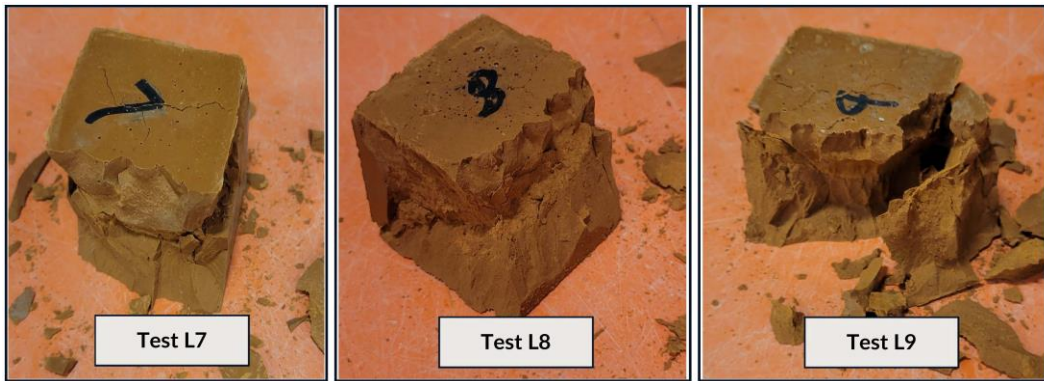
Figure C-11: Images of 28-day Ambient Curing for Tests L7-L9

Figure C-12: Images of Oven Curing for Tests L7-L9
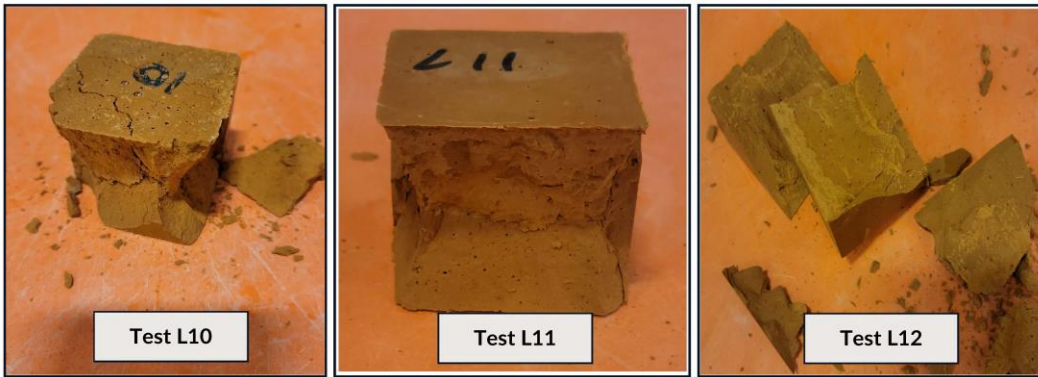
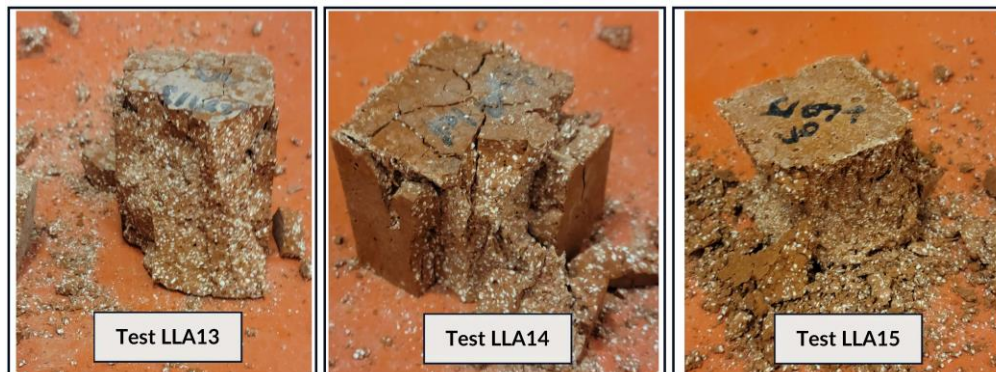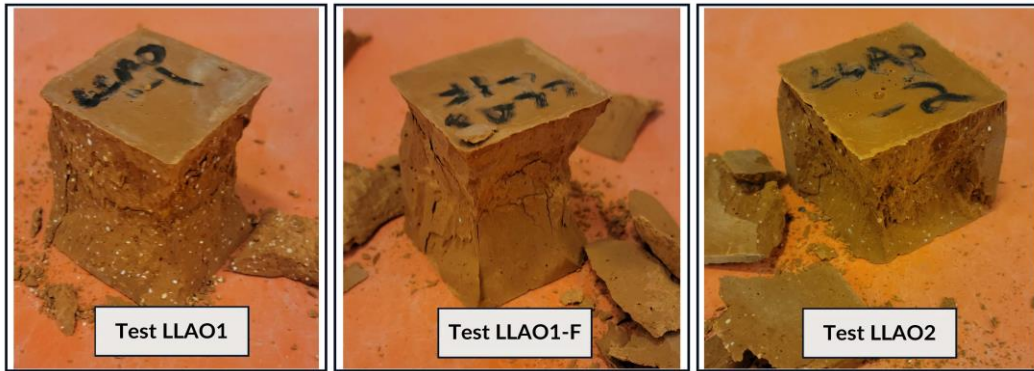**Figure C-13: Images of 28-day Ambient Curing for Tests L10-L12**


Figure C-14: Images of Oven Curing for Tests L10-L12

Figure C-15: Images of 28-day Ambient Curing for Tests L13-L15

Figure C-16: Images of Oven Curing for Tests L14-L15
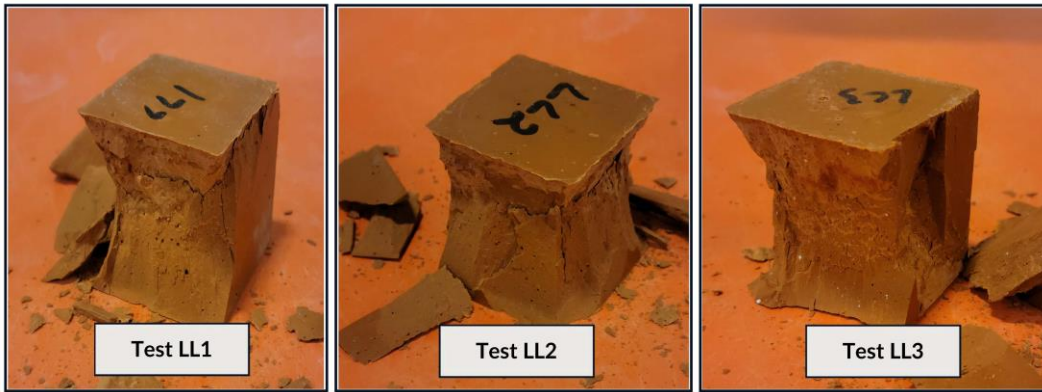
Figure C-17: Images of 28-day Ambient Curing for Tests LL1-LL3

Figure C-18: Images of Oven Curing for Tests LL1-LL3
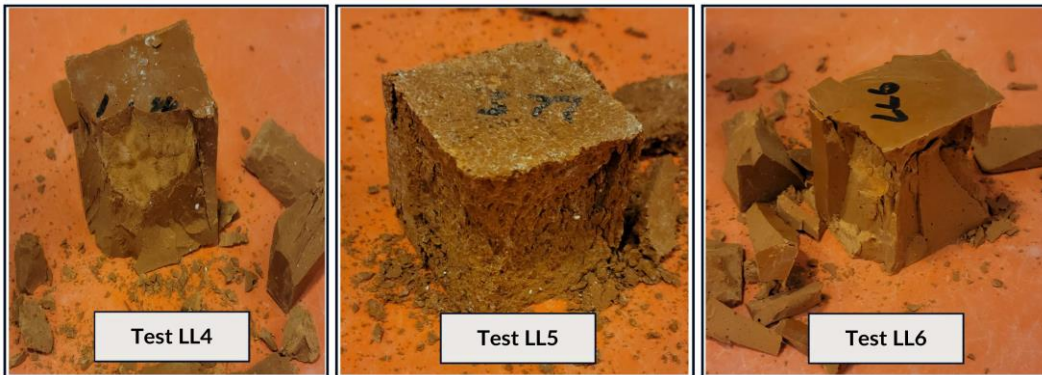
Figure C-19: Images of 28-day Ambient Curing for Tests LL4-LL6
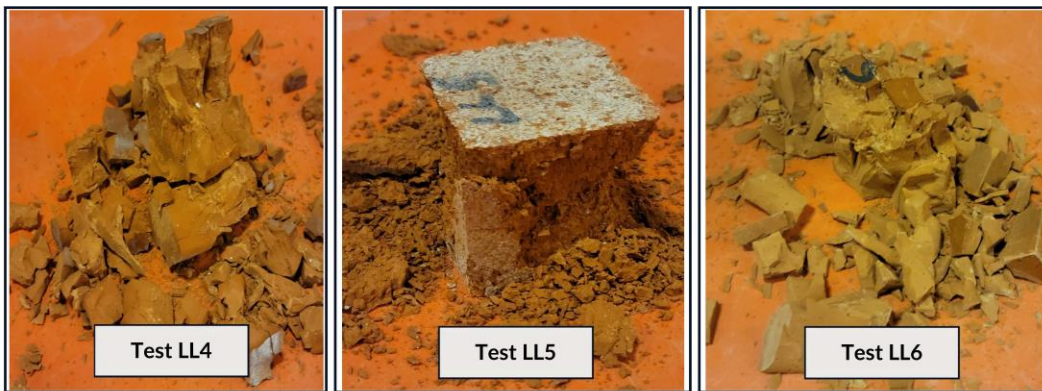
Figure C-20: Images of Oven Curing for Tests LL4-LL6
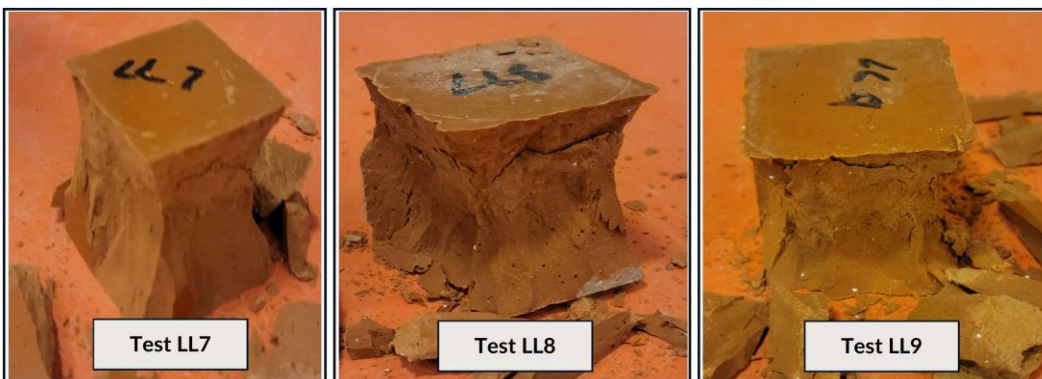
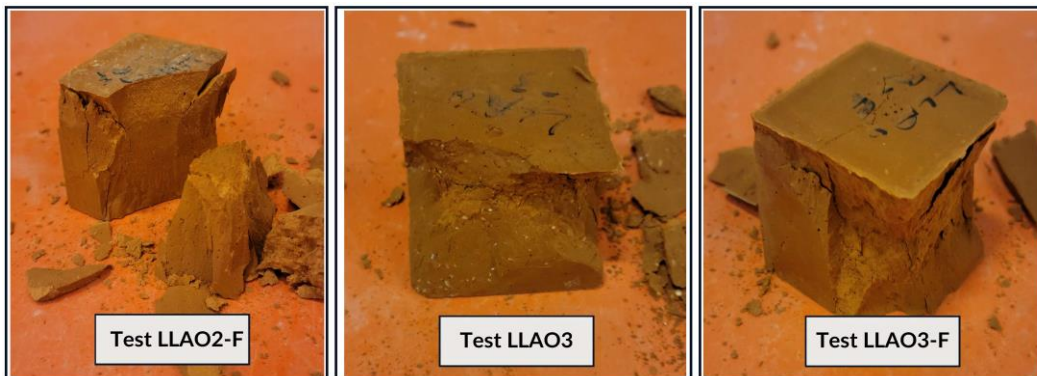**Figure C-21: Images of 28-day Ambient Curing for Tests LL7-LL9**

Figure C-22: Images of Oven Curing for Tests LL7-LL9
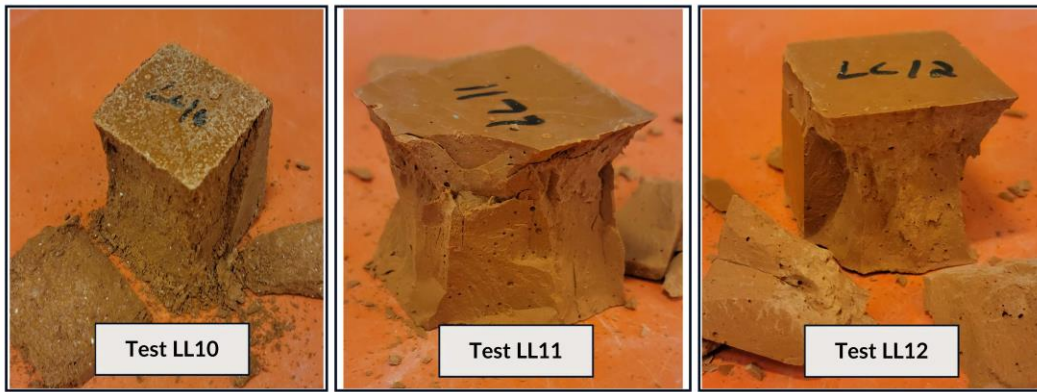
Figure C-23: Images of 28-day Ambient Curing for Tests LL10-LL12

Figure C-24: Images of Oven Curing for Tests LL10-LL13

Figure C-25: Images of 28-day Ambient Curing for Tests LL13-LL15


Figure C-26: Images of Oven Curing for Tests LL13-LL15

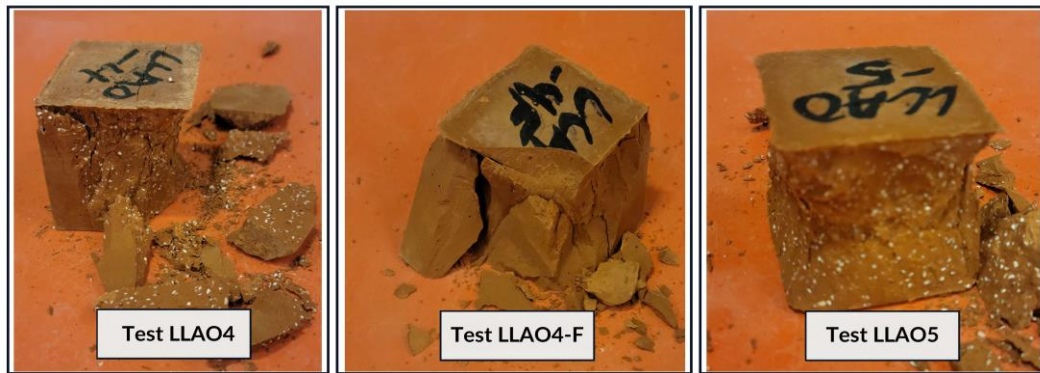**Figure C-27: Images of 28-day Ambient Curing for Tests LLA1-LLA3**

**Figure C-28: Images of Oven Curing for Tests LLA1-LLA3**

Figure C-29: Images of 28-day Ambient Curing for Tests LLA4-LLA6

Figure C-30: Images of Oven Curing for Tests LLA4-LLA6

Figure C-31: Images of 28-day Ambient Curing for Tests LLA7-LLA9

Figure C-32: Images of Oven Curing for Tests LLA7-LLA9

Figure C-33: Images of 28-day Ambient Curing for Tests LLA10-LLA12

Figure C-34: Images of Oven Curing for Tests LLA10-LLA12

Figure C-35: Images of 28-day Ambient Curing for Tests LLA13-LLA15

Figure C-36: Images of Oven Curing for Tests LLA13-LLA15

Figure C-37: Images of 28-day Ambient Curing for LLAO1 to LLAO2
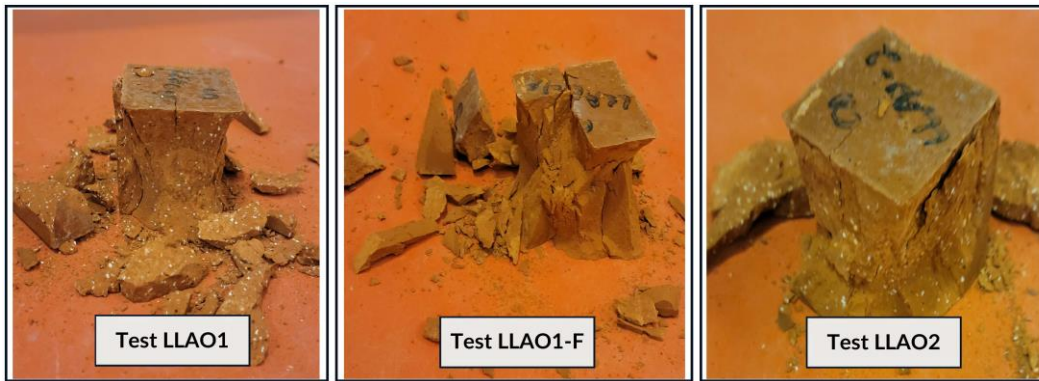
Figure C-38: Images of Oven Curing for LLAO1 to LLAO2

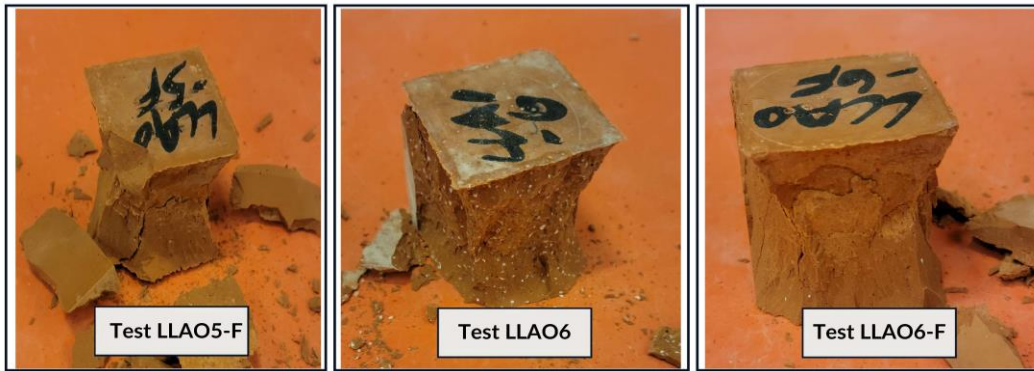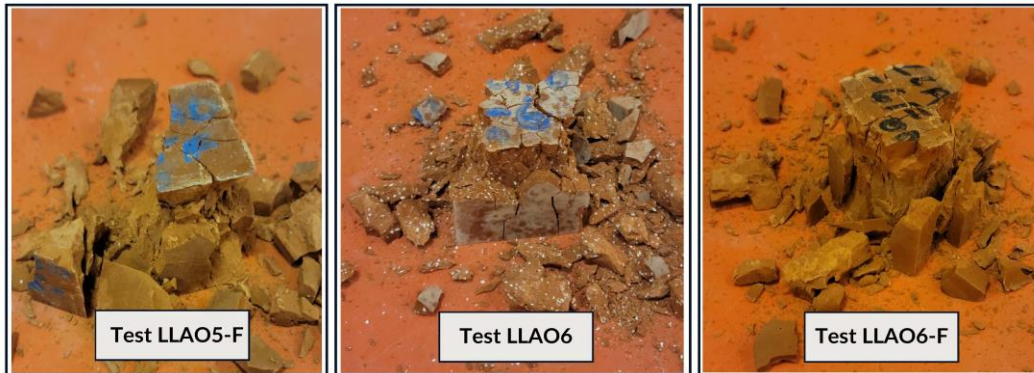**Figure C-39: Images of 28-day Ambient Curing for LLAO2-F to LLAO3-F**
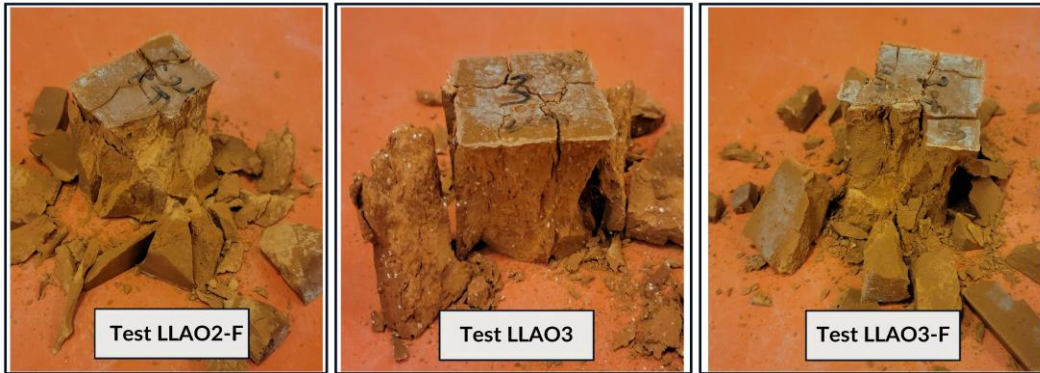
Figure C-40: Images of Oven Curing for LLAO2-F to LLAO3-F

Figure C-41: Images of 28-day Ambient Curing for LLAO4 to LLAO5
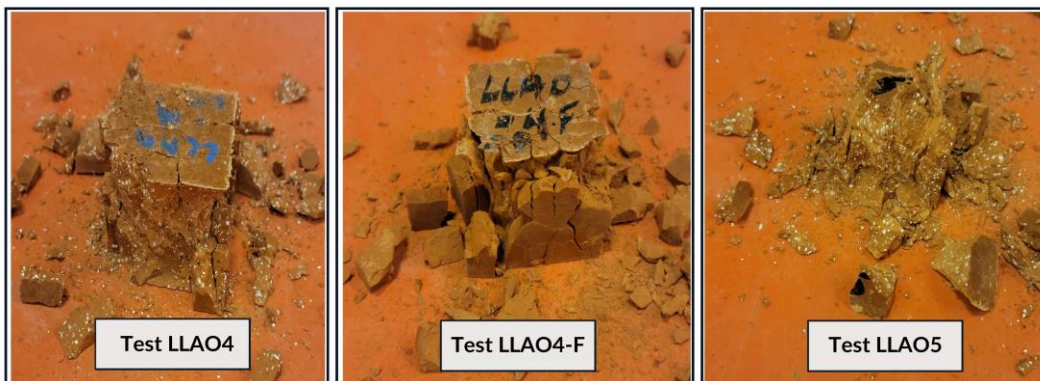
Figure C-42: Images of Oven Curing for LLAO4 to LLAO5

131

Figure C-43: Images of 28-day Ambient Curing for LLAO5-F to LLAO6-F
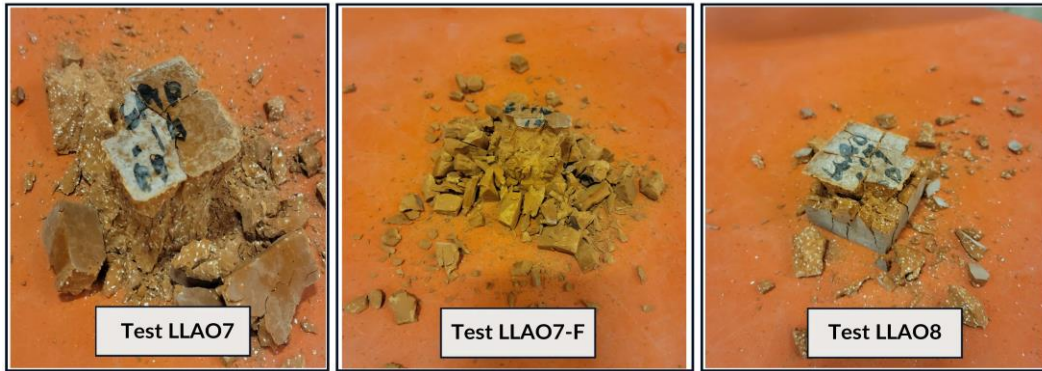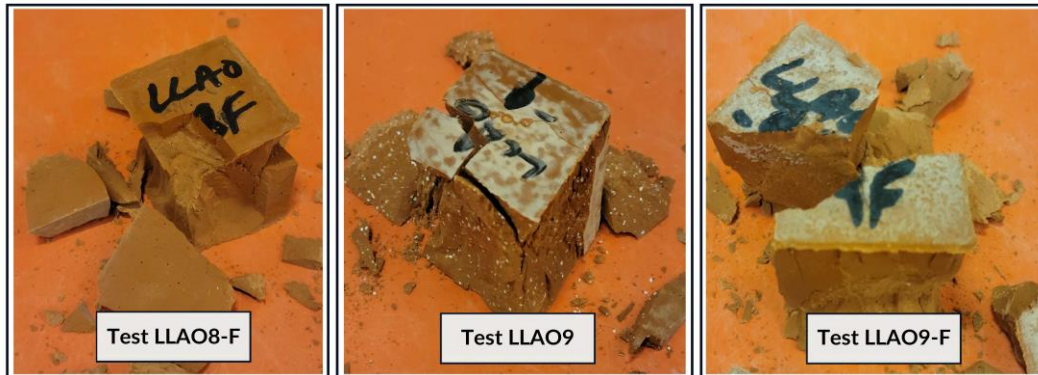

Figure C-44: Images of Oven Curing for LLAO5-F to LLAO6-F
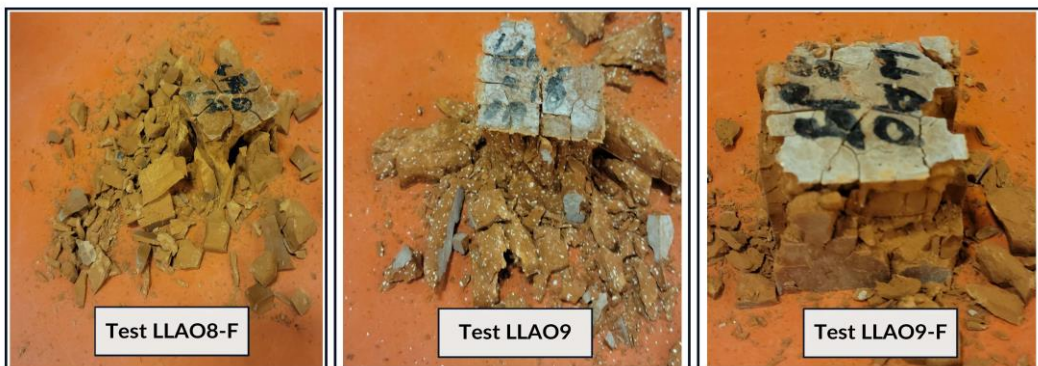

Figure C-45: Images of 28-day Ambient Curing for LLAO7 to LLAO8

Figure C-46: Images of Oven Curing for LLAO7 to LLA8

Figure C-47: Images of 28-day Ambient Curing for LLAO8-F to LLAO9-F

Figure C-48: Images of Oven Curing for LLAO8-F to LLAO9-F